สำนักหอสมุดกลาง พระจอมเกล้าลาดกระบัง

INVESTIGATION OF FLYING HEIGHT IN HELIUM-FILLED DRIVE

E076519

PALITA SUDACHUN

เลขหมู่.....
เลขทะเบียน.....76519
วัน,เดือน,ปี...2.6...ส.ค...2557

b.....
i.....

A THESIS SUBMITTED IN PARTIAL FULFILLMENT

OF THE REQUIREMENT FOR THE DEGREE OF

MASTER OF ENGINEERING IN DATA STORAGE TECHNOLOGY

/INTERNATIONAL COLLEGE

KING MONGKUT'S INSTITUTE OF TECHNOLOGY LADKRABANG

2013

KMITL-2013-IC-M-005-020

This material is reserved for educational use only, not allowed for commercial use.
Forbidden to modify the content, and cite the document when use.

COPYRIGHT 2013

INTERNATIONAL COLLEGE

COLLEGE OF DATA STORAGE TECHNOLOGY AND INNOVATIONS

KING MONGKUT'S INSTITUTE OF TECHNOLOGY LADKRABANG

This thesis is the property of the author. It is not allowed for commercial use.

Forbidden to modify the content, and cite the document when use.

Thesis Title	Investigation of flying height in helium-filled drive
Student	Miss Palita Sudachun
Student ID	52600618
Degree	Master of Engineering
Program	Data Storage Technology
Year	2013
Thesis Advisor	Assoc. Prof. Dr. Mongkol Mongkolwongrojn

ABSTRACT

This thesis aims to investigate the flying height characteristic (static) of the slider head in helium-filled drives for data storage system. The modified Reynolds equations based on the first-order finite difference equation were solved for the rail-pad and the tri-pad slider head. Numerical scheme with finite difference method was implemented to obtain the performance characteristics of the slider head in hard disk drives. The effect of flying height (FH) variation and pressure distribution with varying disk velocity, loading force, and the temperature were investigated numerically.

This study shows that the flying height of the helium-filled drive is very low when compare with the flying height of the air-filled drive.

Index Terms – Helium-filled drive, modified Reynolds equation, flying height, static characteristics of self-acting air bearing

This material is reserved for educational use only, not allowed for commercial use.

Forbidden to modify the content, and cite the document when use.

ACKNOWLEDGEMENTS

I wish to thank my advisor, Assoc. Prof. Dr. Mongkol Mongkolwongrojn from Mechanical Engineering, King Mongkut's Institute of Technology Ladkrabang (KMITL), for offering valuable advice, support and guidance throughout my Master's study.

I would also like to thank Dr. Jesda Panichakorn for help and advice on program simulation and for teaching me the numerical method.

Special appreciation goes to Western Digital (Thailand) Co., Ltd. for my scholarship in graduate study at KMITL and to National Science and Technology Development Agency (NSTDA) for financial support under grant number DSTAR-R&D 02-02-52.

Finally, I am most grateful my parents, family and friends for all their support throughout these years.

PALITA SUDACHUN

King Mongkut's Institute of Technology Ladkrabang

This material is reserved for educational use only, not allowed for commercial use.
Forbidden to modify the content, and cite the document when use.

TABLE OF CONTENTS

	Page
ABSTRACT	I
ACKNOWLEDGEMENTS	II
TABLE OF CONTENTS	III
LIST OF FIGURES	VI
LIST OF TABLES	XI
NOMENCLATURES	XII
CHAPTER 1 INTRODUCTION	1
1.1 Statement and Significance of Research	1
1.2 Related Research	4
1.3 The Objective	16
1.4 Hypothesis of Research	16
1.5 Conceptual of Research	16
1.6 Scope of Research	17
1.7 Research methodology	17
CHAPTER 2 MEGNETIC RECORDING DEVICE	18
2.1 History of the Hard Disk Drive	18
2.2 Construction and Operational Overview of the Hard Disk	19
2.3 Read/Write Heads	22
2.4 Floating Height/Flying Height/Head Gap	23
2.5 Hard Disk Head Sliders, Arms and Actuator	25
2.5.1 Head Sliders	26
2.5.2 Head Arms	28
2.5.3 Head Actuator	29
2.5.4 Voice Coils	30
2.6 Hard Disk Spindle Motor	33
2.7 Hard Disk Platters and Media	34

This material is reserved for educational use only, not allowed for commercial use.
Forbidden to modify the content, and cite the document when use.

TABLE OF CONTENTS (CONT.)

Page

CHAPTER 3 THEORY 37

3.1 Reynolds Equation 37

3.2 Finite difference method 45

3.3 Newton-Raphson's method 47

3.4 Gauss-Seidel Method 48

3.5 Successive Over Relaxation Method (SOR) 49

3.6 Simpson's Rule 50

3.7 Multrigrid method 51

CHAPTER 4 RESEARCH METHODOLOGY 55

4.1 Methodology 55

4.2 Modified Reynolds Equation Solving 56

4.3 Force and moment on slider head in dimensionless form 62

4.4 Support position on slider head 63

4.5 Film Thickness on slider head 63

4.6 Flow chart of simulation program 64

CHAPTER 5 NUMERICAL SIMULATIONS RESULT 66

5.1 Defined the parameter for Rail-pad 66

5.2 Simulation Result for Rail-pad 67

5.2.1 Influence of disk velocity on static characteristics 67

5.2.2 Influence of loading force on static characteristics 72

5.2.3 Influence of temperature on static characteristics 73

5.3 Defined the parameter for Tri-pad 78

5.3.1 Influence of disk velocity on static characteristics 79

5.3.2 Influence of loading force on static characteristics 85

5.3.3 Influence of temperature on static characteristics 87

This material is reserved for educational use only, not allowed for commercial use.

Forbidden to modify the content, and cite the document when use.

TABLE OF CONTENTS (CONT.)

	Page
CHAPTER 6 CONCLUSIONS	92
6.1 Conclusions	92
6.2 Suggestion for future work	93
REFERENCES	94
APPENDIX	96
AUTHOR BOIGRAPHY	104

This material is reserved for educational use only, not allowed for commercial use.
Forbidden to modify the content, and cite the document when use.

LIST OF FIGURES

Figure Page

1.1 INSIC Storage Technologies Areal Density Trends of 2011 from Oracle Corporation. Courtesy of Gary Francis 2

1.2 Head flying above the disk surface 3

1.3 Historical variations ofHMS versus areal density 3

1.4 A Temperature rise with Heater Power and b thermal protrusion with heater power 4

1.5 Gap FH change with the thermal protrusion 5

1.6 A Gap FH change with the environmental temperature in helium (a) and in argon (b) filled drives 6

1.7 Experimental setup 7

1.8 PES comparisons for at head no.7 in air and helium at outer and inner position 8

1.9 Sequence of events of measuring flying height change due to humidity change 9

1.10 Typical read-back amplitude change during humidity increase from 6%to 67% RH at fixed temperature of 52°C 9

1.11 The transducer's FH as a function of when the heating element is turned off..... 10

1.12 Transducer's FH and corresponding FH loss at the different α 11

1.13 Diagram of coupled-filed analysis method..... 12

1.14 ABS design of two thermal actuated sliders..... 12

1.15 Pressure profile of two thermal actuated sliders..... 13

1.16 Pressure loss at 60°C and 80%RH for slider A..... 13

1.17 Flying height vs heat power..... 14

1.18 Flying height vs environmental temperature..... 15

2.1 Areal Density evolution of HDD and flash memory..... 18

2.2 Hard disk heads and platters..... 19

2.3 The tracks and sectors on a disk..... 20

This material is reserved for educational use only, not allowed for commercial use.

Forbidden to modify the content, and cite the document when use.

LIST OF FIGURES (CONT.)

Figure	Page
2.4 Typical hard disk drive components	22
2.5 Read/Write heads and rotary voice coil actuator assembly	23
2.6 Comparison the flying height with human hair and dust particle	24
2.7 Annotated illustration of a typical PC actuator assembly showing the major components	26
2.8 Illustration of head slider	27
2.9 The head arm of a typical recent-design hard drive	28
2.10 A stepper motor actuator	30
2.11 A partially-disassembled voice coil actuator	31
2.12 A hard disk spindle motor	34
2.13 A platter form of a 8", 5.25", 3.5", 2.5", 1.8" and 1"	35
3.1 Cartesian coordinates of film thickness	37
3.2 Equilibrium forces in Cartesian coordinates	38
3.3 Conservation of mass in Cartesian coordinates	41
3.4 Boundary condition and film thickness	45
3.5 Finite difference methods	46
3.6 Flow chart of Newton Raphson method	47
3.7 Intervals for Simpson	50
3.8 Full Multigrid scheme	51
3.9 Distribution from Fine Grid to Coarse Grid	52
3.10 Distribution from Coarse Grid to Fine Grid	53
3.11 Distribution from Coarse Grid to Fine Grid	53
3.12 Distribution from Coarse Grid to Fine Grid	54
4.1 Methodology Flow	55
4.2 Grids for finite difference method	56
4.3 Flying height of slider head	62

This material is reserved for educational use only, not allowed for commercial use.
Forbidden to modify the content, and cite the document when use.

LIST OF FIGURES (CONT.)

Figure	Page
4.4 Force and momentum on slider head	63
4.5 Film thickness	64
4.6 Flow chart of simulation program	65
5.1 The FEMTO form factor of slider dimension for Rail-pad	67
5.2 Comparison FH on Rail-pad of helium and air with various disk velocities at 24mN, 20°C	68
5.3 Comparison on the pressure distribution along the slider head of helium and air at 5400RPM, 20°C, 24mN	68
5.4 Comparison on the pressure distribution along the slider head of helium and air at 7200RPM, 20°C, 24mN	69
5.5 Comparison on the pressure distribution along the slider head of helium and air at 10,000RPM, 20°C, 24mN	69
5.6 Comparison on the pressure distribution along the slider head of helium and air at 5400RPM, 20°C, 24mN	70
5.7 Comparison on the pressure distribution along the slider head of helium and air at 7200RPM, 20°C, 24mN	70
5.8 Comparison on the pressure distribution along the slider head of helium and air at 10,000RPM, 20°C, 24mN	71
5.9 FH comparison between helium and air with loading force change of Rail-pad	72
5.10 Comparison pressure profile of helium on Rail-pad at 24mN & 28mN, 5400RPM, 20°C	73
5.11 FH comparison between helium and air with temperature change of Rail-pad	74
5.12 Comparison Pressure profile of helium on Rail-pad with various temperatures at 5400RPM, 24mN	74
5.13 Comparison Pressure profile of air on Rail-pad with various temperatures at 5400RPM, 24mN	75

This material is reserved for educational use only, not allowed for commercial use.
Forbidden to modify the content, and cite the document when use.

LIST OF FIGURES (CONT.)

Figure Page

5.14 Comparison on the pressure profile along the slider head of helium and air at 5400RPM, 20°C, 24mN 76

5.15 Comparison on the pressure profile along the slider head of helium and air at 5400RPM, 100°C, 24mN 76

5.16 Comparison on the pressure profile along the slider head of helium and air at 5400RPM, 300°C, 24mN 77

5.17 Comparison on the pressure profile along the slider head of helium and air at 5400RPM, 500°C, 24mN 77

5.18 The FEMTO form factor of slider dimension for Tri-pad 79

5.19 Comparison FH on Tri-pas of helium and air with various disk velocities at 20mN, 20°C 80

5.20 Comparison pressure profile of helium with various disk velocities at 20°C, 20mN 81

5.21 Comparison FH on Tri-pad of helium and air at 20°C, 5400RPM, 20mN Pressure profile of helium at 5400RPM, 20mN, 20°C 81

5.22 Comparison FH on Tri-pad of helium and air at 20°C, 7200RPM, 20mN.... 82

5.23 Comparison FH on Tri-pad of helium and air at 20°C, 10000RPM, 20mN 82

5.24 Comparison on the pressure profile along the slider head of helium with various disk velocities – 5400RPM, 7200RPM, 10,000RPM 83

5.25 Comparison on the pressure profile along the slider head of air with various disk velocities – 5400RPM, 7200RPM, 10,000RPM 84

5.26 Comparison FH on Tri-pas of helium and air with various loading force at 5400RPM, 20°C 85

5.27 Comparison pressure profile on Tri-pad of helium with various loading force at 5400RPM, 20°C 86

This material is reserved for educational use only, not allowed for commercial use.
Forbidden to modify the content, and cite the document when use.

LIST OF FIGURES (CONT.)

Figure Page

5.28 Comparison pressure profile on Tri-pad of helium with various loading force (23mN and 25mN) at 5400RPM, 20°C 87

5.29 Comparison FH on Tri-pad of helium and air with various temperatures 87

5.30 Comparison Air bearing number between helium and air with various temperatures 88

5.31 Comparison viscosity on helium and air with various temperatures..... 89

5.32 Comparison density on helium and air with various temperatures..... 89

5.33 Comparison Pressure profile of helium with various temperatures at 7200RPM, 20mN 90

5.34 Comparison Pressure profile of air with various temperatures at 7200RPM, 20mN 90

5.35 Comparison Pressure profile of helium with various temperatures at 7200RPM, 20mN 91

This material is reserved for educational use only, not allowed for commercial use.

Forbidden to modify the content, and cite the document when use.

LIST OF TABLES

Table	Page
1.1 The properties of helium and air	7
5.1 The parameters of the slider head for simulation for Rail-pad	66
5.2 The parameters of the slider head for simulation for Rail-pad	78

This material is reserved for educational use only, not allowed for commercial use.
Forbidden to modify the content, and cite the document when use.

Nomenclatures

a	Surface correction coefficient
B	Rail width
B	Rail width
μ	Dynamic Viscosity
FH	Flying Height
F_0	Normalized Load, $F_0 = \frac{f_0}{P_a}/LW$
f_0	Initial Loading Force
h	Film Thickness
h_a	Reference film thickness
h_{ld}	Leading edge
h_{tr}	Trailing edge
K_n	Knudsen number, $K_n = \lambda_a/h_a$
H	Normalized film thickness, $H = h/h_a$
H_{LD}	Normalized leading edge, $H = h_{ld}/h_a$
H_{TR}	Normalized trailing edge, $H = h_{tr}/h_a$
L	Slider length
p	Pressure
p_a	Atmosphere pressure
P	Normalized Pressure, $P = p/p_a$
R	Length-width ratio, L/W
$\bar{R}$	Gas constant (universal gas constant/molecular weight)
t_m	Absolute temperature
T	Time, ωt
U	Disk velocity
X, Y	Normalized Cartesian coordinates, $X = x/L, Y = y/W$
x_g	Support position

This material is reserved for educational use only, not allowed for commercial use.
Forbidden to modify the content, and cite the document when use.

Nomenclatures (Cont.)

X_G	Normalized support position, $X_G = x_g/L$
x, y	Cartesian coordinates
Q	Poiseullie flow factor, $\emptyset(P,H)$
Λ	Bearing number, $6\eta_a UL/p_a h_a^2$
ε	Relative error
σ	Squeeze number, $12\eta_a \omega L^2/p_a h_a^2$
ω_0	Angular frequency
Z	Normalized translation displacement from disk surface (z/h_a)
M_Z	Normalized mass of slider head $(mh_a\omega_0^2 / p_a LB)$
M_0	Normalized moment, $(m_0 / p_a L^2 B)$

This material is reserved for educational use only, not allowed for commercial use.
Forbidden to modify the content, and cite the document when use.

CHAPTER 1

INTRODUCTION

The digital explosion brought on by the proliferation of the Internet fuelled significant growth in digital content creation and consumption. Coupled with a phenomenal growth in digital tools and equipment, researchers and analysts have put the growth of storage at a 40% compound annual growth rate. The traditional method of increasing tracks per inch (TPI) and bits per inch (BPI) to increase areal density still prevails. However, increasing TPI past a certain point requires other technologies to stabilize performance. Using an inert gas such helium is one technology to use. This has a positive effect on the thermal actuation of the slider head and reduces the vibration of hard disk drives due to large air bearing stiffness. The slider bearing is self-acting with straight rails for the magnetic storage in a hard disk drive. The modified Reynolds equations were formulated. A numerical scheme based on the finite difference method with the Newton-Raphson method was implemented to obtain the static characteristics of slider head in steady state. The main objective of this topic is to investigate the flying height characteristic of a slider head in a helium filled-drive when varying the disk velocity, loading force and temperature. The simulation results shows that the flying height of the slider head in the helium-filled drive is smaller than the flying height in air-filled drives for various disk velocities, loading forces, and temperatures.

1.1 Statement and Significance of Research

The need to expedite new technological advances in areal density in order to fulfill continuing increase in hard disk drive (HDD) demand exists. Areal recording density increases about 30-40% every year as shown in Fig1.1 [1]. Therefore, the study and development on areal density of hard disk drive is very important. There are many factors affecting the design of high capacity storage. One factor which is interesting to study is the reduced distance between the slider head and the disk surface (or what we call "Flying height"). The high precision of the read (playback) /

This material is reserved for educational use only, not allowed for commercial use.
Forbidden to modify the content, and cite the document when use.

write (recording) process will need to be increased when the flying height is small in order to maintain a suitable distance and avoid causing damage to the disk surface. A wide range of development and research projects have focused on the flying height of the slider head, but these projects are restricted by the properties of the air.

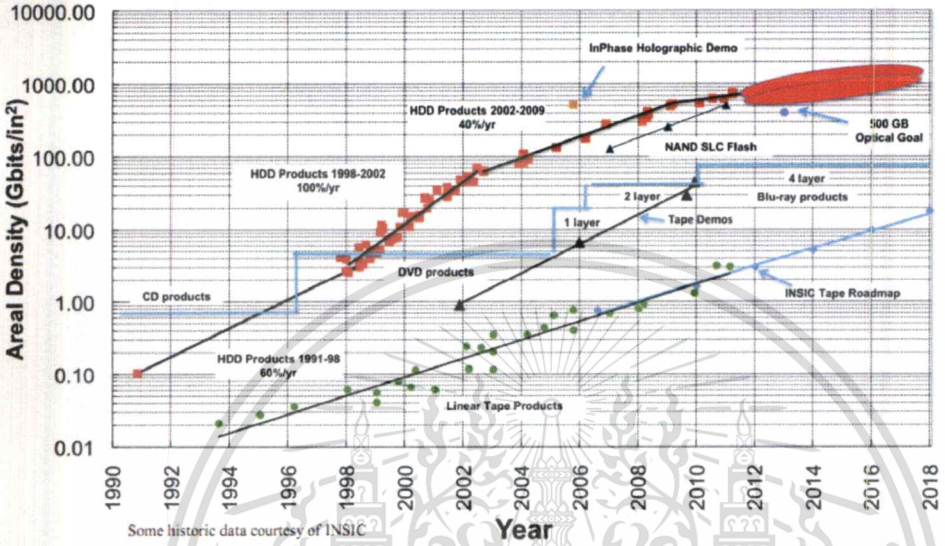

Fig 1.1 INSIC Storage Technologies Areal Density Trends of 2011 from Oracle Corporation. Courtesy of Gary Francis [1]

Thus the use of an inert gas such helium is studied in order to improve the flying height of slider head. Research on using inert gas started in the 1980s when 14 inch disks were normally used [2]. The results showed that the windage loss is reduced by 1/4 and the disk flutter is also reduced by 1/4.6 in helium-filled drives [2]. Also, the vibration from mechanical disturbance is reduced in the helium filled drive, and the positioning error in helium filled drive is less than half of the positioning error in an air-filled drive. These improvements are because of the low density property of helium [3]. In this topic we use the simulation method to study the flying height characteristic of the slider head in the helium-filled drives when the disk velocity, the spring force and the temperature are changed in the fully sealed drives and there is no discussion on the leakage problem.

The magnetic head spacing or the flying height or head-media separation (HMS) is defined here as the mechanical separation between the bottom of the read-write head elements and the top of the magnetic media alloy. Reduction of the magnetic

This material is reserved for educational use only, not allowed for commercial use.
Forbidden to modify the content, and cite the document when use.

spacing has given the greatest return in terms of improving both reader & writer performances and has enabled higher linear and track densities. Figure 1.2 shows the mechanical factors contributed to magnetic spacing. In actual practice, all of these factors have manufacturing tolerances and can be varied. The variations of these spacing factors must be taken into account to define the magnetic spacing budget for the robust design of a magnetic recording system. Interestingly, HMS trend over this areal density (AD) range is going down as shown in Figure 1.3

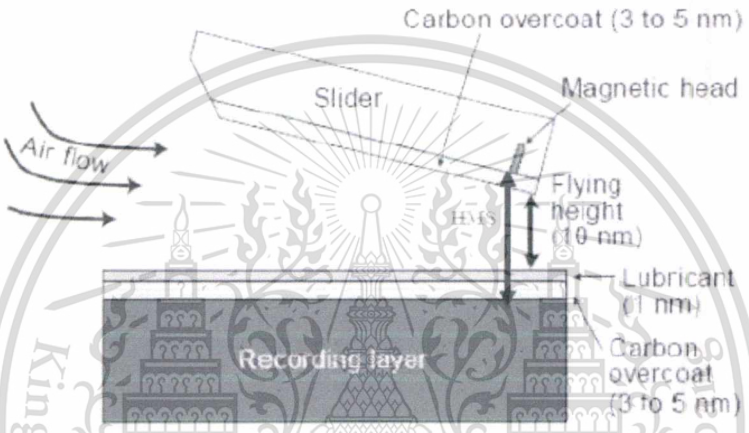

Fig 1.2 Head flying above the disk surface [22]

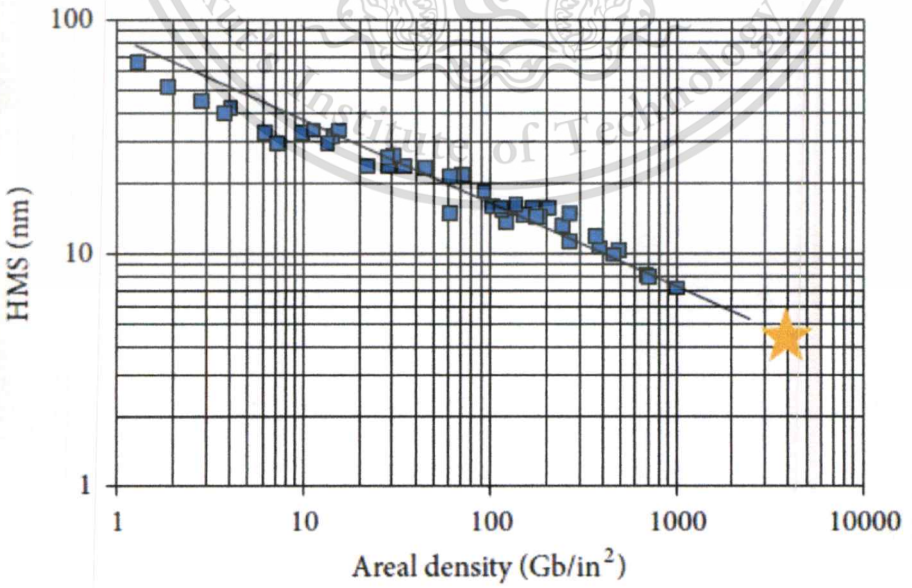

Fig 1.3 Historical variations ofHMS versus areal density [21]

This material is reserved for educational use only, not allowed for commercial use.
Forbidden to modify the content, and cite the document when use.

1.2 Related Research

Zhou, W. D., et al [2] using numerical method and models such as Finite Element model of Thermal Actuated Slider, Air Bearing Model, Heat Transfer Model and Temperature Effects and Gas Properties to investigated the flying height and thermal performance of a thermal actuated slider at inert gas fill HDI. This topic is studied in air, helium and argon. The simulation result showed that with the heater power in the inert gas, the variation of gap flying height (FH) is quiet similar to that in the air. Also, in the helium filled found that the slider's thermal actuation efficiency is slightly better than those in argon and air. The significant parameter on thermal actuation performance is slider protrusion rate, with higher heater power the thermal protrusion is raised and found that the best one is argon and the worst is helium per Fig 1.4.

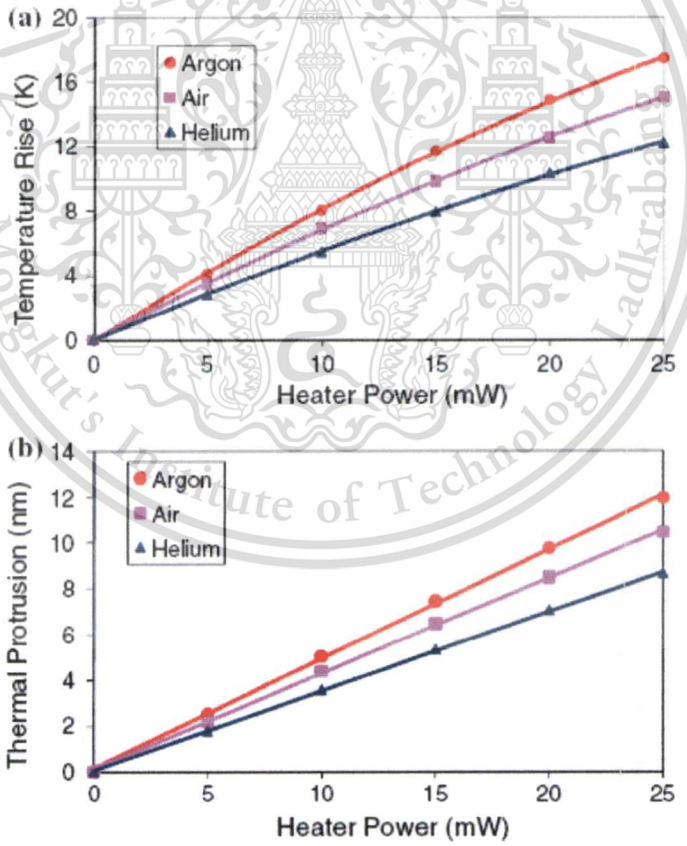

Fig 1.4 A Temperature rise with Heater Power and b thermal protrusion with heater power [2]

This material is reserved for educational use only, not allowed for commercial use.
Forbidden to modify the content, and cite the document when use.

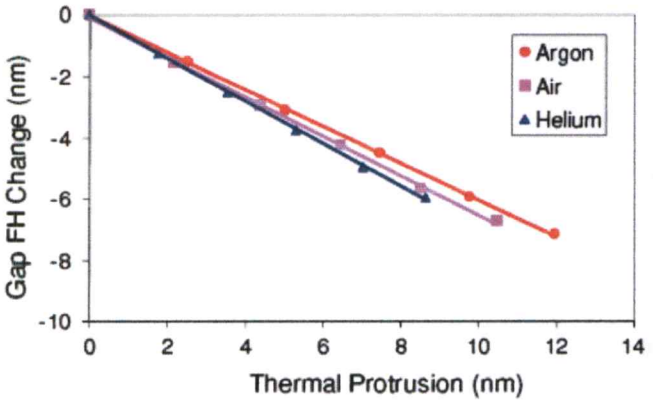

Fig 1.5 Gap FH change with the thermal protrusion [2]

Fig 1.5, the gap flying height is reduced when the thermal protrusion is increased and found that the thermal protrusion rate is lowest in the helium. Then the thermal actuation efficiency is defined as the ratio of the reduction of thermal protrusion [3], with this in the helium is slightly better than that in the argon or the air due to weaker push back effect on helium. The drive must be fully sealed when the inert gas is used as shown in Fig 1.6. The various environmental temperature effects on the gap flying height changes in argon and helium, respectively. The gap FH is slightly decreased in helium as temperature increases in the open drive. This effect is because the mean free path, which increases the Knusen number, thus reduces the load carrying capacity of gas bearing. Besides, the temperature effect of viscosity can help to compensate some FH decrement because the air bearing number will become larger to enhance the slider's load carrying capacity. In the air, the viscosity is increased with the environmental temperature but the effect is still not big enough to change FH's slipping trend.

This material is reserved for educational use only, not allowed for commercial use.
Forbidden to modify the content, and cite the document when use.

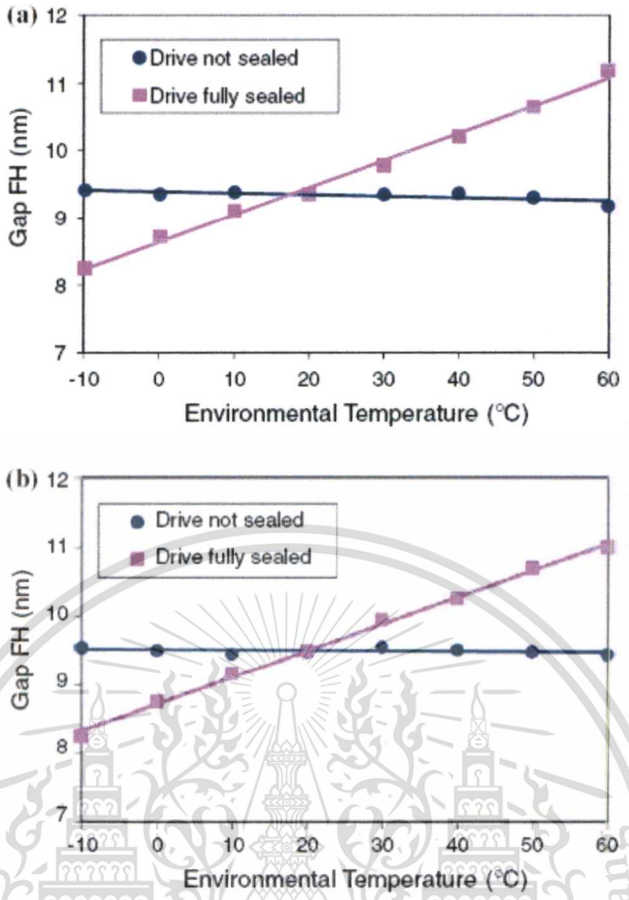

Fig 1.6 A Gap FH change with the environmental temperature in helium (a) and in argon (b) filled drives [2]

Aruga, K., M. Suwa, et al [4] studied on the positioning accuracy of helium and air-filled drives. As the greater positioning is one critical issue for achieve the higher areal density of hard disk drive, the larger windage disturbance at higher rpm applications induced a positioning error then it not easy to increase track density. The experiment is set up [Fig 1.7] for measure the PES spectra of both drives and then calculate the mechanical disturbance then Computer Fluid Dynamic (CFD) is applied for analysis by clarify on air and helium properties comparison on PES, frequency windage and disturbance. Per the representative properties, helium's lightweight provided small windage-loss and small windage-pressure but the dynamic viscosity is larger than air.

This material is reserved for educational use only, not allowed for commercial use.
Forbidden to modify the content, and cite the document when use.

TABLE 1.1 THE PROPERTIES OF HELIUM AND AIR

		Air	Helium	He/Air	(dB)
Density ρ	kg/m^3	1.251	0.179	0.143	-16.9
Kinematic viscosity v	m^2/s	1.380E-05	1.020E-04	7.391	17.4
Thermal conductivity λ	W/mK	0.024	0.142	5.917	15.4
Windage param.	$\rho v^{1/2}$ Åilaminar)	4.647E-03	1.808E-03	0.389	-8.2
Windage param.	$\rho v^{1/5}$ (turbulent)	1.36E-02	2.90E-03	0.214	-13.4
rpm for Re=UR/v=2E4	(ϕ 70㎜)	2,153	15,911		

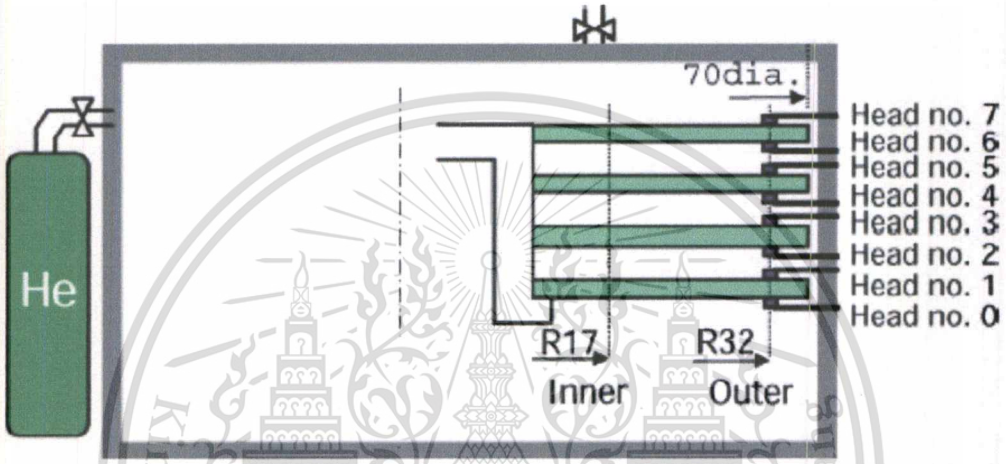

Fig 1.7 Experimental setup [4]

Fig 1.8 present a comparison of PES spectrum for the air- and helium-filled drives at the head between the disk and at the outer disk position. The frequency is displayed from 0 to 23 kHz, the latter being the Nyquist frequency and the dotted line represents the air-filled drive while the solid line is the helium-filled drive. Observed that there are many peak on the air-filled drive and the peak at 2-5 kHz are due to the disk flutter while the peak that more than 10 kHz are mainly the result of arm and suspension resonance.

This material is reserved for educational use only, not allowed for commercial use.
Forbidden to modify the content, and cite the document when use.

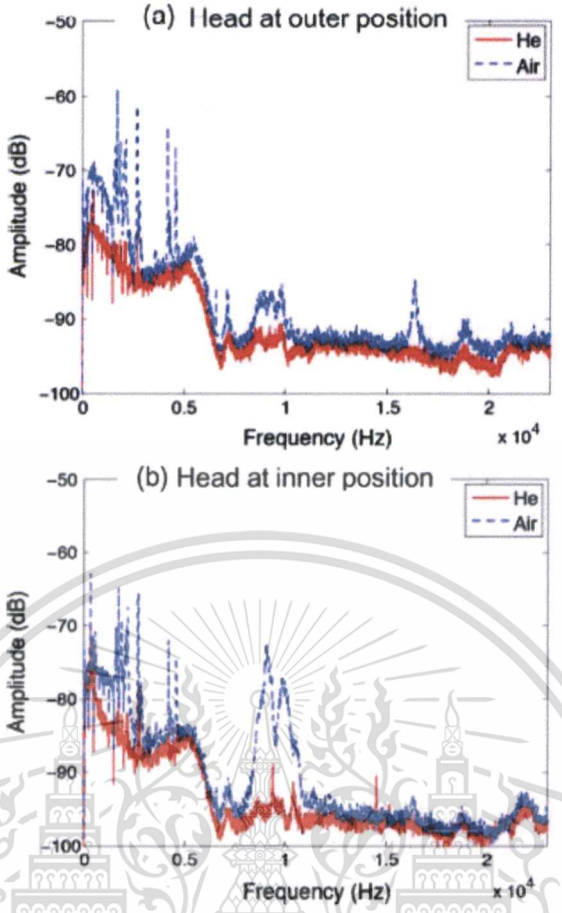

Fig. 1.8 PES comparisons for at head no.7 in air and helium at outer and inner position [4]

In summary, the positioning error in helium-filled drive is less than half of that of air-filled drive. The overall NRRO-6 sigma value of helium-filled drive is 14nm v.s. 34 nm on air, that mean 57% reduction is achieved by replacing air with helium. Almost all disturbances in higher rmp drives are caused by flow induced vibrations and they are verified the effectiveness of using a lighter gas.

Strom, and et al [5] studied on the pressure distribution on a squeeze film air bearing that depends on the water vapor pressure and the saturation vapor of water at ambient temperature. The measurement on relative humidity for the magnetic recording spacing and the numerical model based on the proposed mechanism that match with the experimental data and provide the detailed view of the air bearing response to humidity.

This material is reserved for educational use only, not allowed for commercial use.
Forbidden to modify the content, and cite the document when use.

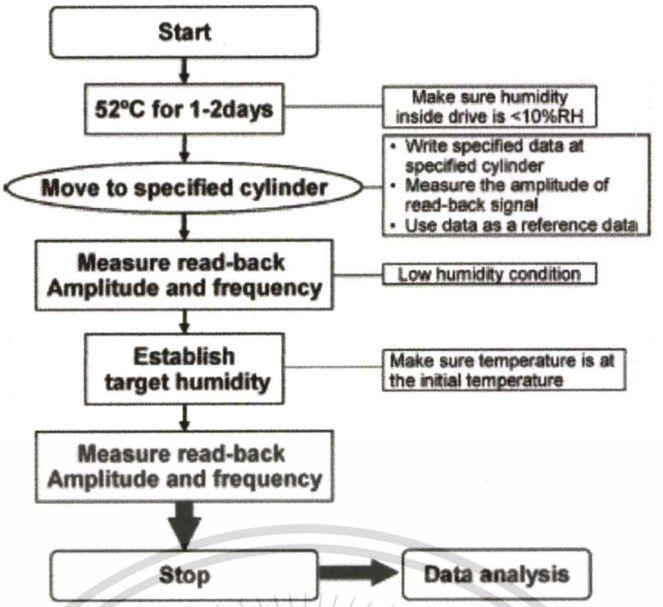

Fig. 1.9 Sequence of events of measuring flying height change due to humidity change [5]

The magnetic recording spacing changes were obtained from measurements of the read signal amplitude following the Wallace expression for the separation loss. Hard disk drive was mounted in an environmental chamber and controlled by computer via Advance Technology Attachment communication interface. Fig 1.10 is typical read-back amplitude change during humidity increase from 6% to 67%RH. The humidity is increased from 6%-67%RH, the read signal amplitude increased from 128 to 138mV, corresponding to a decrease in magnetic spacing of 2.0 nm.

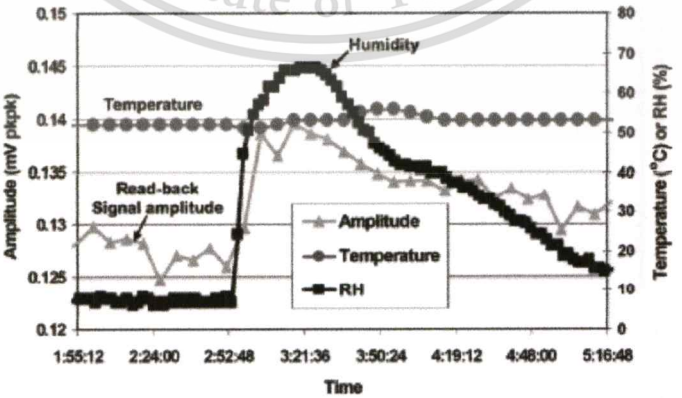

Fig. 1.10 Typical read-back amplitude change during humidity increase from 6% to 67% RH at fixed temperature of 52°C [5]

This material is reserved for educational use only, not allowed for commercial use.
Forbidden to modify the content, and cite the document when use.

They are using a magnetic recording system and qualified the effect of condensation on flying height by measuring the dependence of magnetic spacing on relative humidity and more clarify in the theory and experimental on Flying with vapor condensation on air-filled hard disk drive.

Liu, N., et al [6] studied on thermal flying-height control sliders in hard disk drives filled with air-helium gas mixtures. Reynolds equation was obtained to solve the pressure on the slider's ABS together with the slider disk spacing. Then detailed the structure of the slider's heating element and read-write transducer were modeled and the slider's thermal protrusion is calculated by the finite element method with pressure and heat flux on the ABS as boundary conditions.

Fig 1.11 showed the read-write transducer's FH as a function of friction of helium in the gas mixture (α) when the heating element is turned off without any power supply. When the α is very small, the mean free path and the viscosity is increased that effect to the slider's FH. Those two effects partially offset of each other. As α increase then the mean free path increase faster than the viscosity.

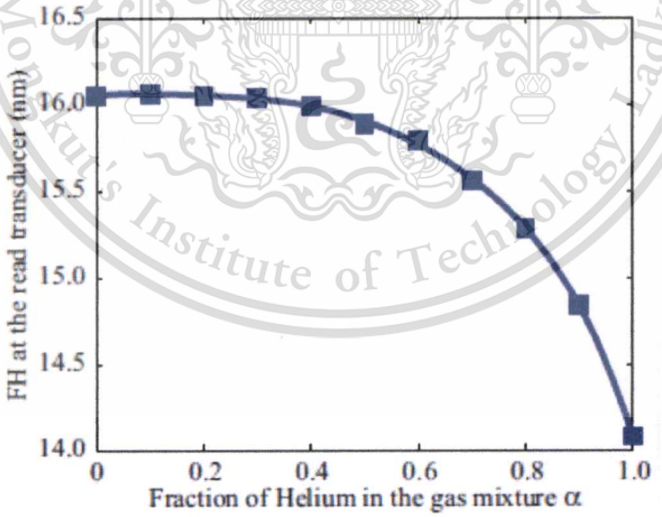

Fig 1.11 The transducer's FH as a function of α when the heating element is turned off [6]

The slider's deformation when the power is applied to the heating element due to the gas pressure on the ABS is negligible and the heat dissipation on the ABS due

This material is reserved for educational use only, not allowed for commercial use.
Forbidden to modify the content, and cite the document when use.

to the gas flow in the hard disk interface (HDI) dominants the change in the slider's deformation with the α.

From the numerical results, the heat dissipation is only significant near the read-write transducer, the local mean free path which is inversely proportional to the local pressure, is on the order of the local flying height (FH). Fig 1.12 showed the thermal conductivity is increase with α then more heat dissipated from the ABS at the given heat power and the maximum temperature rise on the ABS decreases which result in the slider's protrusion decreasing with α.

The FH loss is defined as the difference between the slider's FH without heater power and that when the heating element in turned on. In summary, the performance of thermal flying-height control slider in hard disk drive filled with air-helium mixture is investigated. The thermal conductivity dominates when the α is small, resulting in an increase in the slider's FH.

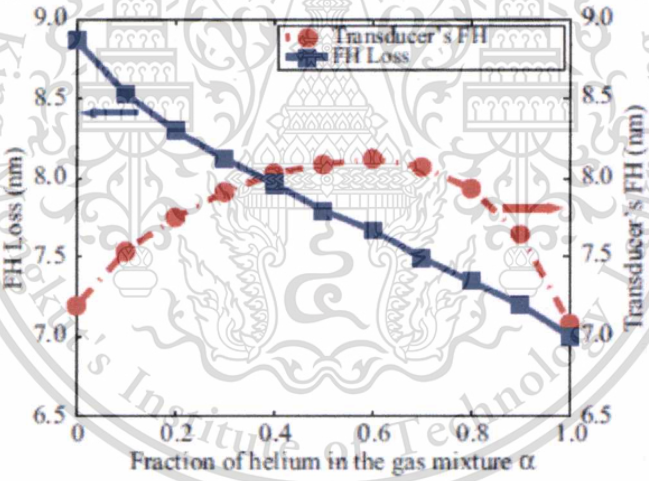

Fig 1.12 Transducer's FH and corresponding FH loss at the different α [6]

Zhou W, and et al [7] studied on the effects of environmental temperature and humidity on thermal flying height adjustment, the couple-filed analysis is applied for this study which included a thermal-structure finite element model to investigate the flying height (FH) change of thermal actuated slider at various environmental conditions. The water vapor's contribution is explained for air bearing pressure loss and a new humidity model is proposed to calculate this pressure loss. The environmental temperature effects and the humidity have significant effects on slider's FH change but their effects on the thermal protrusion height are limited.

This material is reserved for educational use only, not allowed for commercial use.
Forbidden to modify the content, and cite the document when use.

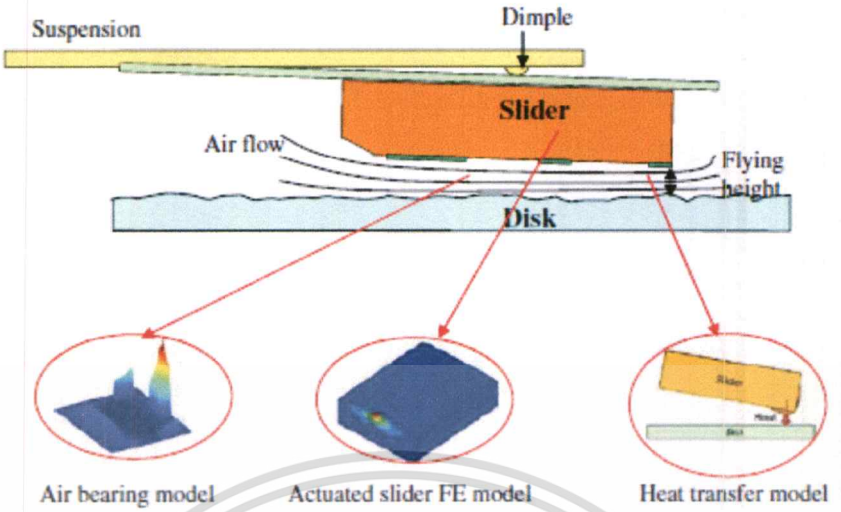

Fig 1.13 Diagram of coupled-filed analysis method [7]

The diagram of coupled-filed analysis method for this study showed in Fig 1.13. The ABS design has a significant effect on thermal actuation performance, per Fig 1.14, the pressure distribution for slider in left hand side has high pressure peak at the location of the head element while the pressure peak for slider in right hand side is move away from the head element and the air pressure on the location of head element is dramatically reduced. The heat from dissipated through the air bearing is prevented from this arrangement and also reduces FH push-back effect.

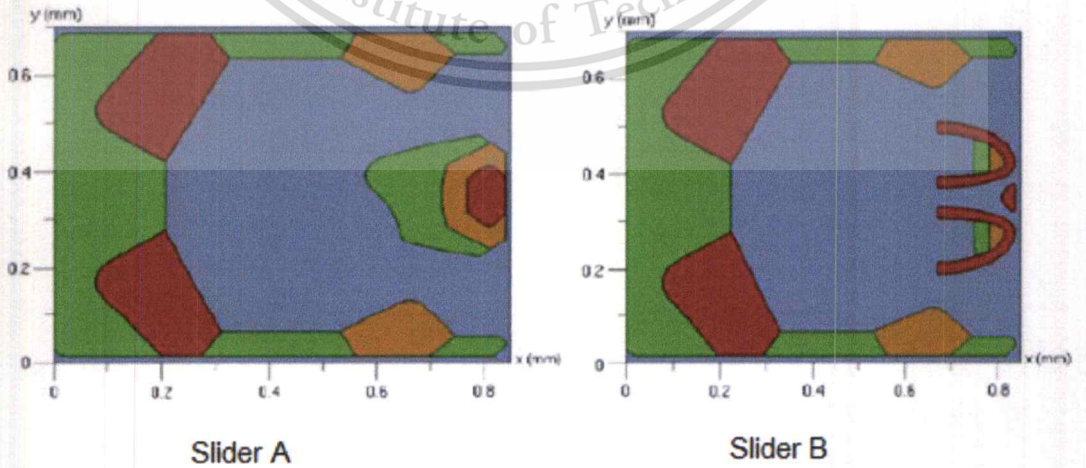

Fig 1.14 ABS design of two thermal actuated sliders [7]

This material is reserved for educational use only, not allowed for commercial use.
Forbidden to modify the content, and cite the document when use.

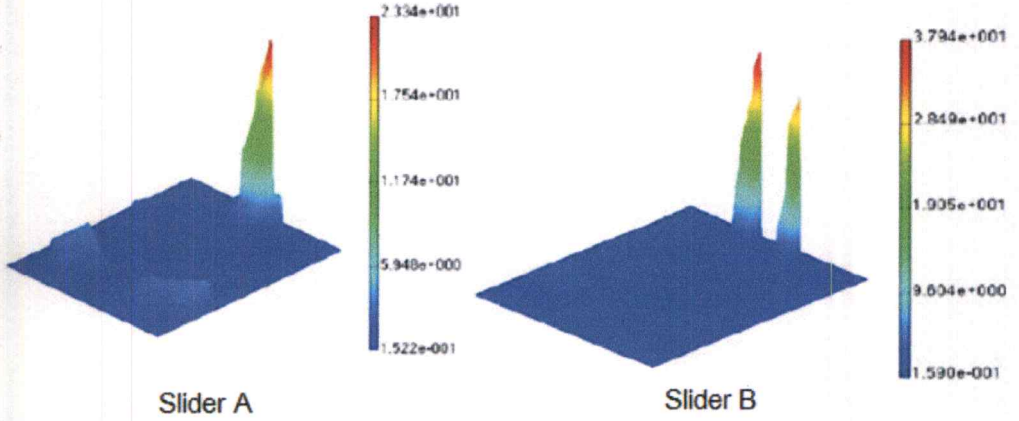

Fig 1.15 Pressure profile of two thermal actuated sliders [7]

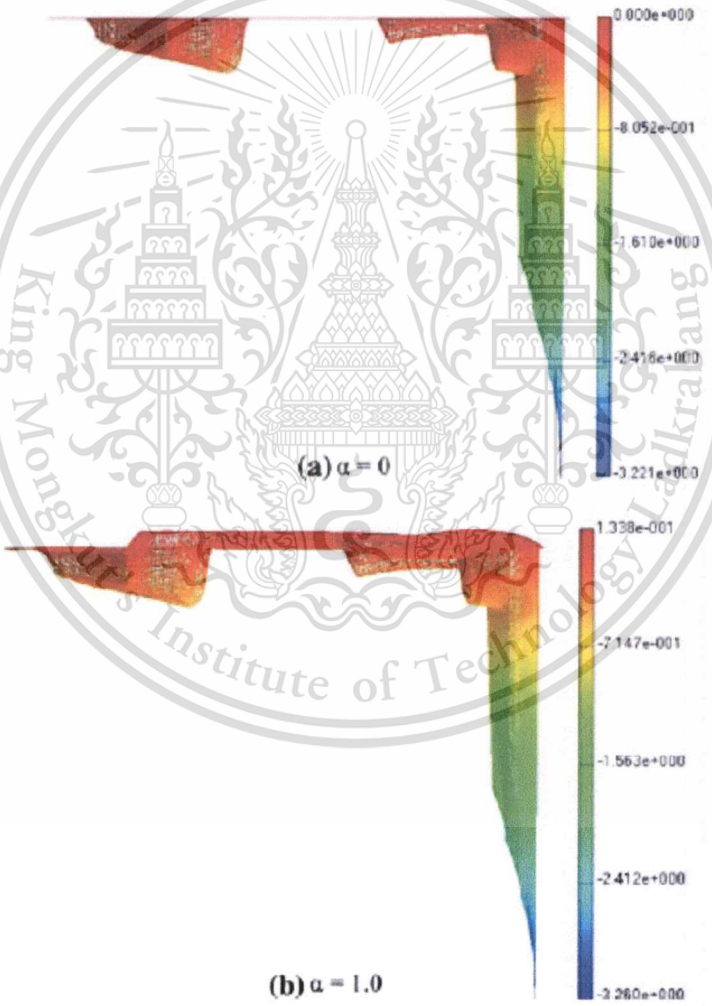

Fig 1.16 Pressure loss at 60°C and 80%RH for slider A [7]

The pressure distribution change in humid air is showed in Fig 1.16, when the ratio of absorb water vapor to the condensed (α) is difference. The pressure drop in the positive pressure (air bearing pressure greater than atmosphere pressure) region

This material is reserved for educational use only, not allowed for commercial use.
Forbidden to modify the content, and cite the document when use.

in both cases look quite similar no matter whether water vapor is condensed (α =0.0) or absorbed (α =1.0) on the disk surface.

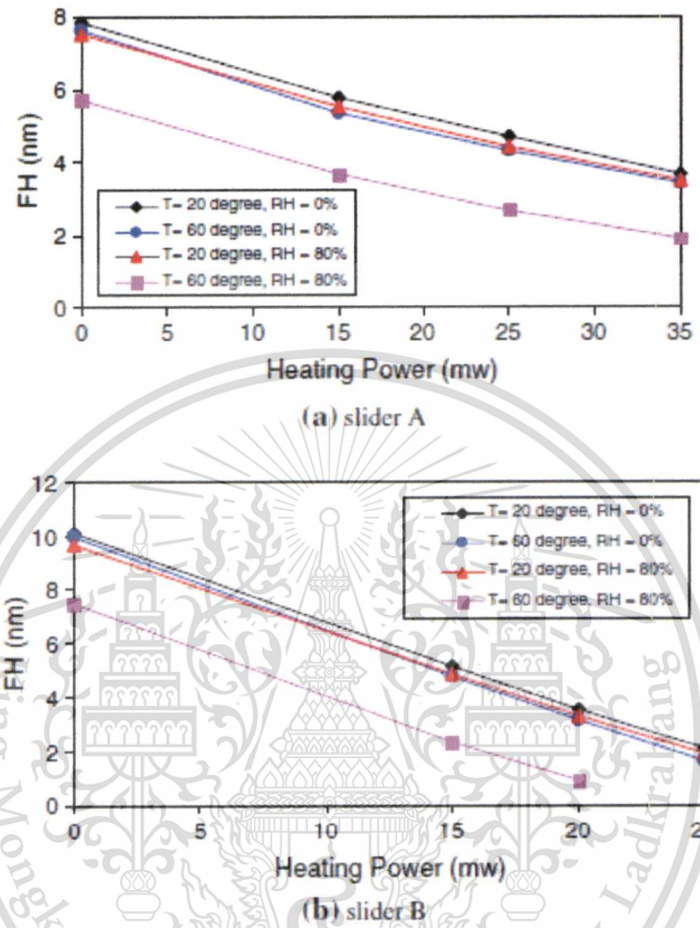

Fig 1.17 Flying height vs heat power [7]

The flying height changes are shown in Fig 1.17 with the various heat power and environmental conditions for slider A and slider B respectively. The relationship is linear between the thermal protrusion and the heat power. The variation of protrusion height due to the environmental temperature and humidity is also not big because the increased mean free path of air at the high environmental temperature will decrease the heat flux from the slider to the disk to create more thermal protrusion.

The variation of gap FH with environmental temperature and RH at heater power of 15mW of slider A and slider B is shown in Fig 1.18. FH has a little changed with environmental temperature from 20°C to 80°C at RH is zero for both sliders while the FH is reduced with high RH.

This material is reserved for educational use only, not allowed for commercial use.
Forbidden to modify the content, and cite the document when use.

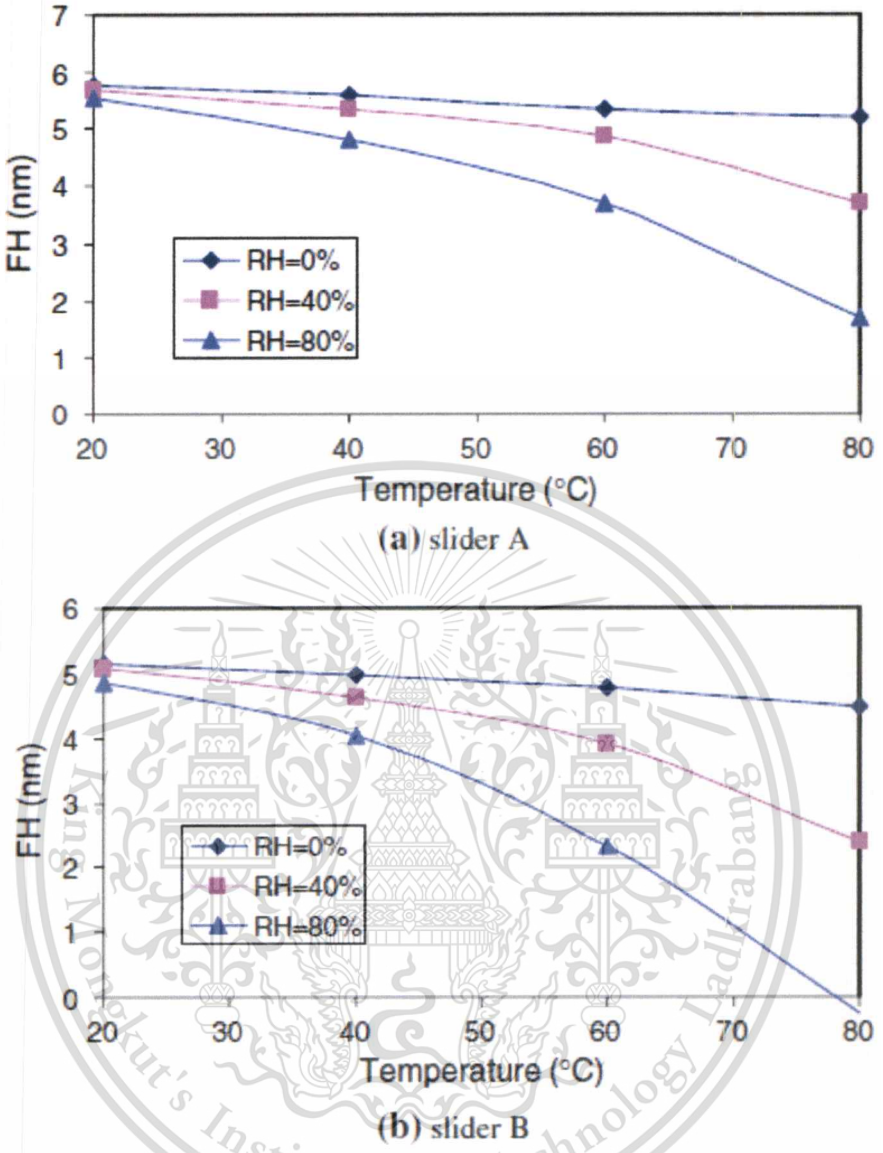

Fig 1.18 Flying height vs environmental temperature [7]

This material is reserved for educational use only, not allowed for commercial use.
Forbidden to modify the content, and cite the document when use.

1.3 The Objective

The main objective of this thesis is to study the flying height characteristic of the slider head with helium-filled drive and air-filled drive by obtaining the modified Reynolds equation and solve numerically by using the finite difference technique and develop computer program to simulate the flying height characteristic of the slider head with various of disk velocity, loading force and temperatures.

1.4 Hypothesis of Research

The Reyolds equation without molecular slip flow conditions is not adequate because the flying height is very low. Therefore, the air films in the self-acting flat air bearing are assumed as the molecular slip flow condition and summary of assumptions are:

1) Surface between slider head and disk surface is flat
2) Newtonian fluid and steady state laminar flow
3) Viscosity is constant
4) Operating temperature is stable
5) Surface tension is neglected
6) Ideal gas
7) Inertia of fluid and gravity are neglected
8) The film thickness is very small when compare with slider head's size
9) Molecular slip flow condition

1.5 Conceptual of Research

To obtain the film pressure distribution between the slider head and the disk surface, applied the modified Reynolds equation and equilibrium conditions. The finite difference method and Newton Raphson technique applied for numerical. Computer program was developed by using FORTRAN language to simulate the flying height characteristic of the flat slider head. The study is on the several of disk velocity, loading force and the temperature of operating.

This material is reserved for educational use only, not allowed for commercial use.
Forbidden to modify the content, and cite the document when use.

สำนักหอสมุดกลาง พระจอมเกล้าลาดกระบัง

1.6 Scope of Research

In this thesis, we studied and focused on the characteristic of flying height in helium- filled drive compared with air-filled drive when the disk velocity, loading force and temperature are changed, just only under static condition. The numerical simulation was obtained in terms of the pressure distribution and the flying height. The scopes of this study are as follow.

1) This study will be focus on flying height characteristic which is different on the disk velocity, loading force and temperature

2) The computer program is developed from the modified Reynolds equation and solves numerically using finite different technique only

This study was expected to see the characteristic of the helium-filled drives is good more that the air-filled drive which same condition.

1.7 Research methodology

This study has been conducted according to the following step:

1) Review literature with related to this topic
2) Studied in the lubrication theory especially the flying height characteristic of slider head and the flying height parameters
3) Finite difference method and Newton Raphson techniques for numerical calculation have been studied
4) Applied the Newton Raphson, and Multrigrid method to obtain the flying height characteristic of slider head with smooth surface
5) Develop computer program with FORTRAN language to solve the static characteristic and the pressure distribution
6) Analyzed simulation result of the static characteristic and the pressure distribution

This material is reserved for educational use only, not allowed for commercial use.
76519
Forbidden to modify the content, and cite the document when use.

CHAPTER 2

MEGNETIC RECORDING DEVICE

2.1 History of the Hard Disk Drive

In magnetic recording technology, the hard disk drive (HDD) is one technology which developed over the past five decades. Tracking back to the early 1950s, IBM invented the first group of 50 aluminum disks (61 cm in diameter each), turning at 3600 revolutions per minute and coated with a fine magnetic layer. This disk could store up to 5 million characters or 5 megabytes with a transfer rate of 8.8 Kbps, weighing more than a ton. [8] The development and investigation of hard disk drives continues until now. Many models of hard disk drives have been introduced to market and the more storage capacity expanded to serve to demand. With the increase of high areal density in the hard disk drive, the one parameter that required improvement is the physical spacing between the read/write element and the disk surface (we call this "flying height, FH").

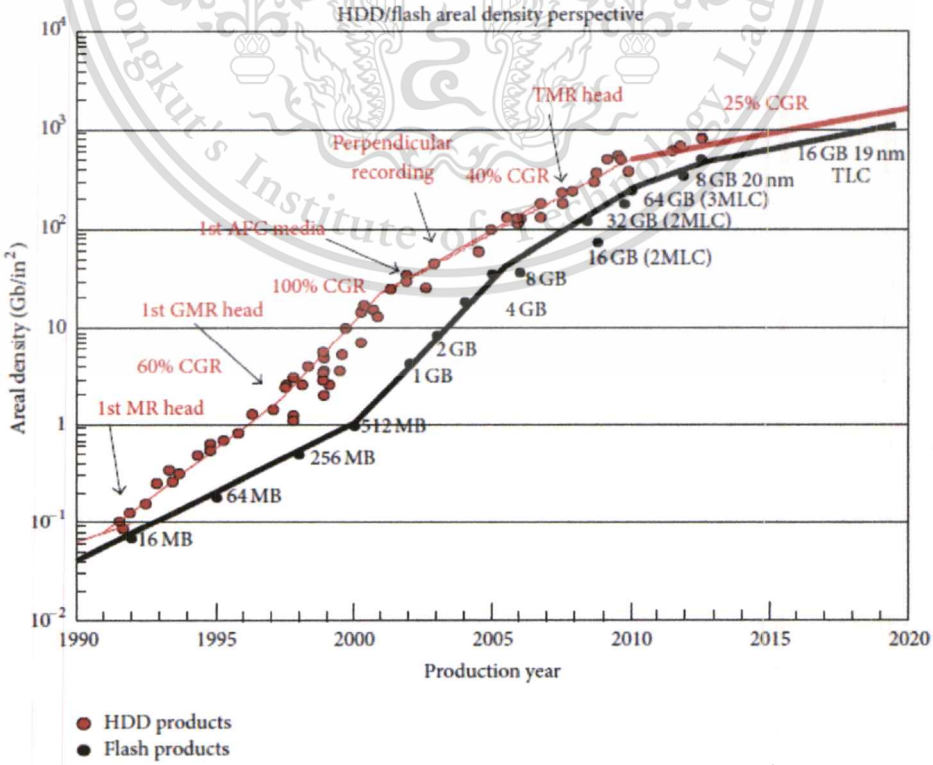

Fig 2.1 Areal Density evolution of HDD and flash memory [9]

This material is reserved for educational use only, not allowed for commercial use.
Forbidden to modify the content, and cite the document when use.

Fig 2.1 shows the areal density evolution of HDD and flash memory over 30 years. The areal density of the hard disk drive continues to increase. In 2015 the target for maximum areal density is 1000 GB/in^2 with 25% of the cumulative annual growth rate (CGR).

2.2 Construction and Operational Overview of the Hard Disk

The hard disk drive is the most important and yet the most mysterious part of a computer system. A hard disk drive is a sealed unit that a PC uses for nonvolatile data storage. Nonvolatile, or semi-permanent, storage means that the storage device retains the data even when no power is supplied to the computer. Because the hard disk drive is expected to retain data until deliberately erased or overwritten, the hard drive is used to store crucial programming and data. As a result, when the hard disk fails, the consequences are usually very serious. To maintain, service, and upgrade a PC system properly, you must understand how the hard disk functions.

A hard disk drive contains rigid, disk-shaped platters, usually constructed of aluminum or glass (see Fig. 2.2). Unlike floppy disks, the platters cannot bend or flex—hence the term hard disk. In most hard disk drives, you cannot remove the platters, which is sometimes called fixed disk drives. Removable hard disk drives are also available. Sometimes this term refers to a device in which the entire drive unit (that is, the disk and the drive) is removable, but it is more commonly used to refer to cartridge drives, where the platters are contained in a removable cartridge.

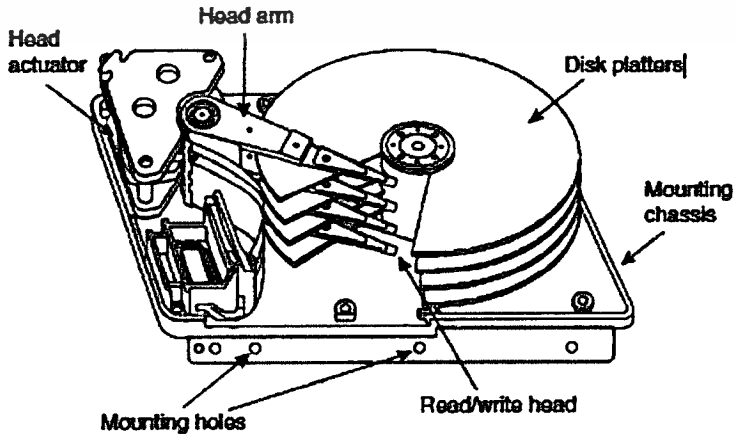

Fig 2.2 Hard disk heads and platters [10]

This material is reserved for educational use only, not allowed for commercial use.
Forbidden to modify the content, and cite the document when use.

The basic physical construction of a hard disk drive consists of spinning disks with heads that move over the disks and store data in tracks and sectors. The heads read and write data in concentric rings called tracks, which are divided into segments called sectors, which normally store 512 bytes each.

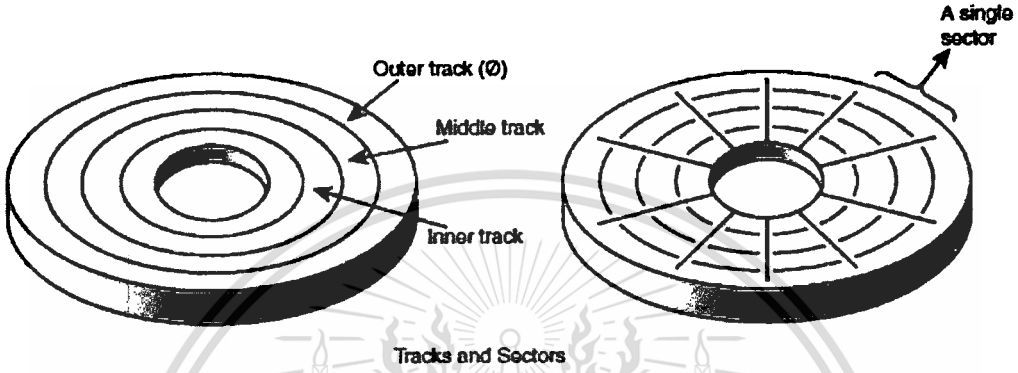

Fig 2.3 The tracks and sectors on a disk [11]

Hard disk drives usually have multiple disks, called platters, that are stacked on top of each other and spin in unison, each with two sides on which the drive stores data. Most drives have two or three platters, resulting in four or six sides, but some PC hard disks have up to 12 platters and 24 sides with 24 heads to read them (Seagate Barracuda 180). The identically aligned tracks on each side of every platter together make up a cylinder (see Fig 2.3). A hard disk drive normally has one head per platter side, with all the heads mounted on a common carrier device or rack. The heads move radically across the disk in unison; they cannot move independently because they are mounted on the same carrier or rack, called an actuator.

Originally, most hard disks spun at 3,600rpm—approximately 10 times faster than a floppy disk drive. For many years, 3,600rpm was pretty much a constant among hard drives. Now, however, most drives spin the disks even faster. While speeds can vary, most modern drives spin the platters at 4,200; 5,400; 7,200; 10,000; or 15,000rpm. High rotational speeds combined with a fast head-positioning mechanism and more sectors per track are what make one hard disk faster than another.

This material is reserved for educational use only, not allowed for commercial use.
Forbidden to modify the content, and cite the document when use.

The heads in most hard disk drives do not (and should not!) touch the platters during normal operation. When the heads are powered off, however, in most drives they land on the ramps as they stop spinning. While the drive is running, a very thin cushion of air keeps each head suspended a short distance above or below the platter. If the air cushion is disturbed by a particle of dust or a shock, the head can come into contact with the platter while it is spinning at full speed. When contact with the spinning platters is forceful enough to do damage, the event is called a head crash. The result of a head crash can be anything from a few lost bytes of data to a completely ruined drive. Most drives have special lubricants on the platters and hardened surfaces that can withstand the daily "takeoffs and landings" as well as more severe abuse.

Many types of hard disk drives are on the market, but nearly all share the same basic physical components. Some differences might exist in the implementation of these components (and in the quality of the materials used to make them), but the operational characteristics of most drives are similar. The basic components of a typical hard disk drive are as follows: The platters, spindle motor, heads, and head actuator mechanisms usually are contained in a sealed chamber called the head disk assembly (HDA). The HDA is usually treated as a single component; it is rarely opened. Other parts external to the drive's HDA, such as the logic boards, bezel, and other configuration or mounting hardware, can be disassembled from the drive.

This material is reserved for educational use only, not allowed for commercial use.
Forbidden to modify the content, and cite the document when use.

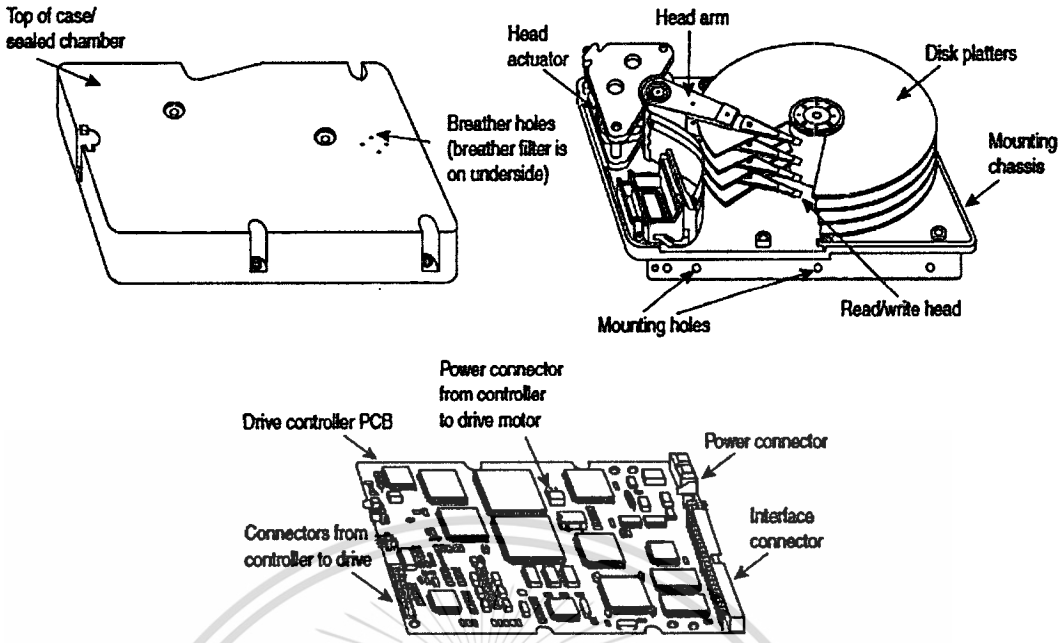

Fig 2.4 Typical hard disk drive components [11]

2.3 Read/Write Heads

A hard disk drive usually has one read/write head for each platter surface (meaning that each platter has two sets of read/write heads—one for the top side and one for the bottom side). These heads are connected, or ganged, on a single movement mechanism. The heads, therefore, move across the platters in unison. Mechanically, read/write heads are simple. Each head is on an actuator arm that is spring-loaded to force the head into contact with a platter. Few people realize that each platter actually is "squeezed" by the heads above and below it. If you could open a drive safely and lift the top head with your finger, the head would snap back down into the platter when you released it. If you could pull down on one of the heads below a platter, the spring tension would cause it to snap back up into the platter when you released it.

This material is reserved for educational use only, not allowed for commercial use.
Forbidden to modify the content, and cite the document when use.

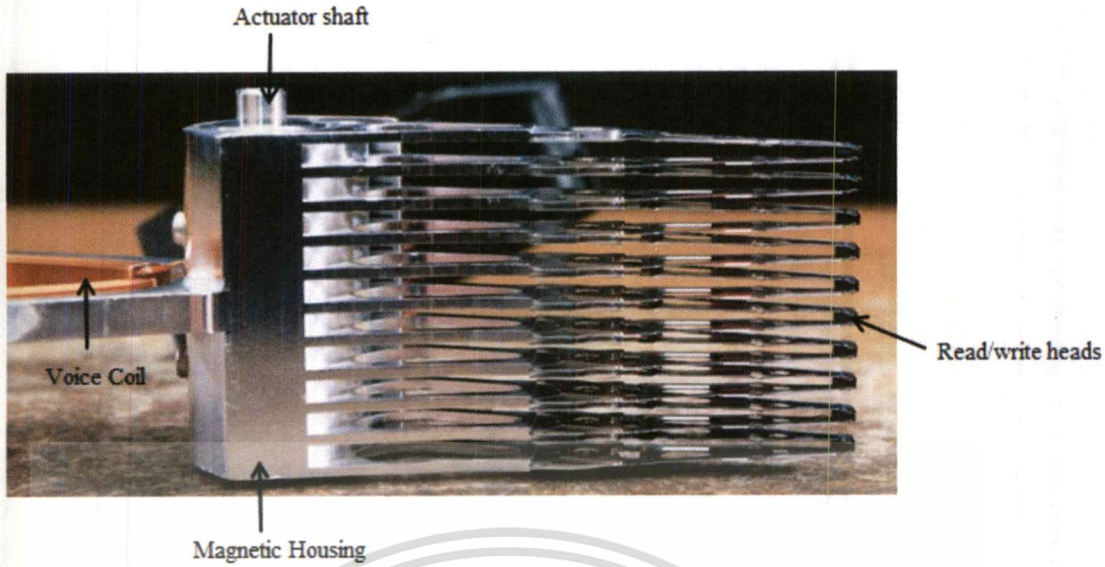

Fig 2.5 Read/Write heads and rotary voice coil actuator assembly [12]

In the early 1960s, hard disk drive recording heads operated at floating heights as large as 200–300 $\mu-inch$; today's drive heads are designed to float as low as 10nm (nanometers) or 0.4 $\mu-inch$ above the surface of the disk. To support higher densities in future drives. The physical separation between the head and disk is expected to drop even further, such that on some drives there will even be contact with the platter surface. New media and head designs will make full or partial contact recording possible [11].

2.4 Floating Height/Flying Height/Head Gap

One distinguishing characteristic of hard disk technology that makes it different from how floppy disks, VCRs and tape decks work is the read/write heads do not make contact with the media. They float over the surface of the disk and do all of their work without ever physically touching the platters they are magnetizing. The amount of space between the heads and the platters is called the floating height or head gap. It is also sometimes called the flying height (which is less accurate because the heads are much more floating than they are flying).

The read/write heads are spring loaded with a weak spring that causes them to press against the platters when the disk is stationary. This is done to ensure that the heads don't drift away from the platters, to maintain an exact floating height is essential for correct operation. The high spin speed causes air to flow under the

This material is reserved for educational use only, not allowed for commercial use.
Forbidden to modify the content, and cite the document when use.

heads and lifts them off the surface of the disk when the disk spins up to operating speed. So the heads really float, they don't fly.

The height at which the heads float is a specific design parameter that is tightly controlled by the engineers that create the drive. The heads can't properly read and write the platter if the height is too great. If it is too small, there is increased chance of a head crash. To increasing areal density means that weaker magnetic fields must be used in storing data on the disks. When this is done the heads must be allowed to ride closer to the platter surface to pick up the weaker signals, which requires other quality improvements to the drive to make sure that there is no chance of a head crash.

Modern hard disks have a floating height of less than five millionths of an inch, with heights decreasing every year. Each time the floating height is decreased, the mechanical aspects of the disk must be adjusted to make sure that the platters are flatter, the alignment of the platter assembly and the read/write heads is perfect, and no dust or dirt is on the surface of the platters. Vibration and shock also become more of a concern, and must be compensated for.

It's actually quite amazing how close to the surface of the disks the heads fly without touching. To put it into perspective, a modern hard disk has a floating height of around three micro inches. A human hair has a thickness of over 2,000 micro inches. In fact, the floating height of a hard disk is smaller than the circuit size of a microprocessor. What's even more amazing is how much abuse these hard disks can take when they are placed in laptop PCs, for example, given these facts, and how much people take this technology for granted.

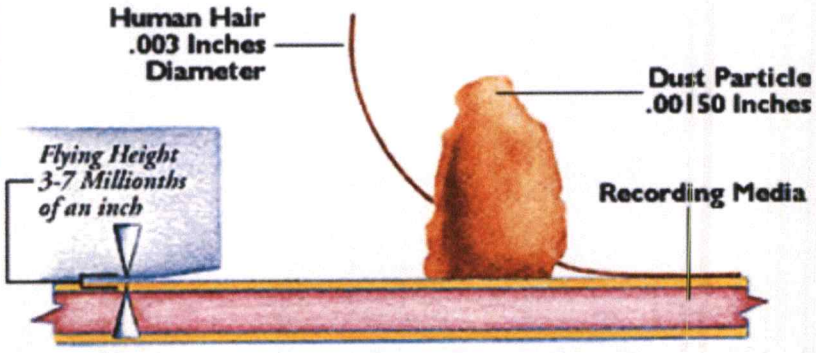

Fig 2.6 Comparison the flying height with human hair and dust particle [13]

This material is reserved for educational use only, not allowed for commercial use.
Forbidden to modify the content, and cite the document when use.

The magnetic fields are made smaller and weaker when the areal density of a drive is increased to improve capacity and performance. To compensate, either the heads must be made more sensitive, or the floating height must be decreased. Each time the floating height is decreased, the mechanical aspects of the disk must be adjusted to make sure that the platters are flatter, the alignment of the platter assembly and the read/write heads is perfect, and no dust or dirt on the surface of the platters. Vibration and shock also become more of a concern, and must be compensated for. This is one reason manufacturers are turning to smaller platters, as well as the use of glass platter substrates.

As the flying height of drives continues to decrease, hard disk engineers are recognizing that we may soon reach the point where it cannot be made any smaller without touching the patter surfaces. There is actually investigation about the possibility of going back to the concept of contact disks, where the head gap is intentionally made zero. This would allow even smaller magnetic fields than is possible in today's drives. Of course, this brings us full circle to the first hard disk experiments in the 1950s. The difference of course is almost 50 years of advances in technology. For example, thin film media is much tougher than the oxide media used on contact disks half a century ago and lubricating agents are much more advanced as well. Even so, it will probably be several years before we know if this technology will be feasible from both an engineering and manufacturing standpoint.

2.5 Hard Disk Head Sliders, Arms and Actuator

The hard disk platters are accessed for read and write operations using the read/write heads mounted on the top and bottom surfaces of each platter. Obviously, the read/write heads do not just float in space; they must be held in an exact position relative to the surfaces they are reading, and furthermore, they must be moved from track to track to allow access to the entire surface of the disk. The heads are mounted onto a structure that facilitates this process. Often called the head assembly or actuator assembly (or even the head-actuator assembly), it is comprised of several different parts.

This material is reserved for educational use only, not allowed for commercial use.
Forbidden to modify the content, and cite the document when use.

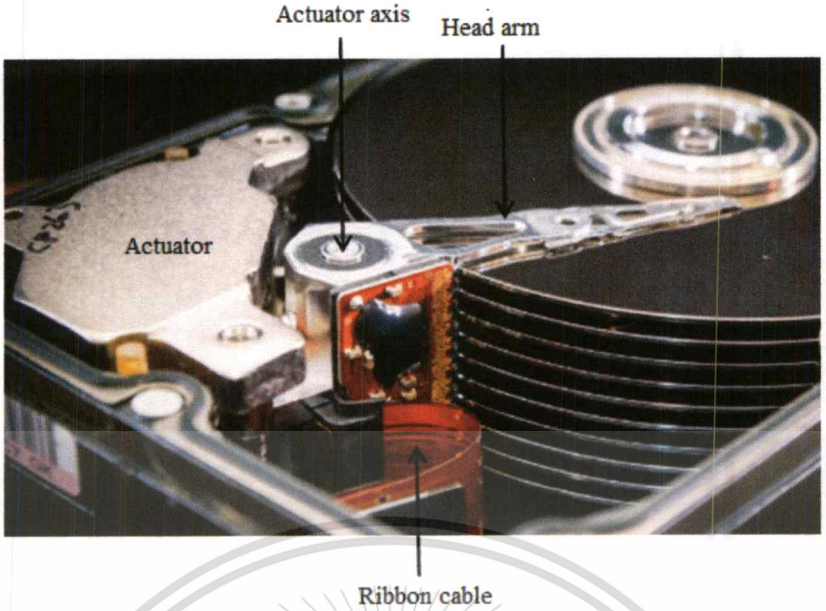

Fig 2.7 Annotated illustration of a typical PC actuator assembly showing the major components. [12]

Fig 2.7 the platters have been removed from the drive to provide a better view of the actuator arms and heads. There are four sliders but only one of each pair is visible. The spindle motor is visible at the top right.

The heads themselves are mounted on head sliders. The sliders are suspended over the surface of the disk at the ends of the head arms. The head arms are all mechanically fused into a single structure that is moved around the surface of the disk by the actuator. It would be an understatement to say that these components are neglected; most people do not even know they exist. Yet they play an important role in the function and performance of the drive. In particular, advances in slider, arm and actuator design are critical to improving the seek time of a hard disk; the impact that the actuator has on performance is discussed in this section.

This section discusses the sliders, arms and actuator of the modern disk drive, as well as explaining the operation of disk drive servo mechanisms and related technologies.

2.5.1 Head Sliders

Hard disk read/write heads are too small to be used without attaching them to a larger unit. This is especially true of modern hard disk heads. Each hard disk head is therefore mounted to a special device called a head slider or just slider for short.

This thesis is reserved for educational use only, not allowed for commercial use.
Forbidden to modify the content, and cite the document when use.

The function of the slider is to physically support the head and hold it in the correct position relative to the platter as the head floats over its surface.

Fig 2.8 Illustration of head slider [14]

Fig 2.8 shown Illustration of head slider that given a special shape to allow them to ride precisely over the platter. Usually they are shaped somewhat like a sled; there are two rails or runners on the outside that support the slider at the correct flying height over the surface of the disk, and in the middle the read/write head itself is mounted, possibly on another rail.

As hard disk read/write heads have been shrinking in size, so have the sliders that carry them. The main advantage of using small sliders is that it reduces the weight that must be yanked around the surface of the platters, improving both positioning speed and accuracy. Smaller sliders also have less surface area to potentially contact the surface of the disk.

The hard disk industry has given names to various generations of slider technology. When the design was first reduced to 50% of the size of the first hard disk sliders, someone decided to call it the nano-slider, where "nano" is the prefix denoting "one billionth". Of course the name is silly, since the sliders have not shrunk by even a factor of 10. The newest sliders have been shrunk from the "nano" size by about another 50% and are being called pico-sliders, which in this author's opinion is an equally silly name, and for the same reason.)

This material is reserved for educational use only, not allowed for commercial use.
Forbidden to modify the content, and cite the document when use.

Each slider is mounted onto a head arm to allow it to be moved over the surface of the platter to which it is mated.

2.5.2 Head Arms

According to figure 2.11, the arm is not solid, but rather has a structural triangular shape. This is done to reduce weight while maintaining rigidity.

Fig 2.9 The head arm of a typical recent-design hard drive [14]

The head arms are thin pieces of metal, usually triangular in shape onto which the head sliders (carrying the read/write heads) are mounted. In a way, the idea here is similar to how the arm of a phonograph is used to move the stylus from the outside of a record to the inside (the similarity ends there). There is one arm per read/write head, and all of them are lined up and mounted to the head actuator to form a single unit. This means that when the actuator moves, all of the heads move together in a synchronized fashion. Heads cannot be individually sent to different track numbers.

The arms themselves are made of a lightweight, thin material, to allow them to be moved rapidly from the inner to outer parts of the drive. Newer designs have replaced solid arms with structural shapes in order to reduce weight and improve performance. This is the same technique used to reduce weight in the construction of airplane wings, for example. Newer drives achieve faster seek times in part by using faster and smarter actuators and lighter, more rigid head arms, allowing the time to switch between tracks to be reduced.

A recent trend in the hard disk industry has been the reduction in the number of platters in various drive families. Even some "flagship" drives in various families now

This material is reserved for educational use only, not allowed for commercial use.
Forbidden to modify the content, and cite the document when use.

only have three or even two platters, where four or five was commonplace a year or so ago. One reason for this trend is that having a large number of head arms makes it difficult to make the drive with high enough precision to permit very fast positioning (on random seeks). This is due to increased weight in the actuator assembly from the extra arms, and also problems aligning all the heads. So in essence, this is a tradeoff that some drive manufacturers are making to improve performance at the expense of capacity. With drive densities now at 20 GB per platter and bound to increase, this is an acceptable design decision for most buyers.

2.5.3 Head Actuator

The actuator is the device used to position the head arms to different tracks on the surface of the platter (actually, to different cylinders, since all head arms are moved as a synchronous unit, so each arm moves to the same track number of its respective surface). The actuator is a very important part of the hard disk, because changing from track to track is the only operation on the hard disk that requires active movement: changing heads is an electronic function, and changing sectors involves waiting for the right sector number to spin around and come under the head (passive movement). Changing tracks means the heads must be shifted, and so making sure this movement can be done quickly and accurately is of paramount importance. This is especially so because physical motion is so slow compared to anything electronic--typically a factor of 1,000 times slower or more. Head actuators come in two general varieties:

Stepper Motors: Originally, hard disk drives used a stepper motor to control the movement of the heads over the surface of the platters. A regular motor turns in a rotary fashion continuously; it can stop at any point in its rotation as it spins around, kind of like the second hand on a wind-up wristwatch. A stepper motor can only stop at predefined "steps" as it turns around, much the way the second hand turns on an electronic, quartz wristwatch. A hard drive using a stepper motor for an actuator attaches the arms to the motor, and each time the motor steps one position clockwise or counterclockwise, the arms move in or out one position. Each position defines a track on the surface of the disk. Stepper motors are also commonly used for both turning the spindle and positioning the head on floppy disk

This material is reserved for educational use only, not allowed for commercial use.
Forbidden to modify the content, and cite the document when use.

drives. If you have a floppy drive, find one of its motors and turn it slowly with your hand; you will feel the discrete step-wise nature of its motion.

Fig 2.10 shows the motor moves in steps, which you can feel if you move the motor shaft by hand. The shaft has two thin strips of metal wrapped around it, which are connected to a pivot that is rigidly attached to the actuator arms. As the motor shaft turns, one half of this "split band" coils onto the shaft and the other half uncoils. When the motor turns in the opposite direction, the process reverses. As this occurs, the pivot moves and in doing so, moves the actuator arms and the hard disk heads.

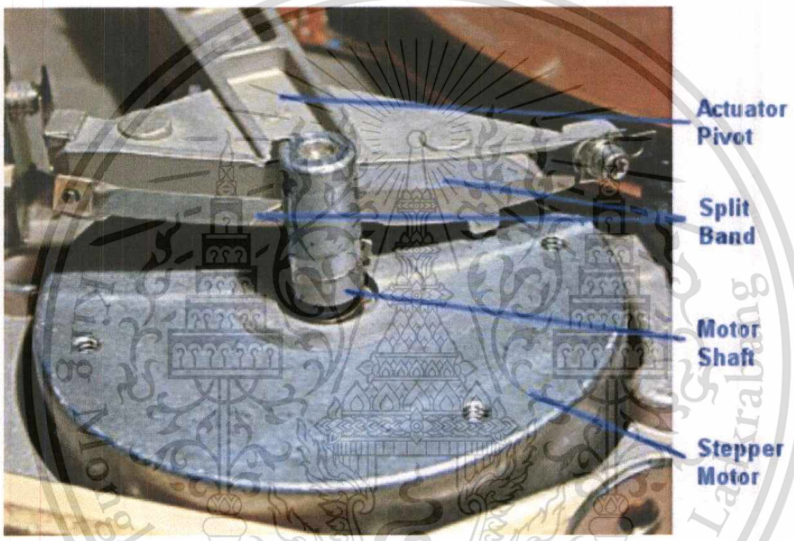

Fig 2.10 A stepper motor actuator [15]

2.5.4 Voice Coils

The actuator in a modern hard disk uses a device called a voice coil to move the head arms in and out over the surface of the platters, and a closed-loop feedback system called a servo system to dynamically position the heads directly over the data tracks. The voice coil works by using electromagnetic attraction and repulsion. A coil is wrapped around a metal protrusion on the end of the set of head arms. This is mounted within an assembly containing a strong permanent magnet. When current is fed to the coil, an electromagnetic field is generated that causes the heads to move in one direction or the other based on attraction or repulsion relative to the permanent magnet. By controlling the current, the heads can be told to move in or out much more precisely than using a stepper motor. The name "voice coil" comes

This material is reserved for educational use only, not allowed for commercial use.
Forbidden to modify the content, and cite the document when use.

from the resemblance of this technology to that used to drive audio speakers, which are also basically electromagnets. All PC hard disk voice coil actuators are rotary, meaning that the actuator changes position by rotating on an axis.

In fig 2.11, the magnet assembly has been unscrewed from its mounting and pulled to the left to expose the coil. The magnet assembly consists of two metal plates (top one easily visible above, and part of the bottom one visible.) The magnet itself is mounted on the underside of the top plate, and spacers used between the plates to create the gap for the coil assembly. Being non-ferrous, the coil moves freely between the plates, rotating the actuator on its axis as its magnetic polarity is changed. (Incidentally, the magnet is strong enough that after removing the spacers between the plates, the bottom plate got "stuck" on the magnet and required considerable effort to remove.)

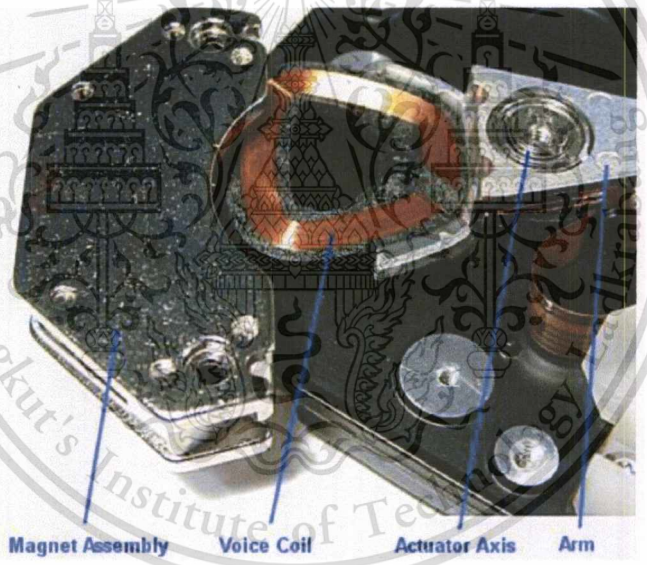

Fig 2.11 A partially-disassembled voice coil actuator [15]

The primary distinction between the two designs is that the stepper motor is an absolute positioning system, while the voice coil is a relative positioning system. Commands given to a stepper motor actuator are generally of the form "Go in this direction to position A, where you'll find item B". Commands to a voice coil actuator are of the form "Go in this direction until you find item B". Consider this analogy. In your backyard you have buried a "secret treasure" and want to tell a friend where to find it. When you buried it, you walked down a path 139 paces to the fourth oak tree, and buried it at the edge of the path. The stepper motor analog would be to

This material is reserved for educational use only, not allowed for commercial use.
Forbidden to modify the content, and cite the document when use.

tell your friend to walk 139 paces down the path, and start digging. The voice coil analog would be to tell him to look for the fourth oak tree and dig there. Obviously, using the "139 paces" method, your friend has a problem: his paces aren't likely to be the same length as yours. In fact, even if you yourself walked out 139 paces twice, you'd probably end up in very different spots, since a "pace" isn't an accurate or repeatable measure. On the other hand, the fourth oak tree will always be the fourth oak tree (barring disastrous chain-saw activity).

Now hard disks of course don't have to use inaccurate measures like "paces", and it's always the same stepper motor accessing the disk, not a "friend", so why is saying "track #139" a big problem? For starters, motors change their characteristics over time, and after a year or two positions #139 might not be where it was when the drive was first formatted. However, they have an even more serious problem: disk components (the platters and the head arms themselves especially) expand and contract with heat. Even if a stepper motor was perfect, it could not properly account for the fact that the disks are changing in size, and therefore, the tracks are literally moving around. If you consider our backyard analogy and think about what it would be like if the oak tree moved a few feet closer to or further from the house based on the day's temperature, you start to realize how inadequate absolute positioning of this form can be.

A stepper motor has no way to compensate for expansion or contraction of the disk: all it can do is go to where "track #139" is supposed to be, and hope it finds it there. If it does not find it because the motor and the disk have become out of sync, errors and data loss result. This is why older disks were so sensitive to temperature, and normally had to be low-level formatted periodically to make sure the tracks lined up with the heads properly. This is also why many drives would fail when first powered up after a weekend, but would work properly after the drive had been allowed to warm up.

The shortcomings of stepper motors were unfortunate but acceptable with old hard disks, because of their relatively low track density. To compensate, tracks could be written fairly wide so that the head would find them even if it was a bit misaligned. The first PC hard disks in 1982 had a track density of only two or three hundred tracks per inch (TPI). Even In 1986, the year Conner Peripherals introduced the first voice coil PC hard disk, density had increased to only about 1,000 TPI.

This material is reserved for educational use only, not allowed for commercial use.
Forbidden to modify the content, and cite the document when use.

Stepper motors are still used to drive floppy disks, for example, because the accuracy demands for floppies are much lower: a 1.44 MB floppy disk has a track density of 135 tracks per inch. In contrast, today's hard disks have densities as high as 30,000 tracks per inch. With data packed this densely, tracks are extremely thin, and a stepper motor lacks the accuracy and stability necessary for proper operation.

All modern hard disks use voice coil actuators. The voice coil actuator is not only far more adaptable and insensitive to thermal issues but also it is much faster and more reliable than a stepper motor. The actuator's positioning is dynamic and is based on feedback from examining the actual position of the tracks. This closed-loop feedback system is also sometimes called a servo motor or servo positioning system and is commonly used in thousands of different applications where precise positioning is important. There are several different ways that the servo positioning system is implemented in PCs; the servo's operation is discussed in its own section.

2.6 Hard Disk Spindle Motor

The spindle motor, also sometimes called the spindle shaft, is responsible for turning the hard disk platters, allowing the hard drive to operate. The spindle motor is sort of a "work horse" of the hard disk. It is not flashy, but it must provide stable, reliable and consistent turning power for thousands of hours of often continuous use, to allow the hard disk to function properly. In fact, many drive failures are actually failures with the spindle motor, not the data storage systems.

In figure 2.12, you can see that it attaches with three screws around its perimeter. The shiny metal is the shaft, which rotates; the dull metal is the base of the motor. The six small screw holes on the top of the shaft are for securing the platters. You can also see a large screw hole in the center top of the shaft, which is used to attach the top cover to the spindle shaft for added stability. The four wire connector attaches to the hard disk logic board.

This material is reserved for educational use only, not allowed for commercial use.
Forbidden to modify the content, and cite the document when use.

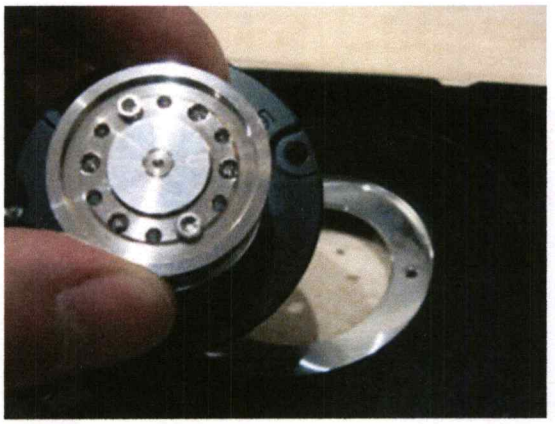

Fig 2.12 A hard disk spindle motor [16]

For many years all hard disks spun at the same speed. In the interests of performance, manufacturers have been steadily ratcheting up their products' spin speeds over the last few years. These higher-speed spindles often have issues related to the amount of heat and vibration they generate. The increased performance and also the new potential issues related to the spindle motor have given it renewed attention in the last few years.

2.7 Hard Disk Platters and Media

Every hard disk contains one or more flat disks that are used to actually hold the data in the drive. These disks are called platters (sometimes also "disks" or "discs"). They are composed of two main substances: a substrate material that forms the bulk of the platter and gives it structure and rigidity, and a magnetic media coating which actually holds the magnetic impulses that represent the data. Hard disks get their name from the rigidity of the platters used, as compared to floppy disks and other media which use flexible "platters" (actually, they aren't usually even called platters when the material is flexible.)

The platters are "where the action is"--this is where the data itself is recorded. For this reason the quality of the platters and particularly, their media coating, is critical. The surfaces of each platter are precision machined and treated to remove any imperfections, and the hard disk itself is assembled in a clean room to reduce the chances of any dirt or contamination getting onto the platters.

The size of the platters in the hard disk is the primary determinant of its overall physical dimensions, also generally called the drive's form factor; most drives are produced in one of the various standard hard disk form factors. Disks are sometimes

This material is reserved for educational use only, not allowed for commercial use.
Forbidden to modify the content, and cite the document when use.

referred to by a size specification; for example, someone will talk about having a "3.5-inch hard disk". When this terminology is used, it usually refers to the disk's form factor, and normally, the form factor is named based on the platter size. The platter size of the disk is usually the same for all drives of a given form factor, though not always, especially with the newest drives, as we will see below. Every platter in any specific hard disk has the same diameter.

The first PCs used hard disks that had a nominal size of 5.25". Today, by far the most common hard disk platter size in the PC world is 3.5". Actually, the platters of a 5.25" drive are 5.12" in diameter, and those of a 3.5" drive are 3.74"; but habits are habits and the "approximate" names are what are commonly used. You will also notice that these numbers correspond to the common sizes for floppy disks because they were designed to be mounted into the same drive bays in the case. Laptop drives are usually smaller, due to laptop manufacturers' never-ending quest for "lighter and smaller". The platters on these drives are usually 2.5" in diameter or less; 2.5" is the standard form factor, but drives with 1.8" and even 1.0" platters are becoming more common in mobile equipment.

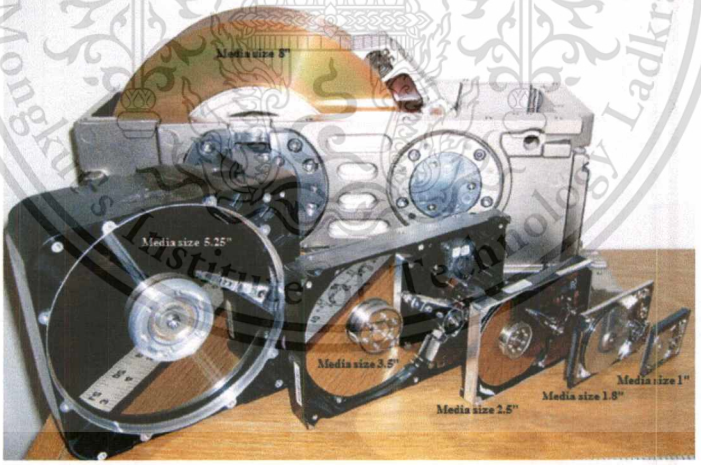

Fig 2.13 A platter form of a 8", 5.25", 3.5", 2.5", 1.8" and 1" [17]

Traditionally, drives extend the platters to as much of the width of the physical drive package as possible, to maximize the amount of storage they can pack into the drive. However, as discussed in the section on hard disk historical trends, the trend overall is towards smaller platters. This might seem counter-intuitive; after all, larger platters mean there is more room to store data,

This material is reserved for educational use only, not allowed for commercial use.
Forbidden to modify the content, and cite the document when use.

so should not it be more cost-effective for manufacturers to make platters as big as possible? There are several reasons why platters are shrinking, and they are primarily related to performance. The areal density of disks is increasing so quickly that the loss of capacity by going to smaller platters is viewed as not much of an issue--few people care when drives are doubling in size every year anyway!--while performance improvements continue to be at the top of nearly everyone's wish list. In fact, several hard disk manufacturers who were continuing to produce 5.25" drives for the "value segment" of the market as recently as 1999 have now discontinued them. (The very first hard disks were 24" in diameter, so you can see how far we have come in 40 or so years.)

This material is reserved for educational use only, not allowed for commercial use.
Forbidden to modify the content, and cite the document when use.

CHAPTER 3

THEORY

3.1 Reynolds Equation

Reynolds equation is the mathematical statement of the classical theory of lubrication. Physically, it can be thought of as an expression of conservation principles for a system made up of lubricant flow between two parallel surfaces. The modified Reynolds equation is established by combination between Navier-Stokes equation and Continuity equation under the assumptions as:

1. Rigid and smooth surface for air bearing and disk.
2. The lubricant property is Newtonian fluid.
3. The viscosity of the lubricant fluid is constant through film.
4. The flow of lubricant fluid is laminar flow.
5. Surface temperature of the head is equal across the head and constant.
6. Lubricate fluid is ideal gas.
7. Lubricate fluid is isothermal.
8. Negligible body force and inertia force because film thickness of fluid is very small
9. No slip condition at boundaries.

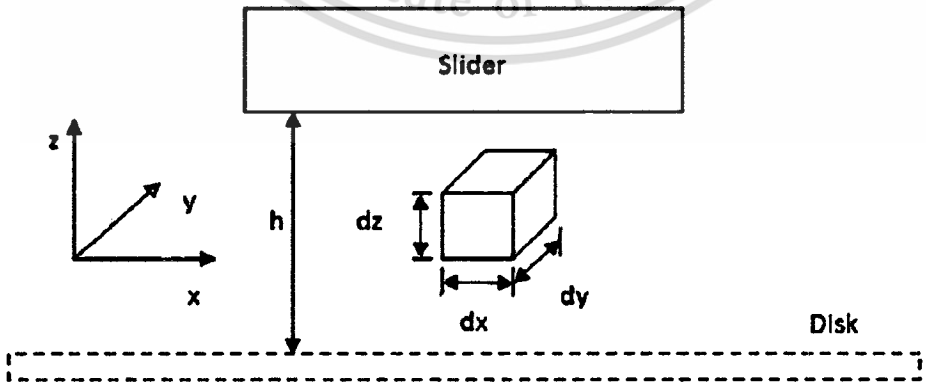

Fig 3.1 Cartesian coordinates of film thickness

This material is reserved for educational use only, not allowed for commercial use.
Forbidden to modify the content, and cite the document when use.

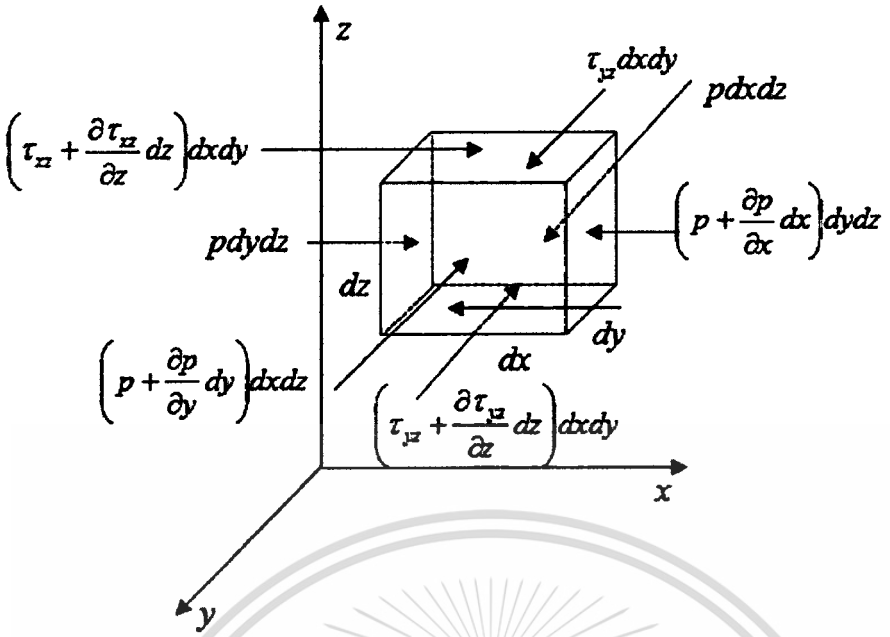

Fig 3.2 Equilibrium forces in Cartesian coordinates

From Fig 3.2, the equilibrium forces in x-direction ($\Sigma F_x = 0$)

$$pdzdy+\left(\tau_{xz}+\frac{\partial\tau_{xz}}{\partial z}dz\right)dxdy=\left(p+\frac{\partial p}{\partial x}dx\right)dydz+\tau_{xz}dxdy \tag{3.1}$$

$$\frac{\partial p}{\partial x}=\frac{\partial\tau_{xz}}{\partial z} \tag{3.2}$$

In y -direction, the equilibrium forces ($\Sigma F_y = 0$)

$$pdzdy+\left(\tau_{yz}+\frac{\partial\tau_{yz}}{\partial z}dz\right)dxdy=\left(p+\frac{\partial p}{\partial y}dy\right)dxdz+\tau_{yz}dxdy \tag{3.3}$$

$$\frac{\partial p}{\partial y}=\frac{\partial\tau_{yz}}{\partial z} \tag{3.4}$$

From Newton's law, the share stress is

$$\tau_{xz}=\mu\frac{\partial u}{\partial z} \tag{3.5}$$

$$\tau_{yz}=\mu\frac{\partial v}{\partial z} \tag{3.6}$$

This material is reserved for educational use only, not allowed for commercial use.
Forbidden to modify the content, and cite the document when use.

Substituting equation (3.5) into (3.2) and substituting equation (3.6) into (3.4) respectively

$$\begin{aligned}\frac{\partial p}{\partial x} &= \frac{\partial \tau_{xz}}{\partial z} \\ &= \frac{\partial}{\partial z}\left(\mu \frac{\partial u}{\partial z}\right) \\ &= \mu \frac{\partial^2 u}{\partial z^2}\end{aligned} \tag{3.7}$$

And,

$$\begin{aligned}\frac{\partial p}{\partial y} &= \frac{\partial \tau_{yz}}{\partial z} \\ &= \frac{\partial}{\partial z}\left(\mu \frac{\partial v}{\partial z}\right) \\ &= \mu \frac{\partial^2 v}{\partial z^2}\end{aligned} \tag{3.8}$$

Integrate (3.7) and (3.8), 2 times

From equation (3.7)

$$\begin{aligned}\int \mu \frac{\partial^2 u}{\partial z^2} dz &= \int \frac{\partial p}{\partial x} dz \\ \mu \frac{\partial u}{\partial z} + C_1 &= \frac{\partial p}{\partial x} z \\ \int \mu \frac{\partial u}{\partial z} dz + \int C_1 dz &= \int \frac{\partial p}{\partial x} z dz \\ \mu(u) + C_1 + C_2 &= \frac{\partial p}{\partial x} \frac{z^2}{2} \\ u &= \frac{1}{\mu}\left(\frac{\partial p}{\partial x}\right)\frac{z^2}{2} + C_1 z + C_2\end{aligned} \tag{3.9}$$

This material is reserved for educational use only, not allowed for commercial use.
Forbidden to modify the content, and cite the document when use.

From equation (3.8)

$$\int \mu \frac{\partial^2 v}{\partial z^2} dz = \int \frac{\partial p}{\partial y} dz$$

$$\mu \frac{\partial v}{\partial z} + D_1 = \frac{\partial p}{\partial x} z$$

$$\int \mu \frac{\partial v}{\partial z} dz + \int D_1 dz = \int \frac{\partial p}{\partial y} z dz \qquad (3.10)$$

$$\mu(v) + D_1 + D_2 = \frac{\partial p}{\partial y} \frac{z^2}{2}$$

$$v = \frac{1}{\mu}\left(\frac{\partial p}{\partial y}\right)\frac{z^2}{2} + D_1 z + D_2$$

From boundary condition

$$z = 0; \quad u = U_1; \quad v = V_1$$
$$z = h; \quad u = U_2; \quad v = V_2$$

Substituting value into (3.9) and (3.10)

$$U_2 = \frac{1}{\mu}\left(\frac{\partial p}{\partial x}\right)\frac{0^2}{2} + C_1(0) + C_2$$
$$C_2 = U_2$$

$$U_1 = \frac{1}{\mu}\left(\frac{\partial p}{\partial x}\right)\frac{h^2}{2} + C_1(h) + U_2$$

$$C_1 = \frac{1}{h}\left(\left(U_1 - U_1 - \frac{1}{\mu}\frac{\partial p}{\partial x}\right)\left(\frac{h^2}{2}\right)\right)$$

From equation (3.9)

$$u = \frac{1}{2\mu}\left(\frac{\partial p}{\partial x}\right)z^2 + \frac{(U_1 - U_2)}{h} z - \frac{1}{\mu}\left(\frac{\partial p}{\partial x}\right)\left(\frac{h}{2}\right)z + U_2$$
$$= \frac{1}{2\mu}\left(\frac{\partial p}{\partial x}\right)\left(z^2 - zh\right) + \left(U_1 - U_2\right)_1\left(\frac{z}{h}\right) + U_2 \qquad (3.11)$$

From equation (3.10)

$$v = \frac{1}{2\mu}\left(\frac{\partial p}{\partial y}\right)z^2 + \frac{(V_1 - V_2)}{h} z - \frac{1}{\mu}\left(\frac{\partial p}{\partial y}\right)\left(\frac{h}{2}\right)z + V_2$$
$$= \frac{1}{2\mu}\left(\frac{\partial p}{\partial y}\right)\left(z^2 - zh\right) + \left(V_1 - V_2\right)_1\left(\frac{z}{h}\right) + V_2 \qquad (3.12)$$

This material is restricted for educational use only. Not allowed for commercial use.
Forbidden to modify the content, and cite the document when use.

Flow rate in x-direction; q_x in equation (3.9)

$$\begin{aligned} q_x &= \int_0^h u dz \\ &= \frac{1}{2\mu}\frac{\partial p}{\partial x}\int_0^h (z^2 - zh)dz + \left(\frac{U_1 - U_2}{h}\right)\int_0^h z dz + U_2\int_0^h dz \\ &= \frac{1}{2\mu}\frac{\partial p}{\partial x}\left(\frac{h^3}{3} - \frac{h^2}{2}\right) + \left(\frac{U_1 - U_2}{h}\right)\frac{h^2}{2} + U_2 h \\ &= \frac{h^3}{12\mu}\frac{\partial p}{\partial x} + \left(\frac{U_1 + U_2}{2}\right)h \end{aligned} \tag{3.13}$$

Flow rate in y-direction; q_y in equation (3.10)

$$\begin{aligned} q_y &= \int_0^h v dz \\ &= \frac{1}{2\mu}\frac{\partial p}{\partial y}\int_0^h (z^2 - zh)dz + \left(\frac{V_1 - V_2}{h}\right)\int_0^h z dz + V_2\int_0^h dz \\ &= \frac{1}{2\mu}\frac{\partial p}{\partial y}\left(\frac{h^3}{3} - \frac{h^2}{2}\right) + \left(\frac{V_1 - V_2}{h}\right)\frac{h^2}{2} + V_2 h \\ &= \frac{-h^3}{12\mu}\frac{\partial p}{\partial y} + \left(\frac{V_1 + V_2}{2}\right)h \end{aligned} \tag{3.14}$$

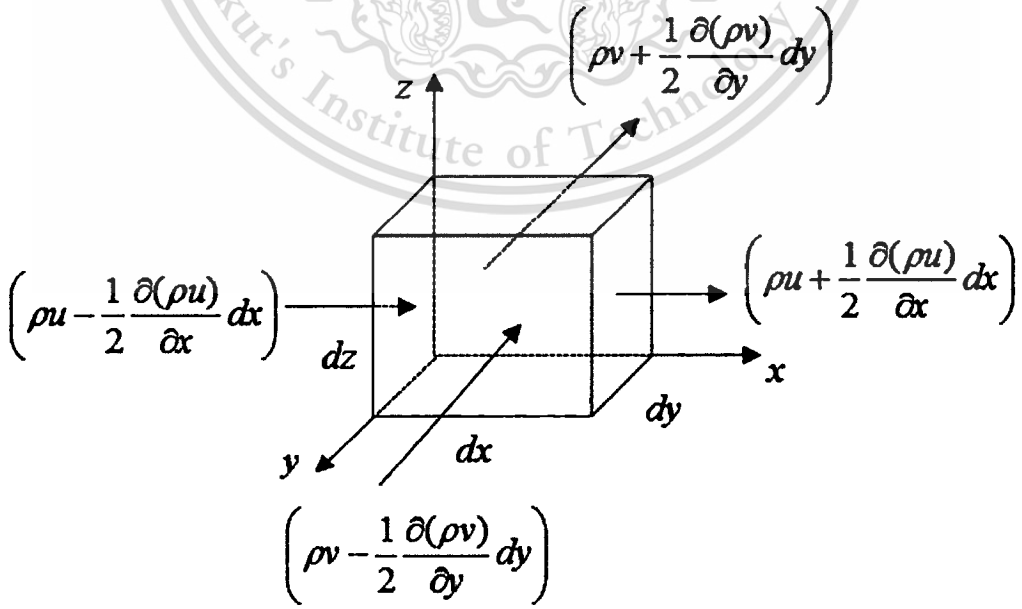

Fig 3.3 Conservation of mass in Cartesian coordinates

This material is reserved for educational use only, not allowed for commercial use.
Forbidden to modify the content, and cite the document when use.

From continuity equation

$$\left(\rho u+\frac{1}{2}\frac{\partial(\rho u)}{\partial x}dx\right)dydz+\left(\rho v+\frac{1}{2}\frac{\partial(\rho v)}{\partial y}dy\right)dxdz-\left(\rho u1\frac{1}{2}\frac{\partial(\rho u)}{\partial x}dx\right)dydz$$
$$-\left(\rho v-\frac{1}{2}\frac{\partial(\rho v)}{\partial y}dy\right)dxdz=-\frac{\partial\rho}{\partial t}dxdydz \tag{3.14}$$

$$\frac{\partial(\rho u)}{\partial x}+\frac{\partial(\rho v)}{\partial y}=-\frac{\partial\rho}{\partial t}$$
$$\frac{\partial(\rho u)}{\partial x}+\frac{\partial(\rho v)}{\partial y}+\frac{\partial\rho}{\partial t}=0 \tag{3.15}$$

Integrate equation (3.15)

$$\int_0^h\left[\frac{\partial(\rho u)}{\partial x}+\frac{\partial(\rho v)}{\partial y}+\frac{\partial\rho}{\partial t}\right]dz=0$$
$$\frac{\partial}{\partial x}\left(\rho\int_0^h udz\right)+\frac{\partial}{\partial y}\left(\rho\int_0^h vdz\right)+\frac{\partial(\rho h)}{\partial t}=0 \tag{3.16}$$

Substituting equation (3.13) and (3.14) into (3.16)

$$\frac{\partial}{\partial x}\left(\frac{-\rho h^3}{12\mu}\frac{\partial p}{\partial x}\right)+\frac{\partial}{\partial x}\left(\frac{\rho(U_1+U_2)h}{2}\right)+\frac{\partial}{\partial y}\left(\frac{-\rho h^3}{12\mu}\frac{\partial p}{\partial y}\right)+\frac{\partial}{\partial y}\left(\frac{\rho(V_1+V_2)h}{2}\right)+\frac{\partial(\rho h)}{\partial t}=0$$

$$\frac{\partial}{\partial x}\left(\frac{\rho h^3}{12\mu}\frac{\partial p}{\partial x}\right)+\frac{\partial}{\partial y}\left(\frac{\rho h^3}{12\mu}\frac{\partial p}{\partial y}\right)=6\frac{\partial}{\partial x}\left(\rho(U_1+U_2)h\right)+12\frac{\partial}{\partial y}\rho(V_1+V_2)h+12\frac{\partial(\rho h)}{\partial t}$$

When $V_1=V_2=0$ and $U_1=U, U_2=0, (\mu=\eta)$

$$\frac{\partial}{\partial x}\left(\frac{\rho h^3}{\eta}\frac{\partial p}{\partial x}\right)+\frac{\partial}{\partial y}\left(\frac{\rho h^3}{\eta}\frac{\partial p}{\partial y}\right)=6\frac{\partial\rho Uh}{\partial x}+12\frac{\partial(\rho h)}{\partial t} \tag{3.17}$$

From ideal gas condition

$$\frac{p}{\rho}=\overline{R}T_m \tag{3.18}$$

When $\overline{R}$ is gas constant, T_m is absolute temperature.

This material is reserved for educational use only, not allowed for commercial use.
Forbidden to modify the content, and cite the document when use.

Also, from isothermal process

$$\frac{p}{\rho}=1 \text{ or } \rho = p \tag{3.19}$$

Substituting equation (3.19) into (3.17)

$$\frac{\partial}{\partial x}\left(\frac{ph^3}{\eta}\frac{\partial p}{\partial x}\right)+\frac{\partial}{\partial y}\left(\frac{ph^3}{\eta}\frac{\partial p}{\partial y}\right)=6\frac{\partial pUh}{\partial x}+12\frac{\partial(ph)}{\partial t} \tag{3.20}$$

From Burg dorfer equation at ambient pressure

$$\eta=\frac{\eta_a}{1+(6a\lambda/h)};\ a \text{ is surface correction coefficient} \tag{3.21}$$

From $\frac{p}{p_a}=\frac{\rho}{p_a}=\frac{\lambda_a}{\lambda}$ and $Kn=\frac{\lambda_a}{h_a}$ substituting into (3.21)

$$\eta=\frac{\eta_a}{1+(6aKnp_ah_a/ph)} \tag{3.22}$$

Substituting equation (3.22) into (3.20)

$$\frac{\partial}{\partial x}\left(ph^3\left(1+\frac{6aKnp_ah_a}{ph}\right)\frac{\partial p}{\partial x}\right)+\frac{\partial}{\partial y}\left(ph^3\left(1+\frac{6aKnp_ah_a}{ph}\right)\frac{\partial p}{\partial y}\right)=6\eta U\frac{\partial ph}{\partial x}+12\eta\frac{\partial(ph)}{\partial t} \tag{3.23}$$

Where

$$X=\frac{x}{L};Y=\frac{y}{B};H=\frac{h}{h_a};P=\frac{p}{p_a};Kn=\frac{\lambda}{h_a};T=\omega t;\Lambda=\frac{6\eta_aUL}{p_ah_a^2};\sigma=\frac{12\eta_a\omega L^2}{p_ah_a^2}$$

Thus, the modified Reynolds equation in general term (dimensionless) is

$$\frac{\partial}{\partial X}\left(PH^3\left(1+\frac{6aKn}{PH}\right)\frac{\partial P}{\partial X}\right)+R^2\frac{\partial}{\partial Y}\left(PH^3\left(1+\frac{6aKn}{PH}\right)\frac{\partial P}{\partial Y}\right)=\Lambda\frac{\partial PH}{\partial X}+\sigma\frac{\partial PH}{\partial T} \tag{3.24}$$

This material is reserved for educational use only, not allowed for commercial use.
Forbidden to modify the content, and cite the document when use.

Consider in static condition, the Reynolds equation is reduced to

$$\frac{\partial}{\partial X}\left(PH^3\left(1+\frac{6aKn}{PH}\right)\frac{\partial P}{\partial X}\right)+R^2\frac{\partial}{\partial Y}\left(PH^3\left(1+\frac{6aKn}{PH}\right)\frac{\partial P}{\partial Y}\right)=\Lambda\frac{\partial PH}{\partial X} \tag{3.25}$$

where

H = Normalized film thickness $\left(h/h_a\right)$

T = Time $\left(\omega t\right)$

Λ = Bearing number $\left(6\eta_a UL/p_a h_a^{\,2}\right)$

σ = Squeeze number $\left(12\eta_a \omega L^2/p_a h_a^2\right)$

Kn = Knudsen number $\left(\lambda/h_a\right)$

η_a = Gas viscosity

λ_a = Mean free molecular path of gas

ω_0 = Angular frequency

p_a = Atmospheric pressure

h_a = Reference film thickness

$Q(P,H)=\phi(P,H)PH^3$ and $\phi(P,H)$ = Poiseulille flow factor. These factors are taken into account of the air rare faction effects based on linearized Boltzmann equation which can be defined according to flow regimes with First-order slip model;

$$\phi(P,H)=a_0+a_1\left(\frac{Kn}{PH}\right) \tag{3.26}$$

The boundary conditions used is,

$$P(0,Y)=P(1,Y)=P_a \tag{3.27}$$

Where

X = Normalized Cartesian coordinates, $X=x/L$

Y = Normalized Cartesian coordinates, $Y=y/W$

P = Normalized pressure $\left(p/p_a\right)$

R = Length-width ratio, L/W; (L = slider length, W = slider width)

This material is reserved for educational use only, not allowed for commercial use.
Forbidden to modify the content, and cite the document when use.

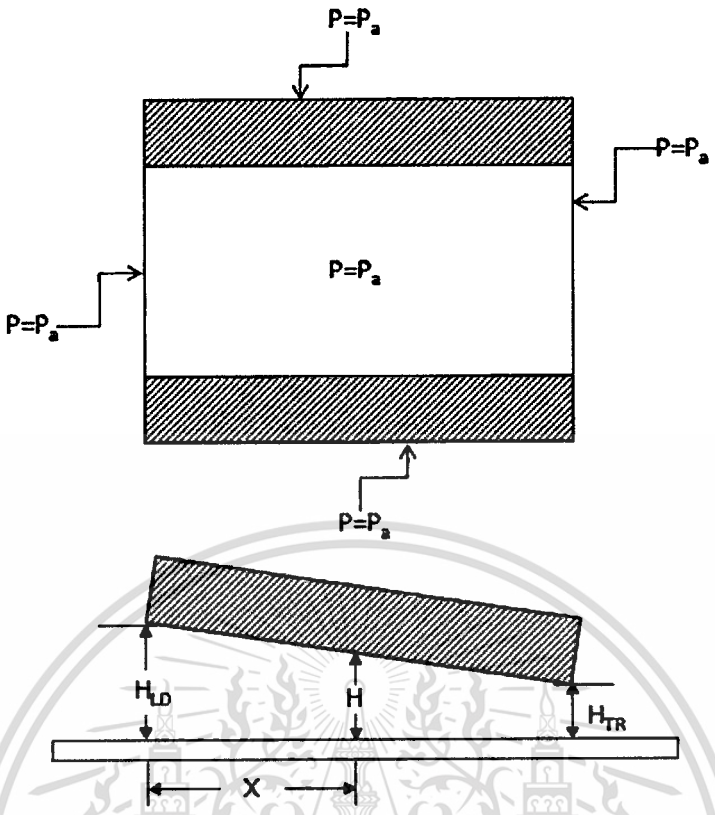

Fig 3.4 Boundary condition and film thickness

The film thickness at any position follows

$$h_{x,y} = h_{TR} + (L - x)\left(\frac{h_{LD} - h_{TR}}{L}\right) \tag{3.28}$$

Rewrite in dimensionless form

$$H_{X,Y} = H_{TR} + (L - X)(H_{LD} - H_{TR}) \tag{3.29}$$

3.2 Finite difference method

The finite difference equation is the approximate equation of derivative equations. It is an importance for numerical analysis. The finite different method consists of transforming the partial derivative equations over a small interval to algebraic equations. By assuming that u is function of the independent variables x and y, we can then divided the $x-y$ plan in mesh points equal to $\delta x = h$ &$\delta y = k$ as showed below

This material is reserved for educational use only, not allowed for commercial use.
Forbidden to modify the content, and cite the document when use.

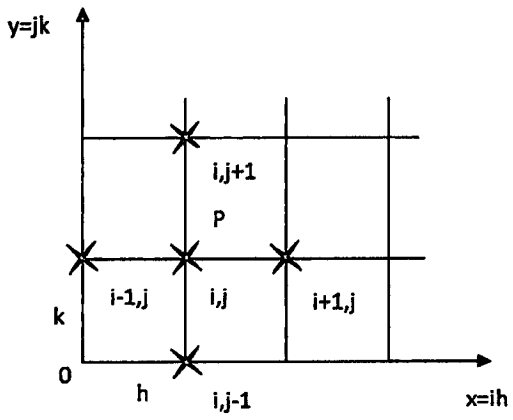

Fig 3.5 Finite difference method

We can evaluate u at point P by

$$u_P = u(ih, jk) = u_{i,j} \tag{3.30}$$

The value of the first derivative at P can be evaluated by three approximation approaches

Central difference

$$\left(\frac{\partial u}{\partial x}\right)_p = \left(\frac{\partial u}{\partial x}\right)_{i,j} \cong \frac{u_{i+1,j} - u_{i-1,j}}{2h} \tag{3.31}$$

$$\left(\frac{\partial u}{\partial y}\right)_p = \left(\frac{\partial u}{\partial y}\right)_{i,j} \cong \frac{u_{i,j+1} - u_{i,j-1}}{2k} \tag{3.32}$$

Forward difference

$$\left(\frac{\partial u}{\partial x}\right)_p = \left(\frac{\partial u}{\partial x}\right)_{i,j} \cong \frac{u_{i+1,j} - u_{i,j}}{h} \tag{3.33}$$

$$\left(\frac{\partial u}{\partial y}\right)_p = \left(\frac{\partial u}{\partial y}\right)_{i,j} \cong \frac{u_{i,j+1} - u_{i,j}}{k} \tag{3.34}$$

Backward difference

$$\left(\frac{\partial u}{\partial x}\right)_p = \left(\frac{\partial u}{\partial x}\right)_{i,j} \cong \frac{u_{i,j} - u_{i-1,j}}{h} \tag{3.35}$$

$$\left(\frac{\partial u}{\partial y}\right)_p = \left(\frac{\partial u}{\partial y}\right)_{i,j} \cong \frac{u_{i,j} - u_{i,j-1}}{k} \tag{3.36}$$

This material is used for educational use only, not allowed for commercial use.
Forbidden to modify the content, and cite the document when use.

The value of the second derivative at P could also be evaluated by

$$\left(\frac{\partial^2 u}{\partial x^2}\right)_p = \left(\frac{\partial^2 u}{\partial x^2}\right)_{i,j} \cong \frac{u_{i+1,j} - 2u_{i,j} + u_{i-1,j}}{h^2} \tag{3.37}$$

$$\left(\frac{\partial^2 u}{\partial y^2}\right)_p = \left(\frac{\partial^2 u}{\partial y^2}\right)_{i,j} \cong \frac{u_{i,j+1} - 2u_{i,j} + u_{i,j-1}}{k^2} \tag{3.38}$$

3.3 Newton-Raphson's method

The Newton-Raphson's method is a root-finding algorithm using the first few terms of the Taylor series of a function in the vicinity of a suspected root. This work the latter term is reserved to the application of Newton's method for computing square roots. For $f(x)$ a polynomial, Newton's method is essentially the same as Horner's method.

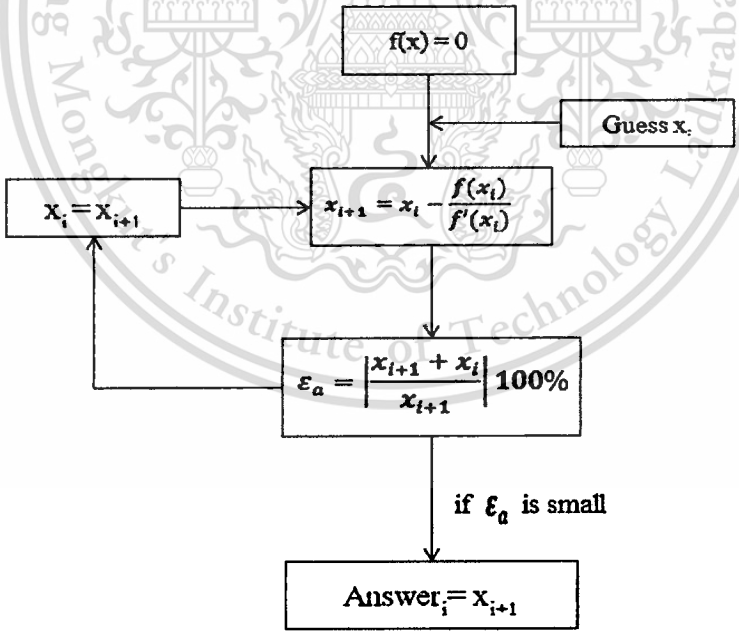

Fig 3.6 Flow chart of Newton-Raphson's method

This material is reserved for educational use only, not allowed for commercial use.
Forbidden to modify the content, and cite the document when use.

The Taylor series of $f(x)$ about the point x_0 is given by

$$f(x_0+\varepsilon)=f(x_0)+f'(x_0)\varepsilon+\frac{1}{2}f''(x_0)\varepsilon^2+... \tag{3.39}$$

Use only first order terms,

$$f(x_0+\varepsilon)\approx f(x_0)+f'(x_0)\varepsilon \tag{3.40}$$

The equation of the tangent line to the curve at $(x_0, f(x_0))$. Therefore, $(x_1, 0)$ is the location where the tangent line intersects x-axis. A graph therefore gives a good intuitive idea of why Newton's method works at a well-chosen starting point and why it might diverge with a poorly-chosen starting point.

The expression above can be used to estimate the amount of offset needed to land closer to the root starting from an initial guess x_0. Setting $f(x_0,\varepsilon)=0$ and $\varepsilon \equiv \varepsilon_0$ give

$$\varepsilon_0=-\frac{f(x_0)}{f'(x_0)} \tag{3.41}$$

Unfortunately, this procedure can be unstable near a horizontal asymptote or a local extremism. However, with a good initial choice of the root's position, the algorithm can be applied iteratively to obtain

$$x_{n+1}=x_n-\frac{f(x_n)}{f'(x_n)} \tag{3.42}$$

For n=1, 2, 3, an initial point x_0 that provides safe convergence of Newton's method is called an approximate zero.

3.4 Gauss-Seidel Method

The Gauss-Seidel method is a technique for solving the n equations of the linear system $Ax = b$ in sequence

$$x_i^k=\frac{b_i-\sum_{j<i}a_{ij}x_j^k-\sum_{j>i}a_{ij}x_j^{k-1}}{aii},\ i=1,2,3,\ldots,n \tag{3.43}$$

This material is reserved for educational use only, not allowed for commercial use.
Forbidden to modify the content, and cite the document when use.

There are two important characteristics of the Gauss-Seidel method should be noted. Firstly, the computations appear to be serial. Since each component of the new iteration depends upon all previously computed components, the updates cannot be done simultaneously as in the Jacobi method. Secondly, the new iterated value $x^{(k)}$ depends on the order in which the equations are examined. If this ordering is changed, the components of the new iterates (and not just their order) will also change.

The iterations are stopped when the absolute relative approximate error is less than a pre-specified tolerance for all unknowns.

$$\left|\epsilon_a\right|_i = \left|\frac{x_i^{new} - x_i^{old}}{x_i^{new}}\right| \times 100 \tag{3.44}$$

3.5 Successive Over Relaxation Method (SOR)

The successive over relaxation method (SOR) is a method of solving a linear system for equations $Ax = b$ derives by extrapolating the Gauss-Seidel method. This extrapolation takes the form of a weight average between the previous iterate and the computed Gauss-Seidel iterate successively for each component.

$$x_i^{(k)} = \omega\bar{x}^{(k)} + (1+\omega)x_i^{(k-1)} \tag{3.45}$$

Where $\bar{x}$ denotes a Guss-Seidel iterate and ω is the extrapolation factor. The idea is to choose a value for ω that will accelerate the rate of convergence of iterate to the solution.

If $\omega = 1$, the SOR method simplifies to the Gauss-Seidel method. A theorem due to Kahan (1958) shows that SOR fails to converge if ω is outside the interval (0, 2). In general, it is not possible to compute in advance the value of e to ω that will maximize the rate of convergence of SOR. Frequently, some heuristic estimate is used, such as $\omega = 2 - O(h)$ where h h is the mesh spacing of the discretization of the underlying physical domain.

This material is reserved for educational use only, not allowed for commercial use.
Forbidden to modify the content, and cite the document when use.

3.6 Simpson's Rule

Simpson's rule is a numerical method that approximates the value of a definite integral by using quadratic polynomials. We consider the definite integral

$$\int_a^b f(x)dx \tag{3.46}$$

We assume that $f(x)$ is continuous on $[a,b]$ and we divide $[a,b]$ into an even number n of subintervals of equal length

$$\Delta x = \frac{b-a}{n} \tag{3.47}$$

using the n + 1 points

$$x_0 = a,\ x_1 = a+\Delta x,\ x_2 = a+2\Delta x, \ldots, x_n = a+n\Delta x = b \tag{3.48}$$

We can compute the value of $f(x)$ at these points.

$$y_0 = f(x_0),\ y_1 = f(x_1),\ y_2 = f(x_2), \ldots, y_n = f(x_n) \tag{3.49}$$

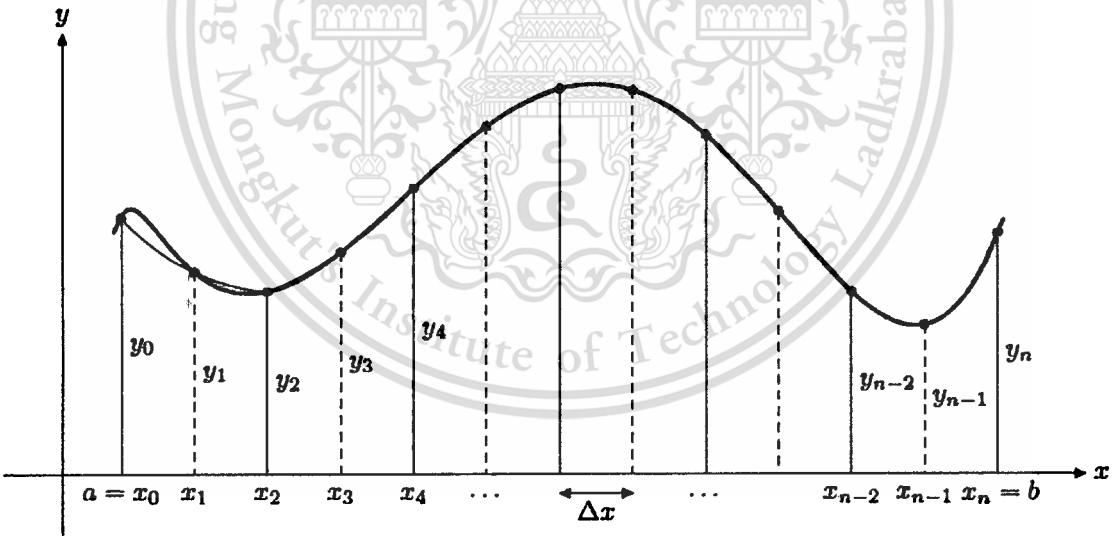

Fig 3.7 Intervals Δx for Simpson

We can estimate the integral by adding the areas under the parabolic arcs through three successive points. By simplifying,

This material is reserved for educational use only, not allowed for commercial use.
Forbidden to modify the content, and cite the document when use.

$$\int_a^b f(x)dx \approx \frac{\Delta x}{3}(y_0+4y_1+y_2)+\frac{\Delta x}{3}(y_2+4y_3+y_4)+\ldots+\frac{\Delta x}{3}(y_{n-2}+4y_{n-1}+y_n) \quad (3.50)$$

3.7 Multrigrid method

To obtain accurate and efficient solutions, the Multrigrid method is applied. This method is commonly used in implementations for non-linear equation [18]. The technique involves a sequence of "grids" to accurately determine the convergence iteratively. The flow for Multigrid is as below [19], with a pictorial representation presented in Fig. 3.7 below.

1) Initialize $f^h, f^{2h}, f^{4h}, \ldots, f^H$
2) Solve on coarsest grid $v^H = (A^H)^{-1} f^H$
3) Interpolate initial guess $v^{2h} \leftarrow I_{4h}^{2h} v^{4h}$
4) Perform V-cycle $v^{2h} \leftarrow MV^{2h}(v^{2h}, f^{2h})$

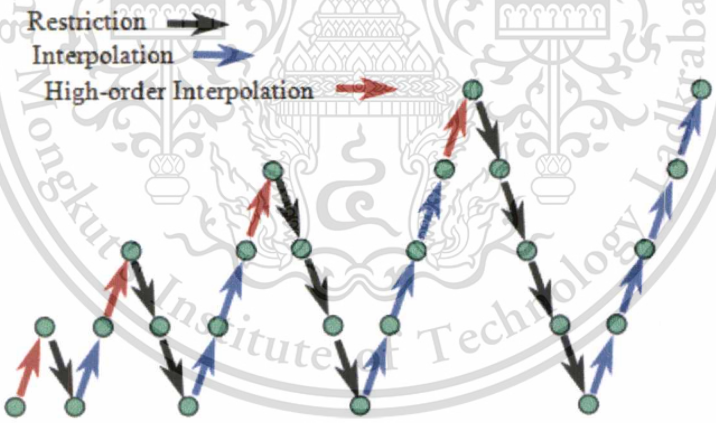

Fig 3.8 Full Multigrid scheme [20]

This material is reserved for educational use only, not allowed for commercial use.
Forbidden to modify the content, and cite the document when use.

Distribution from Fine Grid to Coarse Grid

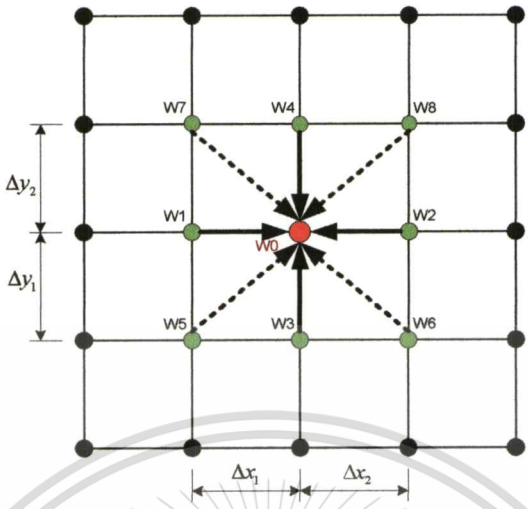

Fig 3.9 Distribution from Fine Grid to Coarse Grid [20]

Where

$$\Delta x_1 = x_i - x_{i-1} \qquad \Delta x_2 = x_{i+1} - x_i \qquad \Delta y_1 = y_j - y_{j-1} \qquad \Delta y_2 = y_{j+1} - y_j$$

$$\Delta = \min(\Delta x_1, \Delta x_2, \Delta y_1, \Delta y_2)$$

$$W_1 = \frac{\Delta}{\Delta x_1} \quad W_2 = \frac{\Delta}{\Delta x_2} \quad W_3 = \frac{\Delta}{\Delta y_1} \quad W_4 = \frac{\Delta}{\Delta y_2}$$

$$W_0 = W_1 + W_2 + W_3 + W_4$$

$$W_5 = \frac{1}{4}(W_1 + W_3) \qquad W_6 = \frac{1}{4}(W_2 + W_3)$$

$$W_7 = \frac{1}{4}(W_1 + W_4) \qquad W_8 = \frac{1}{4}(W_2 + W_4)$$

$$W_T = W_0 + W_1 + W_2 + W_3 + W_4 + W_5 + W_6 + W_7 + W_8$$

$$P_{i,j} = \left(\frac{1}{W_T}\right)\left(W_0 P_{i,j} + W_1 P_{i-1,j} + W_2 P_{i+1,j} + W_3 P_{i,j-1} + W_4 P_{i,j+1} + W_5 P_{i-1,j-1} + W_6 P_{i+1,j-1} + W_7 P_{i-1,j+1} + W_8 P_{i+1,}\right.$$

This material is reserved for educational use only, not allowed for commercial use.
Forbidden to modify the content, and cite the document when use.

Distribution from Coarse Grid to Fine Grid

First Step, distribute from dark node to green node

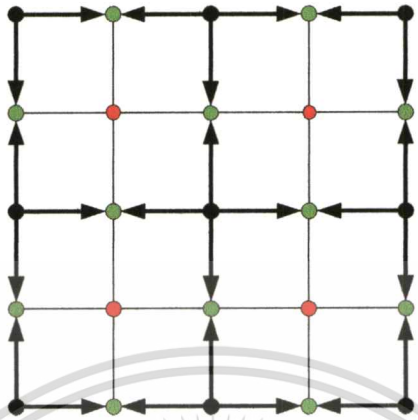

Fig 3.10 Distribution from Coarse Grid to Fine Grid [20]

After that, distribute grid from dark and green node to red node

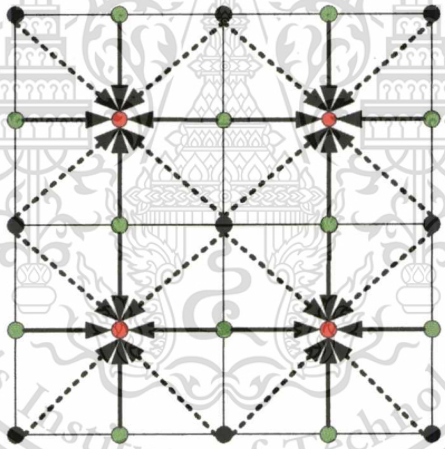

Fig 3.11 Distribution from Coarse Grid to Fine Grid [20]

Where

$$\Delta x_1 = x_i - x_{i-1} \qquad \Delta x_2 = x_{i+1} - x_i \qquad \Delta y_1 = y_j - y_{j-1} \qquad \Delta y_2 = y_{j+1} - y_j$$

$$\Delta = \min\left(\Delta x_1, \Delta x_2, \Delta y_1, \Delta y_2\right)$$

This material is reserved for educational use only, not allowed for commercial use.
Forbidden to modify the content, and cite the document when use.

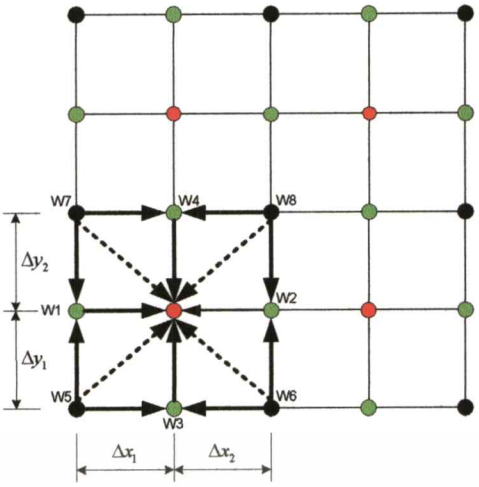

Fig 3.12 Distribution from Coarse Grid to Fine Grid

$$W_1 = \frac{\Delta}{\Delta x_1} \quad W_2 = \frac{\Delta}{\Delta x_2} \quad W_3 = \frac{\Delta}{\Delta y_1} \quad W_4 = \frac{\Delta}{\Delta y_2}$$

$$W_5 = \frac{1}{4}(W_1 + W_3) \quad W_6 = \frac{1}{4}(W_2 + W_3) \quad W_7 = \frac{1}{4}(W_1 + W_4)$$

$$W_8 = \frac{1}{4}(W_2 + W_4) \quad W_T = W_1 + W_2 + W_3 + W_4 + W_5 + W_6 + W_7 + W_8$$

$$P_{i-1,j} = \left(\frac{1}{W_5 + W_7}\right)\left(W_5 P_{i-1,j-1} + W_7 P_{i-1,j+1}\right) \quad P_{i+1,j} = \left(\frac{1}{W_6 + W_8}\right)\left(W_6 P_{i+1,j-1} + W_8 P_{i+1,j+1}\right)$$

$$P_{i,j-1} = \left(\frac{1}{W_5 + W_6}\right)\left(W_5 P_{i-1,j-1} + W_6 P_{i+1,j-1}\right) \quad P_{i,j+1} = \left(\frac{1}{W_7 + W_8}\right)\left(W_7 P_{i-1,j+1} + W_8 P_{i+1,j+1}\right)$$

$$P_{i,j} = \left(\frac{1}{W_T}\right)\left(W_1 P_{i-1,j} + W_2 P_{i+1,j} + W_3 P_{i,j-1} + W_4 P_{i,j+1} + W_5 P_{i-1,j-1} + W_6 P_{i+1,j-1} + W_7 P_{i-1,j+1} + W_8 P_{i+1,j+1}\right)$$

This material is reserved for educational use only, not allowed for commercial use.
Forbidden to modify the content, and cite the document when use.

CHAPTER 4

RESEARCH METHODOLOGY

4.1 Methodology

Below is the methodology flow chart for this study, starting from Modified the Reynolds equation then use the FORTRAN for simulation and the last is analysis the data.

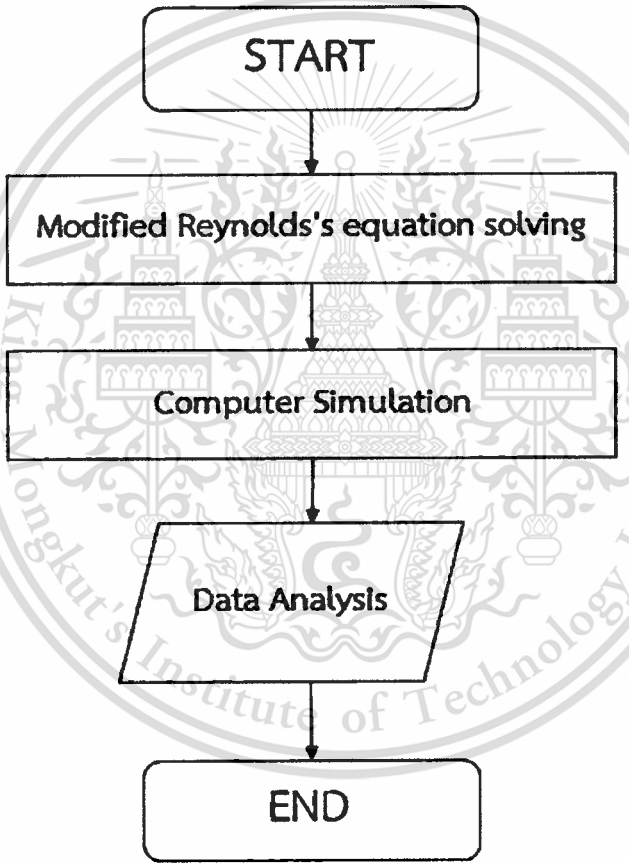

Fig 4.1 Methodology Flow

This material is reserved for educational use only, not allowed for commercial use.
Forbidden to modify the content, and cite the document when use.

4.2 Modified Reynolds Equation Solving

The modified Reynolds equation is highly non-linear equation and cannot be solved using exact form. Therefore, the numerical method is important and necessary to obtain flow solutions. Numerical method is applied to approximate the flow solutions by discretization using Finite Difference Method. In this work, the Central Difference Scheme (4.1) is applied to estimate the spatial terms of Modified Reynolds equation (4.2)

$$\frac{df(x)}{dx} \approx \frac{f(x+\Delta x)-f(x)}{\Delta x} \tag{4.1}$$

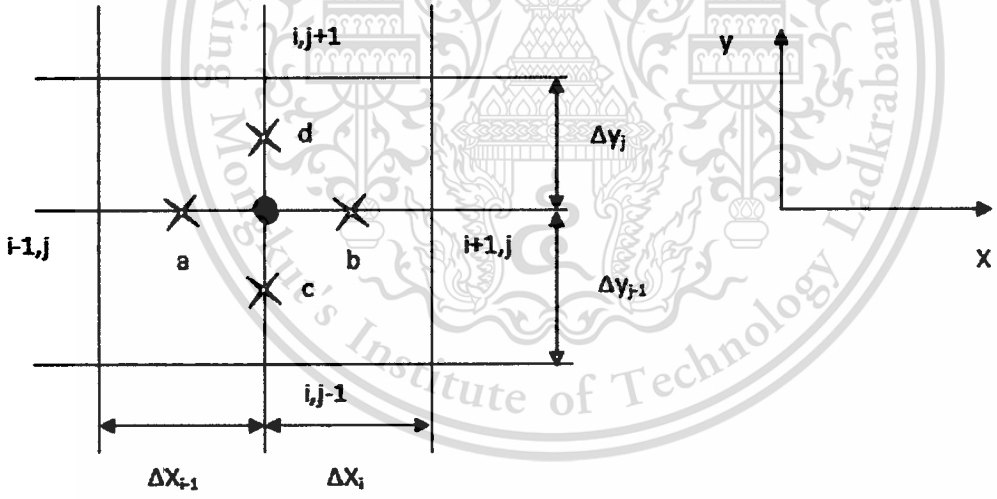

Fig 4.2 Grids for finite difference method

$$\frac{\partial}{\partial X}\left(Q(P)H^3\frac{\partial P}{\partial X}\right)+\frac{\partial}{\partial Y}\left(Q(P)H^3\frac{\partial P}{\partial Y}\right)-\Lambda\frac{\partial(PH)}{\partial X}=0 \tag{4.2}$$

The discretization solution for the first, second, and third terms of the left hand side is shown as equation (4.3), (4.4), and (4.5), respectively

This material is reserved for educational use only, not allowed for commercial use.
Forbidden to modify the content, and cite the document when use.

First Term

$$\left.\frac{\partial}{\partial X}\left(Q(P)H^3\frac{\partial P}{\partial X}\right)\right|_{i,j} \approx \frac{QH^3\left.\frac{\partial P}{\partial X}\right|_b - QH^3\left.\frac{\partial P}{\partial X}\right|_a}{(\Delta x_{i-1}+\Delta x_i)/2}$$

$$= QH^3\Big|_{i+\frac{1}{2},j}\frac{P_{i+1,j}-P_{i,j}}{\Delta x_i} - QH^3\Big|_{i-\frac{1}{2},j}\frac{P_{i,j}-P_{i-1,j}}{\Delta x_{i-1}}$$

$$= \frac{1}{(x_{i-1}+x_i)}\left\{\begin{array}{l}\dfrac{H^3_{i+\frac{1}{2},j}}{\Delta x_i}[Q(P_{i+1,j})+Q(P_{i,j})][P_{i+1,j}-P_{i,j}] \\ -\dfrac{H^3_{i-\frac{1}{2},j}}{\Delta x_{i-1}}[Q(P_{i,j})+Q(P_{i-1,j})][P_{i,j}-P_{i-1,j}]\end{array}\right\} \quad (4.3)$$

Second term

$$\left.\frac{\partial}{\partial Y}\left(Q(P)H^3\frac{\partial P}{\partial Y}\right)\right|_{i,j} \approx \frac{QH^3\left.\frac{\partial P}{\partial Y}\right|_d - QH^3\left.\frac{\partial P}{\partial Y}\right|_c}{(\Delta y_{j-1}+\Delta y_j)/2}$$

$$= QH^3\Big|_{i,j+\frac{1}{2}}\frac{P_{i,j+1}-P_{i,j}}{\Delta y_j} - QH^3\Big|_{i,j-\frac{1}{2}}\frac{P_{i,j}-P_{i,j-1}}{\Delta y_{j-1}}$$

$$= \frac{1}{(y_{j-1}+y_j)}\left\{\begin{array}{l}\dfrac{H^3_{i,j+\frac{1}{2}}}{\Delta y_j}[Q(P_{i,j+1})+Q(P_{i,j})][P_{i,j+1}-P_{i,j}] \\ -\dfrac{H^3_{i,j-\frac{1}{2}}}{\Delta y_{j-1}}[Q(P_{i,j})+Q(P_{i,j-1})][P_{i,j}-P_{i,j-1}]\end{array}\right\} \quad (4.4)$$

This material is reserved for educational use only, not allowed for commercial use.
Forbidden to modify the content, and cite the document when use.

Third term

$$\Lambda \frac{\partial (PH)}{\partial X}\bigg|_{i,j} \approx \Lambda \frac{(P_{i+1,j}H_{i+1,j} - P_{i-1,j}H_{i-1,j})}{(\Delta x_{i-1} + \Delta x_i)} \tag{4.5}$$

Substitute equations (4.3), (4.4), and (4.5) into equation (4.1)

$$f_{i,j} = \frac{1}{(x_{i-1} + x_i)} \left\{ \begin{array}{l} \dfrac{H^3_{i+\frac{1}{2},j}}{\Delta x_i}[Q(P_{i+1,j}) + Q(P_{i,j})][P_{i+1,j} - P_{i,j}] \\ -\dfrac{H^3_{i-\frac{1}{2},j}}{\Delta x_{i-1}}[Q(P_{i,j}) + Q(P_{i-1,j})][P_{i,j} - P_{i-1,j}] \end{array} \right\}$$
$$+ \frac{1}{(y_{j-1} + y_j)} \left\{ \begin{array}{l} \dfrac{H^3_{i,j+\frac{1}{2}}}{\Delta y_j}[Q(P_{i,j+1}) + Q(P_{i,j})][P_{i,j+1} - P_{i,j}] \\ -\dfrac{H^3_{i,j-\frac{1}{2}}}{\Delta y_{j-1}}[Q(P_{i,j}) + Q(P_{i,j-1})][P_{i,j} - P_{i,j-1}] \end{array} \right\}$$
$$-\Lambda \frac{(P_{i+1,j}H_{i+1,j} - P_{i-1,j}H_{i-1,j})}{(\Delta x_{i-1} + \Delta x_i)} \tag{4.6}$$

$$f_{i,j}(P_{i-1,j}, P_{i,j}, P_{i+1,j}, P_{i,j+1}, P_{i,j+1}) = 0 \tag{4.7}$$

The boundary conditions $P = P_{atm}$ is applied

$$P_{1,j} = P_{i,1} = 1 \qquad ; (1 \le i \le i_{\max}, 2 \le j \le i_{\max-1}) \tag{4.8}$$

Linearization $f_{i,j}$ by Newton-Raphson's is given by

$$f_{ij} = f^*_{i,j} + \frac{\partial f_{ij}}{\partial P_{22}}\Delta P_{22} + \frac{\partial f_{ij}}{\partial P_{23}}\Delta P_{23} + \ldots + \frac{\partial f_{ij}}{\partial P_{mn}}\Delta P_{mn} + \ldots + \frac{\partial f_{ij}}{\partial P_{MN}}\Delta P_{MN} \tag{4.9}$$

This material is reserved for educational use only, not allowed for commercial use.
Forbidden to modify the content, and cite the document when use.

For $f_{ij} = 0 \qquad ;2 \le i \le M, 2 \le j \le N$ (4.10)

Therefore,

$$f_{i,j}^{*} + \sum_{m=2}^{M}\sum_{n=2}^{N} \frac{\partial f_{ij}}{\partial P_{mn}} \Delta P_{mn} = 0 \tag{4.11}$$

For $m = 1, \quad n = j$, the equation (4.11) can be rewritten as

$$f_{i,j}^{*} + \sum_{i=2}^{M}\sum_{j=2}^{N} \frac{\partial f_{ij}}{\partial P_{ij}} \Delta P_{ij} = 0 \tag{4.12}$$

From equation (4.12) at $m = 1, n = j$, the derivative term can be expressed as,

$$\frac{\partial f_{ij}}{\partial P_{ij}} = \frac{1}{(\Delta x_{i-1} + \Delta x_i)} \left\{ \begin{array}{l} \dfrac{H^3_{i+\frac{1}{2},j}}{\Delta x_i} \left[\left(\dfrac{\partial Q(P_{i,j})}{\partial P_{ij}} (P_{i+1,j} - P_{i,j}) \right) - \left(Q(P_{i+1,j}) + Q(P_{i,j}) \right) \right] \\ - \dfrac{H^3_{i-\frac{1}{2},j}}{\Delta x_{i-1}} \left[\left(\dfrac{\partial Q(P_{i,j})}{\partial P_{ij}} (P_{i,j} - P_{i-1,j}) \right) + \left(Q(P_{i,j}) + Q(P_{i-1,j}) \right) \right] \end{array} \right\}$$

$$+ \frac{H^3_{i,j}}{(\Delta y_{j-1} + \Delta y_j)} \left\{ \begin{array}{l} \dfrac{1}{\Delta y_j} \left[\left(\dfrac{\partial Q(P_{i,j})}{\partial P_{ij}} (P_{i,j+1} - P_{i,j}) \right) - \left(Q(P_{i,j+1}) + Q(P_{i,j}) \right) \right] \\ - \dfrac{1}{\Delta y_{j-1}} \left[\left(\dfrac{\partial Q(P_{i,j})}{\partial P_{ij}} (P_{i,j} - P_{i,j-1}) \right) - \left(Q(P_{i,j}) + Q(P_{i,j-1}) \right) \right] \end{array} \right\} \tag{4.13}$$

From equation (4.13) at $m = i-1, n = j$, the derivative term can be expressed as,

$$\frac{\partial f_{ij}}{\partial P_{i-1,j}} = \frac{1}{(\Delta x_{i-1} + \Delta x_i)} \left\{ \frac{-H^3_{i+\frac{1}{2},j}}{\Delta x_{i-1}} \left[\left(\frac{\partial Q(P_{i-1,j})}{\partial P_{i-1,j}} (P_{i,j} - P_{i-1,j}) \right) - \left(Q(P_{i,j}) + Q(P_{i-1,j}) \right) \right] \right\}$$

$$- \frac{\Lambda H_{i-1}}{(\Delta x_{i-1} + \Delta x_i)} \tag{4.14}$$

This material is reserved for educational use only, not allowed for commercial use.
Forbidden to modify the content, and cite the document when use.

From equation (4.14) at $m=i+1, n=j$, the derivative term can be expressed as,

$$\frac{\partial f_{ij}}{\partial P_{i+1,j}} = \frac{1}{(\Delta x_{i-1}+\Delta x_i)}\left\{\frac{H^3_{i+\frac{1}{2},j}}{\Delta x_{i-1}}\left[\left(\frac{\partial Q(P_{i+1,j})}{\partial P_{i+1,j}}(P_{i+1,j}-P_{i-1,j})\right)+\left(Q(P_{i+1,j})+Q(P_{i,j})\right)\right]\right\}$$

$$-\frac{\Lambda H_{i+1}}{(\Delta x_{i-1}+\Delta x_i)} \qquad (4.15)$$

From equation (4.15) at $m=i, n=j+1$, the derivative term can be expressed as,

$$\frac{\partial f_{ij}}{\partial P_{i,j+1}} = \frac{H^3_{i,j}}{(\Delta y_{j-1}+\Delta y_j)}\left\{\frac{1}{\Delta y_j}\left[\left(\frac{\partial Q(P_{i,j+1})}{\partial P_{i,j+1}}(P_{i,j+1}-P_{i,j})\right)+\left(Q(P_{i,j+1})+Q(P_{i,j})\right)\right]\right\} \qquad (4.16)$$

From equation (4.16) at $m=i, n=j-1$, the derivative term can be expressed as,

$$\frac{\partial f_{ij}}{\partial P_{i,j-1}} = \frac{H^3_{i,j}}{(\Delta y_{j-1}+\Delta y_j)}\left\{\frac{1}{\Delta y_{j-1}}\left[\left(\frac{\partial Q(P_{i,j-1})}{\partial P_{i,j-1}}(P_{i,j}-P_{i,j-1})\right)+\left(Q(P_{i,j})+Q(P_{i,j-1})\right)\right]\right\} \qquad (4.17)$$

Other cases, the derivative term can be expressed as,

$$\frac{\partial f_{ij}}{\partial P_{mn}} = 0 \qquad (4.18)$$

Newton-Raphson's technique is used to linearize and can be written in general form as expressed in equation (4.18). Linearized Reynolds equation is shown in the matrix. The Gauss Seidel technique is applied to obtain the pressure values.

$$[A]\{\Delta P\} = \{-f^*\} \qquad (4.19)$$

This material is reserved for educational use only, not allowed for commercial use.
Forbidden to modify the content, and cite the document when use.

$$[A]=\begin{bmatrix}
\frac{\partial f_{22}}{\partial P_{22}} & \frac{\partial f_{22}}{\partial P_{23}} & & \frac{\partial f_{22}}{\partial P_{2N}} & \frac{\partial f_{22}}{\partial P_{32}} & & \frac{\partial f_{22}}{\partial P_{3N}} & & \frac{\partial f_{22}}{\partial P_{MN}} \\
\frac{\partial f_{23}}{\partial P_{22}} & \frac{\partial f_{23}}{\partial P_{23}} & \cdots & \frac{\partial f_{23}}{\partial P_{2N}} & \frac{\partial f_{23}}{\partial P_{32}} & \cdots & \frac{\partial f_{23}}{\partial P_{3N}} & \cdots & \frac{\partial f_{23}}{\partial P_{MN}} \\
\vdots & \vdots & \cdots & \vdots & \vdots & \cdots & \vdots & \cdots & \vdots \\
\frac{\partial f_{mn}}{\partial P_{22}} & \frac{\partial f_{mn}}{\partial P_{23}} & \vdots & \frac{\partial f_{mn}}{\partial P_{2N}} & \frac{\partial f_{mn}}{\partial P_{32}} & \vdots & \frac{\partial f_{mn}}{\partial P_{3N}} & \vdots & \frac{\partial f_{mn}}{\partial P_{mn}} \\
\vdots & \vdots & \cdots & \vdots & \vdots & \cdots & \vdots & \cdots & \vdots \\
\frac{\partial f_{MN}}{\partial P_{22}} & \frac{\partial f_{MN}}{\partial P_{22}} & \vdots & \frac{\partial f_{MN}}{\partial P_{2N}} & \frac{\partial f_{MN}}{\partial P_{32}} & \vdots & \frac{\partial f_{MN}}{\partial P_{3N}} & \vdots & \frac{\partial f_{MN}}{\partial P_{mn}}
\end{bmatrix} \tag{4.20}$$

$$\{\Delta P\}=\begin{bmatrix}
\Delta P_{22} \\
\Delta P_{23} \\
\vdots \\
\Delta P_{mn} \\
\vdots \\
\Delta P_{MN}
\end{bmatrix} \tag{4.21}$$

$$\{-f^*\}=\begin{bmatrix}
-f_{22}^* \\
-f_{23}^* \\
\vdots \\
-f_{mn}^* \\
\vdots \\
-f_{MN}^*
\end{bmatrix} \tag{4.22}$$

And,

$$\Delta P_{mn} = P_{mn}^{(k)} - P_{mn}^{(k-1)} \quad \text{, or} \quad P_{mn}^{(k)} = P_{mn}^{(k-1)} + \Delta P_{mn} \tag{4.23}$$

This material is reserved for educational use only, not allowed for commercial use.
Forbidden to modify the content, and cite the document when use.

An equation (4.19) shows the new pressure using Gauss Seidel iteration, where n is the number of iteration. The termination of iteration is determined by the pressure convergence and accuracy in equation (4.20).

$$\frac{\sum_{m=2}^{M}\sum_{n=2}^{N}\left|\Delta P_{mn}\right|}{\sum_{m=2}^{M}\sum_{n=2}^{N}\left|P_{mn}^{(k)}\right|} \le \varepsilon \qquad ; \varepsilon \text{ is relative error} \tag{4.24}$$

4.3 Force and moment on slider head in dimensionless form

The force on slider head can be obtained by integrating pressure divided by area as follows:

$$W = \int_0^1\int_0^1 (P-1)dXdY \tag{4.25}$$

The moment on slider head can be found as following:

$$X_G W = \int_0^1\int_0^1 X(P-1)dXdY \tag{4.26}$$

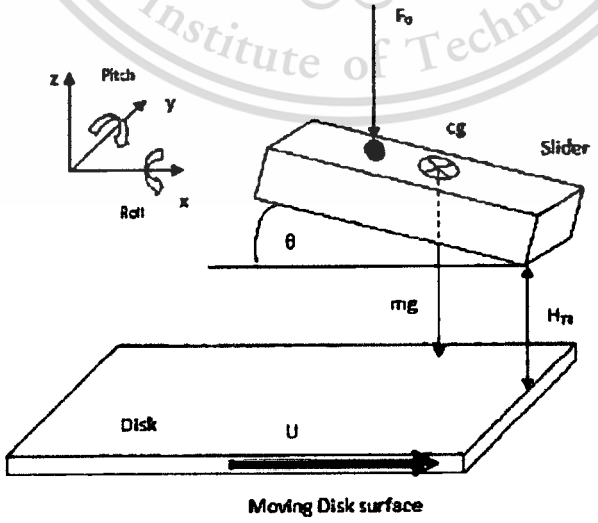

Fig 4.3 Flying height of slider head

This material is reserved for educational use only, not allowed for commercial use.
Forbidden to modify the content, and cite the document when use.

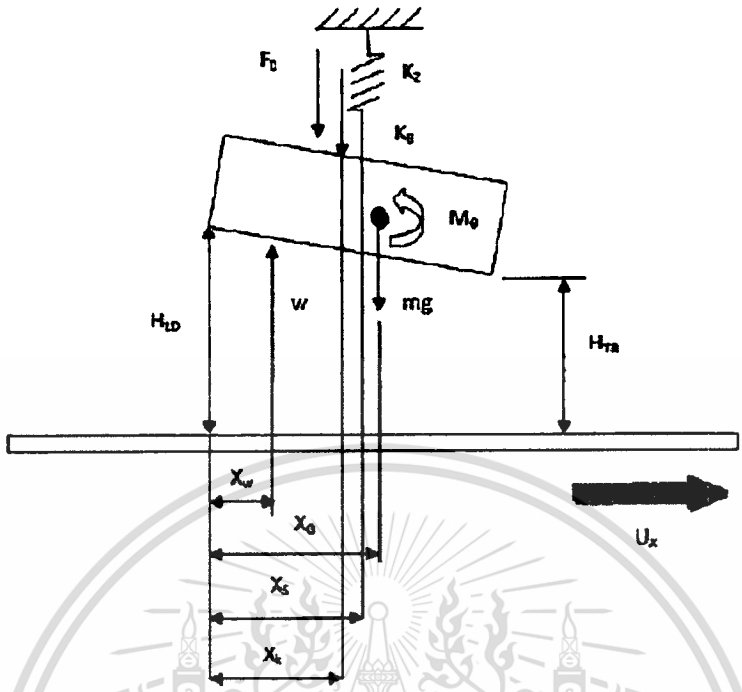

Fig 4.4 Force and momentum on slider head

4.4 Support position on slider head

We can find support position on slider head:

$$X = \frac{1}{W}\int_0^1\int_0^1 X\left(P-1\right)dXdY \tag{4.27}$$

$$Y = \frac{1}{W}\int_0^1\int_0^1 Y\left(P-1\right)dXdY \tag{4.28}$$

4.5 Film Thickness on slider head

The equation of flying height is analyzed from the surface of air bearing of head slider that can be written in dimensionless form as equation (4.29).

$$H = H_{TR} + (1-X)(H_{LD} - H_{TR}) \tag{4.29}$$

This material is reserved for educational use only, not allowed for commercial use.
Forbidden to modify the content, and cite the document when use.

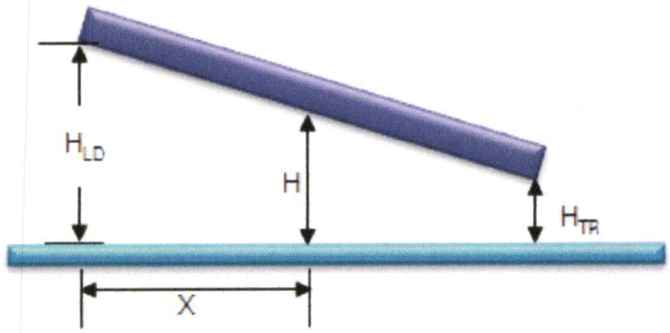

Fig 4.5 Film thickness

Where $H = h/h_a$ is normalized film thickness, h_a is reference film thickness, $H_{TR} = h_{TR}/h_a$ is normalized trailing edge, $H_{LD} = h_{LD}/h_a$ is normalized leading edge, H is film thickness, h_{TR} is trailing edge, h_{LD} is leading edge.

The equation of flying height is analyzed from the surface of air bearing of head slider that can be written in dimensionless form as equation below:

$$H = H_{TR} + (1 - X_1)(H_{LD} - H_{TR}); \quad (0 \le x \le x_1) \text{ and } (0 \le y \le y_1)$$

$$H = H_{TR} + (1 - X_2)(H_{LD} - H_{TR}); \quad (x_2 \le x \le L)$$

4.6 Flow chart of simulation program

Computer program is developed using FORTRAN language to simulate the flying height characteristics and pressure distribution of the slider head as Figure 4.6 demonstrates the developed program.

The computation software starts with defining the Film Thickness given by equation (4.29). The pressure boundary condition at the edge of slider is set as 1. For this simulation, velocity and rail width are independent parameters while Rail length is fixed as 850 μm. Once all parameters are defined, the film thickness is expressed in $x - y$ dimension. $P(i, j)$ is computed by using the modified Reynolds equation.

This material is reserved for educational use only, not allowed for commercial use.
Forbidden to modify the content, and cite the document when use.

Newton-Raphson's shown in equation 4.9 is applied. Gauss-Seidel technique with SOR is used to obtain the pressure $P(i, j)$. If the error from Gauss-Seidel is less than the specified error, the software will start calculating the total force from the pressure using the Simpson's Rule. The next step, balance force condition is utilized to check whether or not the defined flying height is correct. If the difference between total force and the applied force from gram load is less than 0.0001, the software will generate text file for pressure distribution and flying height. If not, it will return to the film thickness loop and re-define again.

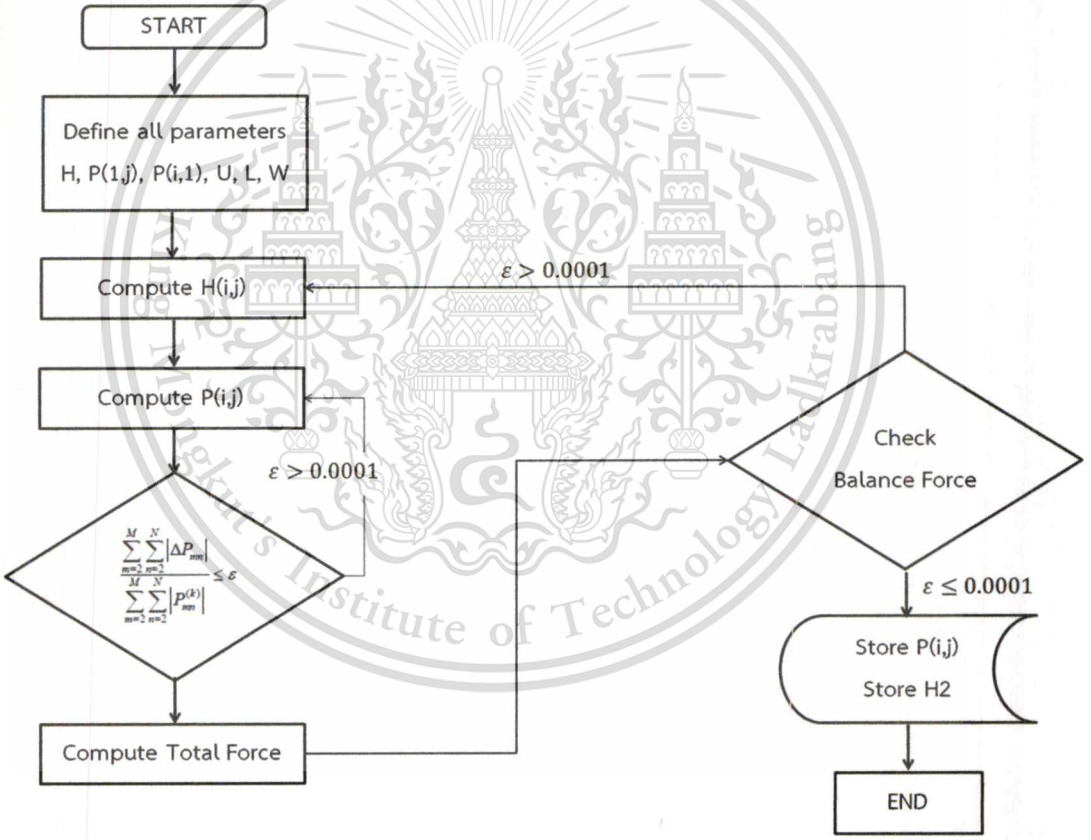

Fig 4.6 Flow chart of simulation program

This material is reserved for educational use only, not allowed for commercial use.
Forbidden to modify the content, and cite the document when use.

CHAPTER 5

NUMERICAL SIMULATIONS RESULT

5.1 Defined the parameter for Rail-pad

In this study we focus on the characteristic of flying height when the parameters in the list are changed, in Table 5.1. The simulation is performed with the FEMTO form factor of slider dimension, 700μm in width and 850μm in lenght (Fig 5.1).

TABLE 5.1

THE PARAMETERS OF THE SLIDER HEAD FOR SIMULATION FOR RAIL-PAD

Symbol	Discretion	Dimension		Unit
		Helium	Air	
L	Slider lenght	850		μm
W	Slider width	700		μm
B	Slider rail width	112.5		μm
f_0	Loading force	22 – 28		Nm
P_a	Ambient Pressure	1.013x10-5		Pa
U	Disk velocity (2.5")	5400 - 10000		PRM
T	Temperature	20-500		$°C$
η	Viscosity	$1.956x10^{-5}$	1.821x10-5	$Pa.s$
ρ	Density	0.167	1.205	kg/m^3
k	Thermal Conductivity	0.148	0.026	W/mk
λ	Mean Free Path	165.5	63.5	nm

This material is reserved for educational use only, not allowed for commercial use.
Forbidden to modify the content, and cite the document when use.

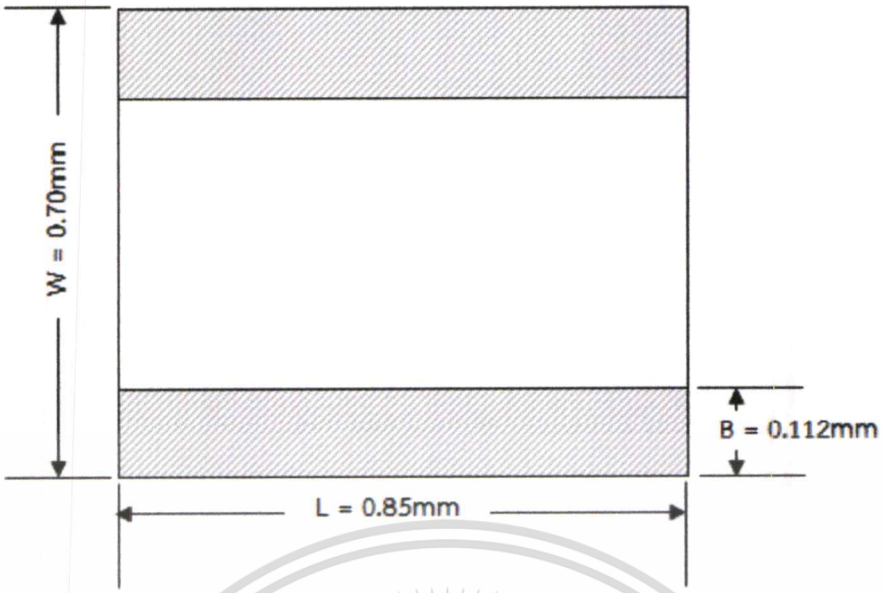

Fig 5.1 the FEMTO form factor of slider dimension for Rail-pad

5.2 Simulation Result for Rail-pad

5.2.1 Influence of disk velocity on static characteristics

The comparison of flying height between helium and air is shown in Fig 5.2, this is focused on 20°C and loading force 24mN by varying the disk velocity from 5000RPM to 15,000RPM. It found that the disk velocity is effect to flying height and the trend of flying height is increased when disk velocity is increased due to larger mass flow rate. As demonstrated in Fig 5.2, the disk velocity significantly influences the flying height in the case of helium with leading edge. With the same velocity, helium can provided low flying height. This is because the effect of the dynamic viscosity, shear stress and air bearing properties. The benefit from this is the capacity of read/write process can be increased due to the slider head can close to disk surface.

This material is reserved for educational use only, not allowed for commercial use.
Forbidden to modify the content, and cite the document when use.

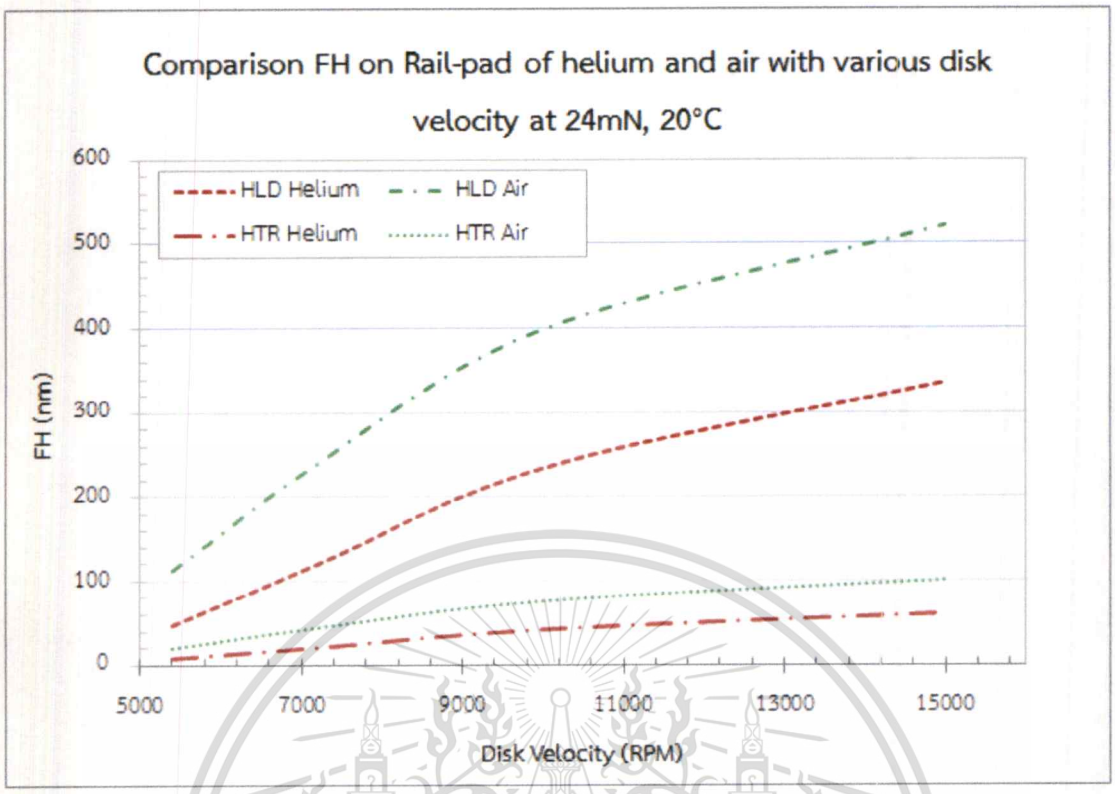

Fig 5.2 Comparison FH on Rail-pad of helium and air with various disk velocities at 24mN, 20°C

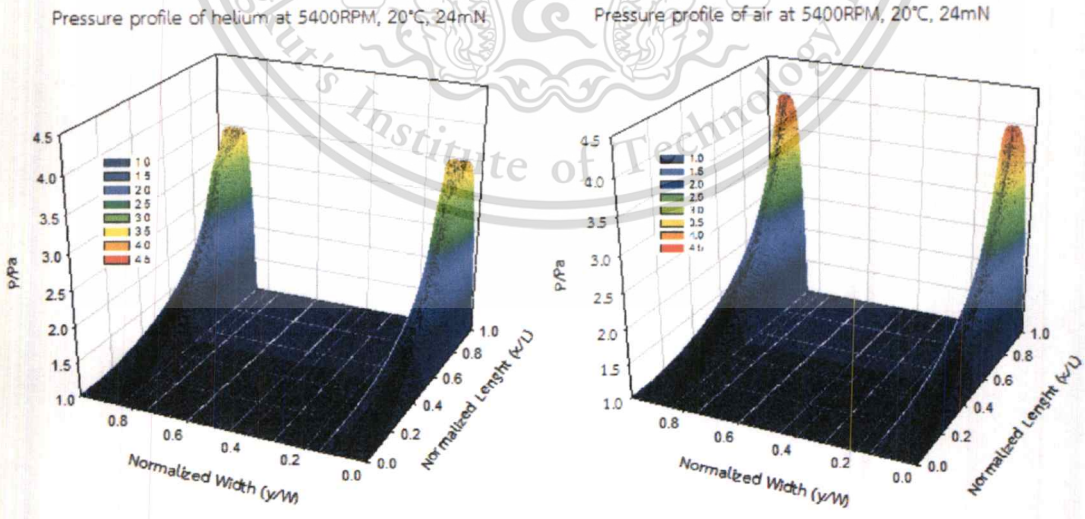

Fig 5.3 Comparison on the pressure distribution along the slider head of helium and air at 5400RPM, 20°C, 24mN

This material is reserved for educational use only, not allowed for commercial use.
Forbidden to modify the content, and cite the document when use.

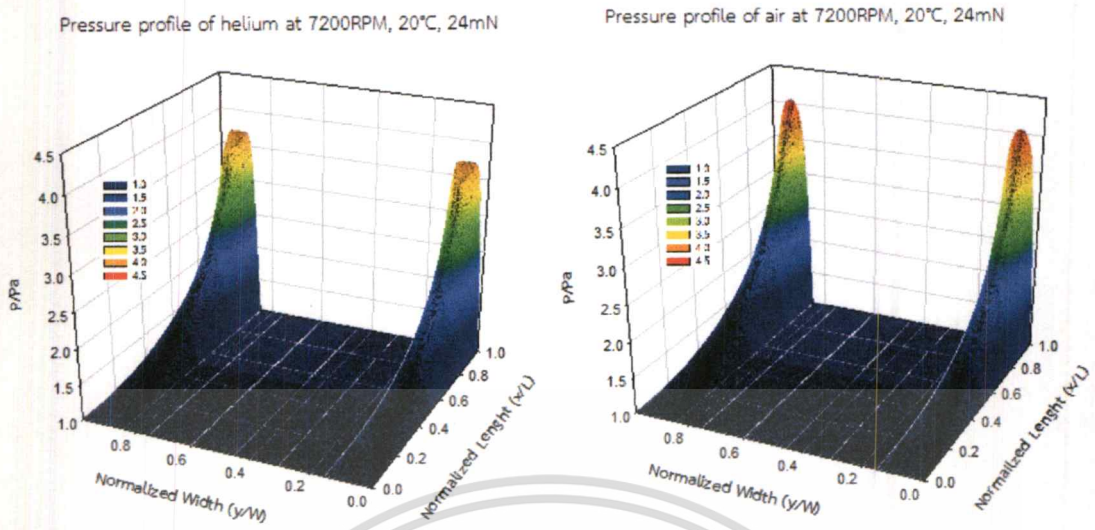

Fig 5.4 Comparison on the pressure distribution along the slider head of helium and air at 7200RPM, 20°C, 24mN

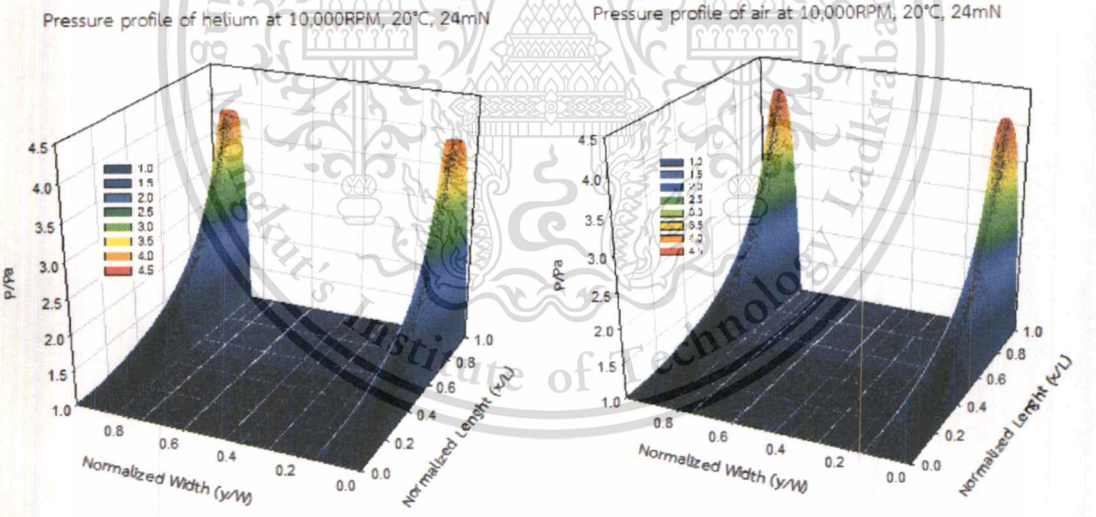

Fig 5.5 Comparison on the pressure distribution along the slider head of helium and air at 10,000RPM, 20°C, 24mN

This material is reserved for educational use only, not allowed for commercial use.
Forbidden to modify the content, and cite the document when use.

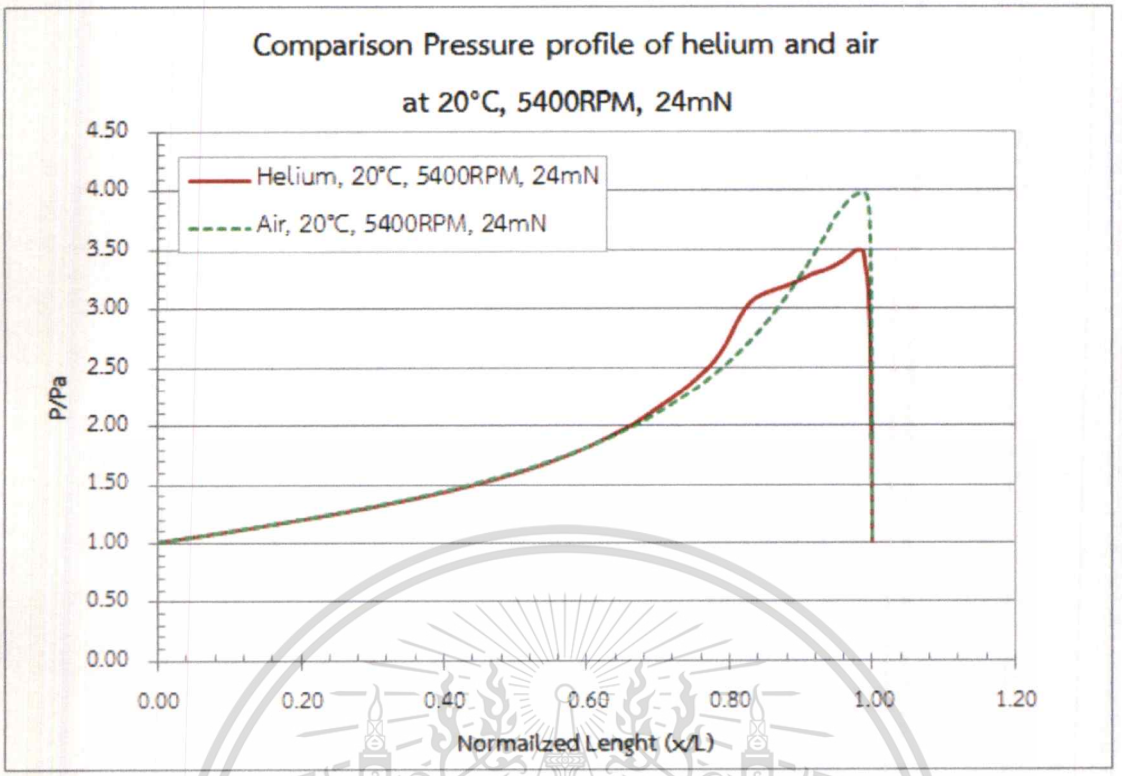

Fig 5.6 Comparison on the pressure distribution along the slider head of helium and air at 5400RPM, 20°C, 24mN

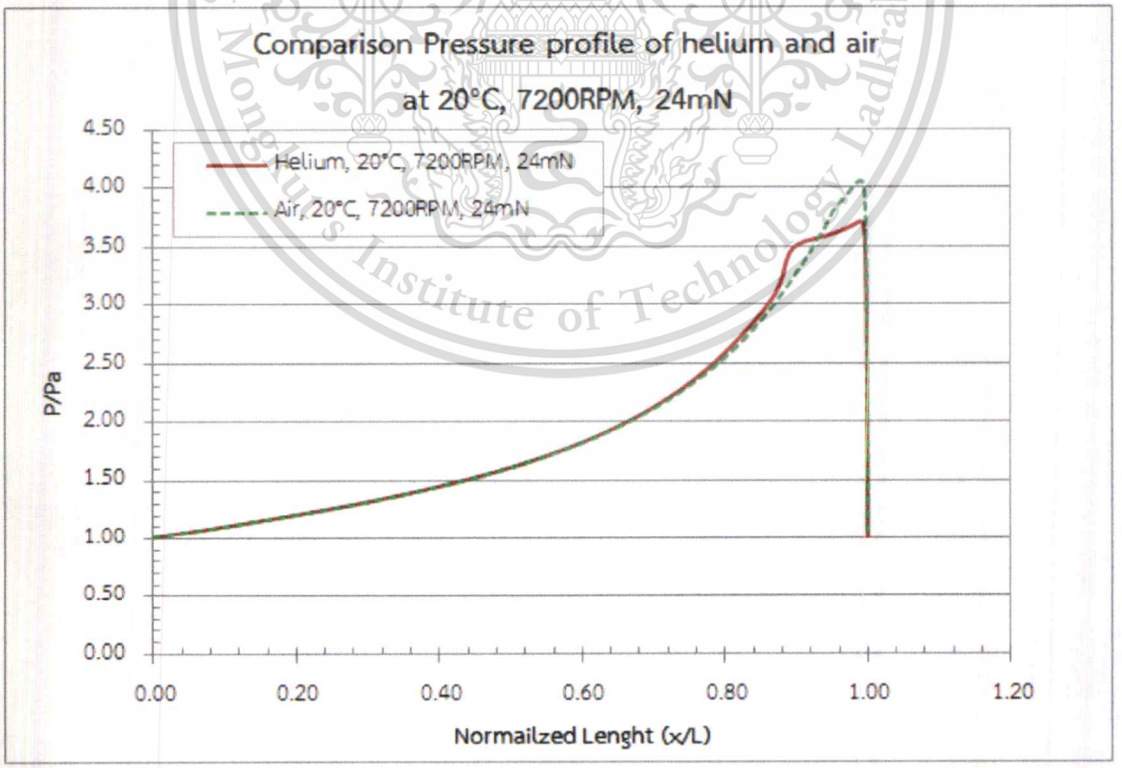

Fig 5.7 Comparison on the pressure distribution along the slider head of helium and air at 7200RPM, 20°C, 24mN

This material is reserved for educational use only, not allowed for commercial use.
Forbidden to modify the content, and cite the document when use.

Fig 5.3 until Fig 5.5 exhibit the pressure distribution along the slider lenght with contour plot for helium and air at 20°C, 24mN, 5400RPM, 7200RPM and 10,000RPM, respectively. The pressure is affected when the disk velocity is changed. At higher velocity is provided a low pressure at the trailing edge of the slider head for both helium and air.

By the way, in same disk velocity pressure of helium is slightly lower than air. In Fig 5.6 until 5.8 showed comparison between helium and air in each disk velocity, 544RPM, 7200RPM and 10,000RPM, respectively. This is because in high disk velocity provided high air bearing number then the pressure has to reduce in order to balance mass conservation.

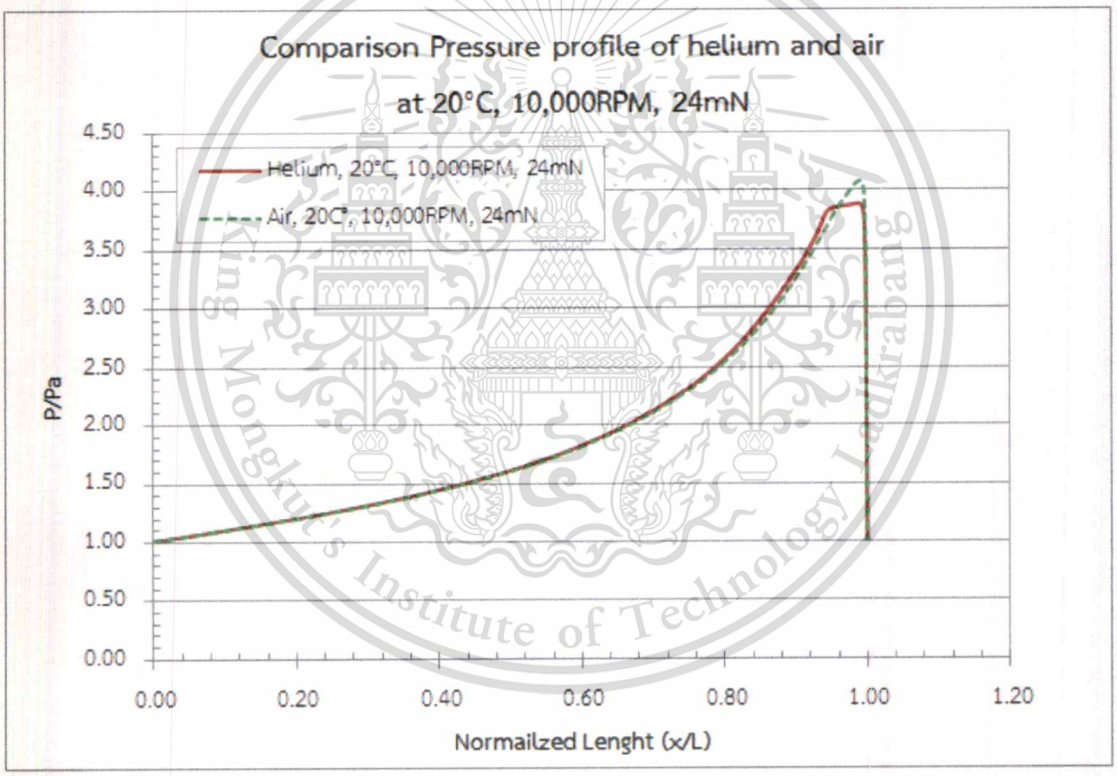

Fig 5.8 Comparison on the pressure distribution along the slider head of helium and air at 10,000RPM, 20°C, 24mN

This material is reserved for educational use only, not allowed for commercial use.
Forbidden to modify the content, and cite the document when use.

5.2.2 Influence of loading force on static characteristics

The comparison of flying height of helium and air with various loading force is shown in Fig 5.9. The simulation is focus only on 20°C and disk velocity 5400RPM by various loading force from 20mN and 24mN. It found that the loading force is significant effect to flying height at leading edge and the trend of flying height is decreased when the loading force is increased due to high pressure under slider head. As demonstrated in Fig 5.9, the loading force significantly influences the flying height in the case of helium. With the same loading force, helium can provided low flying height. This is because the effect of the density and dynamic viscosity of helium.

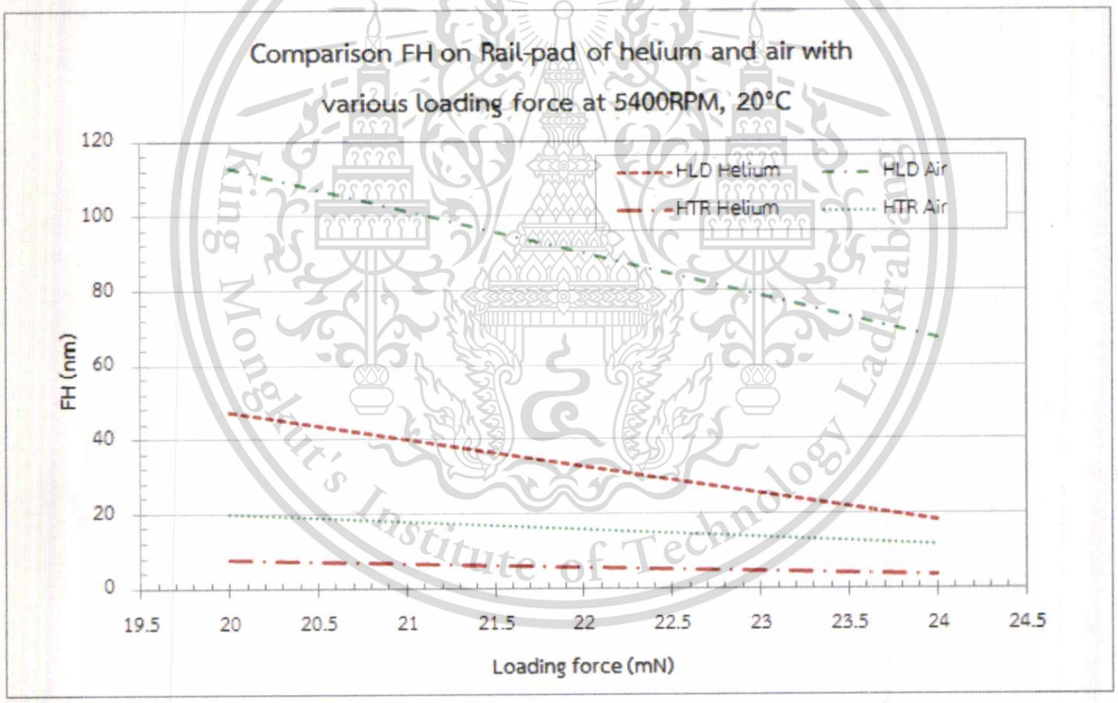

Fig 5.9 FH comparison between helium and air with loading force change of Rail-pad

This material is reserved for educational use only, not allowed for commercial use.
Forbidden to modify the content, and cite the document when use.

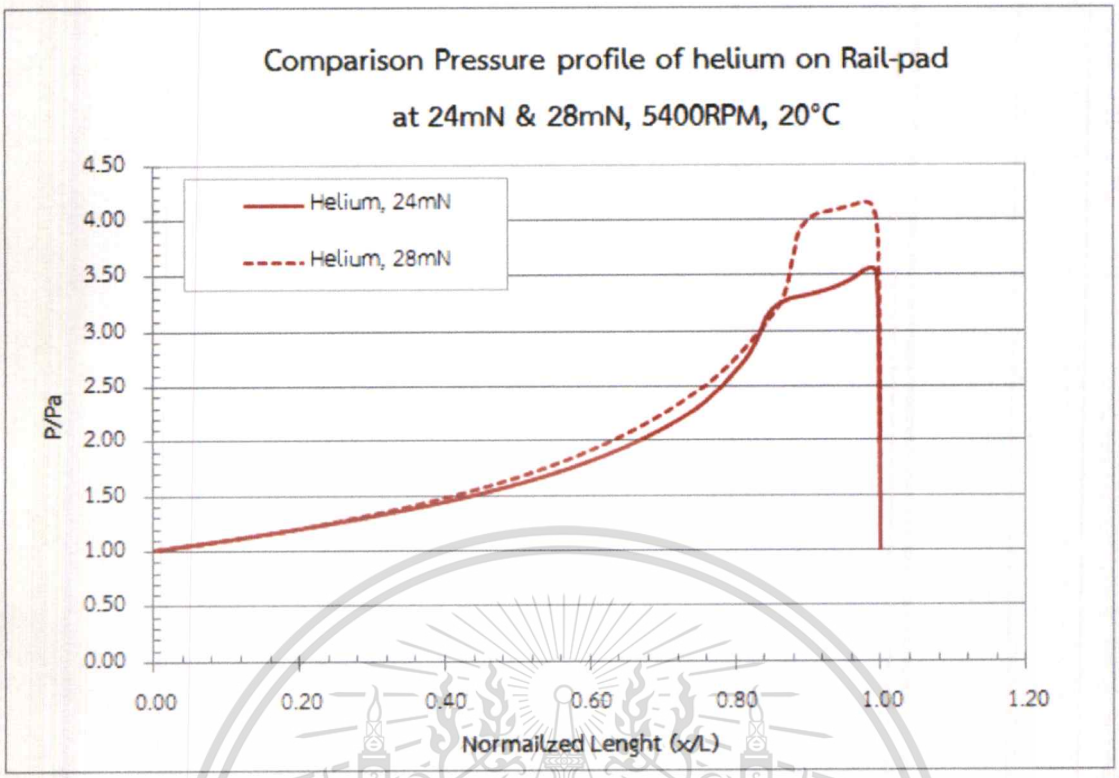

Fig 5.10 Comparison pressure profile of helium on Rail-pad at 24mN & 28mN, 5400RPM, 20°C

Compared on pressure profile of helium at 24mN and 28mN force (per Fig 5.10) will see in 28mN force is provided high maximum pressure more than 24mN forces.

5.2.3 Influence of temperature on static characteristics

The comparison of flying height on Rail-pad for helium and air with various temperatures at 5400RPM, 24mN is showed as Fig. 5.10. The temperature is varying from 20°C to 500°C. It found that the inside temperature is effect to flying height and the trend of flying height is increased when the temperature is increased due to high pressure under slider head. As demonstrated in Fig 5.10, the temperature significantly influences the flying height in both helium and air. With the same temperature, helium can provided low flying height. This is because the effect of the thermal conductivity properties.

This material is reserved for educational use only, not allowed for commercial use.
Forbidden to modify the content, and cite the document when use.

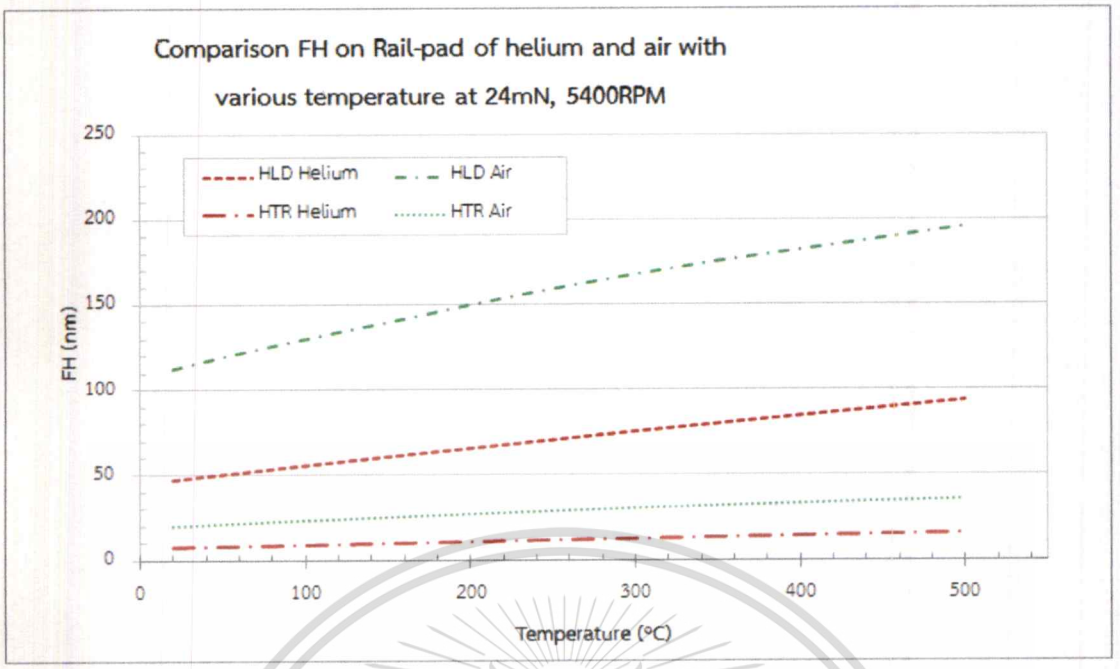

Fig 5.11 FH comparison between helium and air with temperature change of Rail-pad

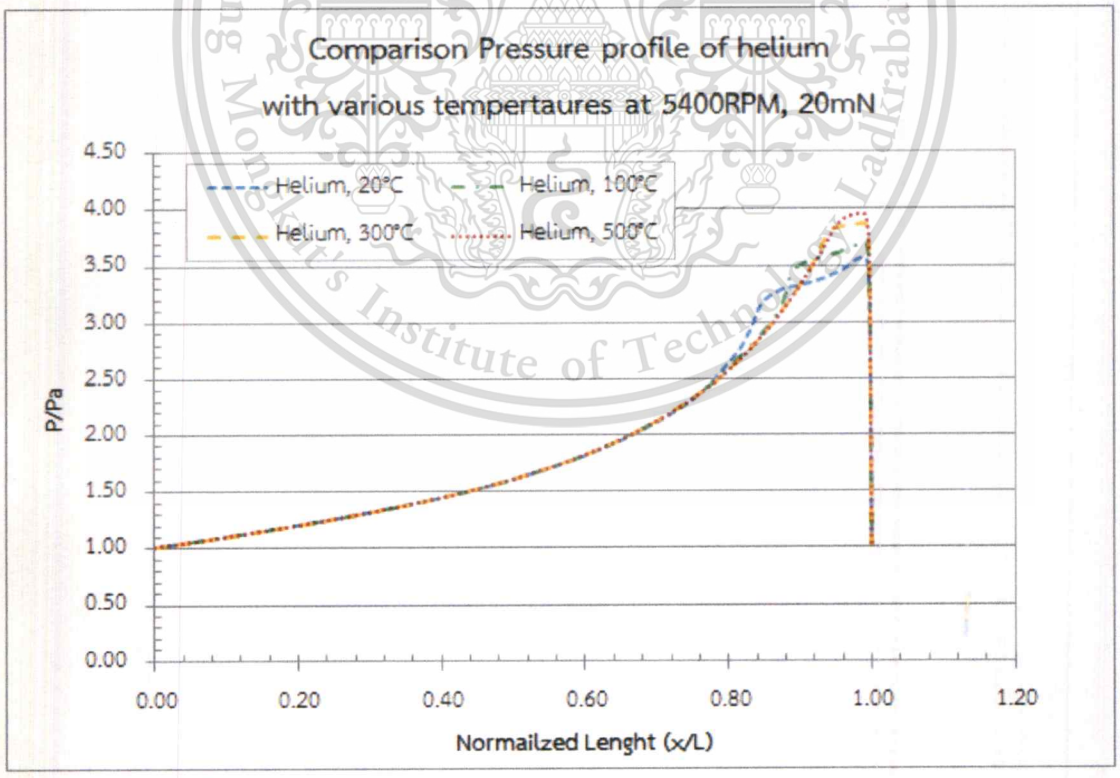

Fig 5.12 Comparison Pressure profile of helium on Rail-pad with various temperatures at 5400RPM, 24mN

This material is reserved for educational use only, not allowed for commercial use.
Forbidden to modify the content, and cite the document when use.

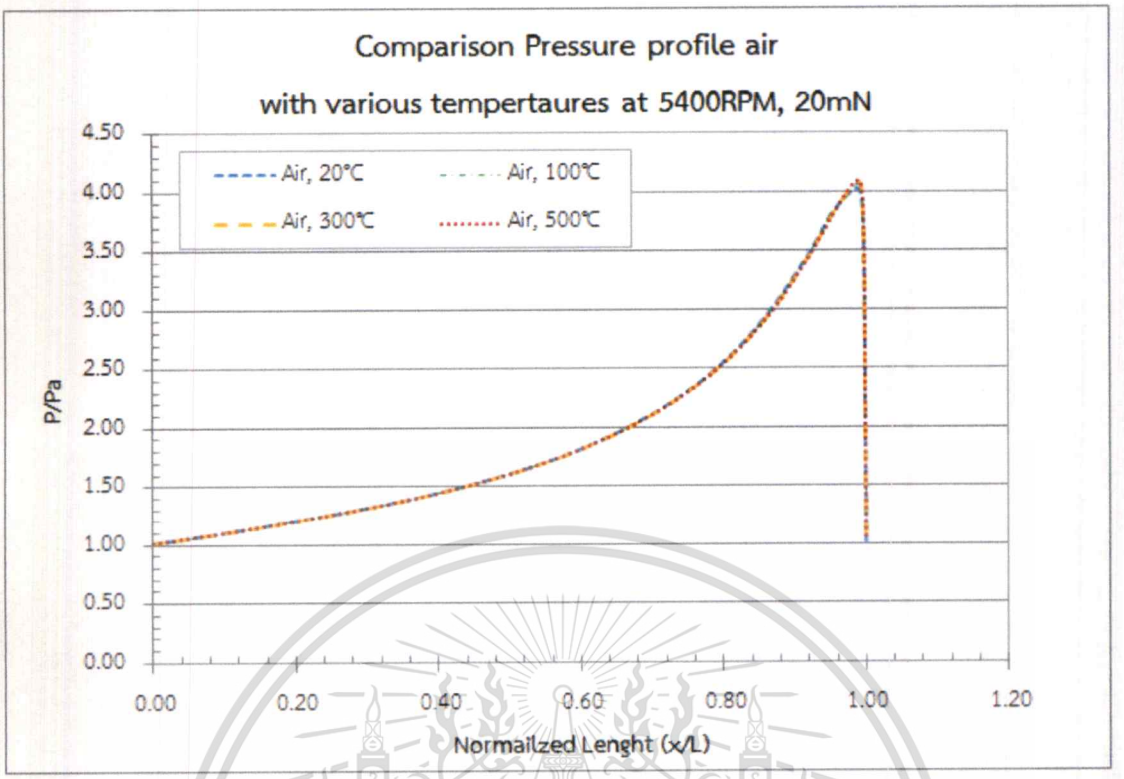

Fig 5.13 Comparison Pressure profile of air on Rail-pad with various temperatures at 5400RPM, 24mN

In Fig 5.11 showed the flying height comparison of helium on Rail-pad when the temperature is changed. The high temperature is investigated to see the significant effected with flying height at leading edge. For helium, the pressure profile is increased with temperature increased while the maximum pressure in air is quiet comparable (per Fig. 5.12 and Fig 5.13, respectively). This is because of the thermal conductivity of helium is larger than the air.

Fig 5.14 until 5.17 showed pressure profile comparison between helium and air with temperature is changed in contour plot.

This material is reserved for educational use only, not allowed for commercial use.
Forbidden to modify the content, and cite the document when use.

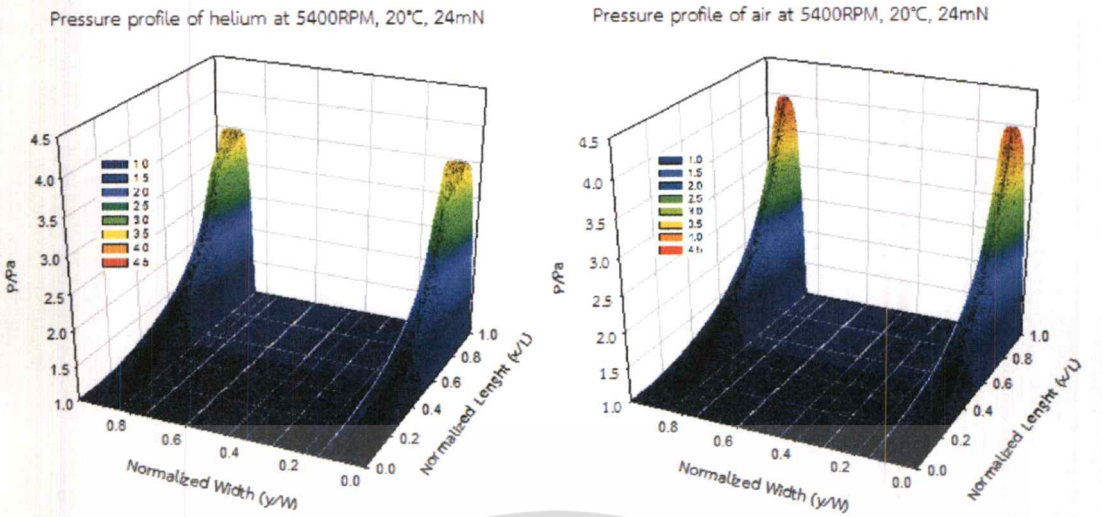

Fig 5.14 Comparison on the pressure profile along the slider head of helium and air at 5400RPM, 20°C, 24mN

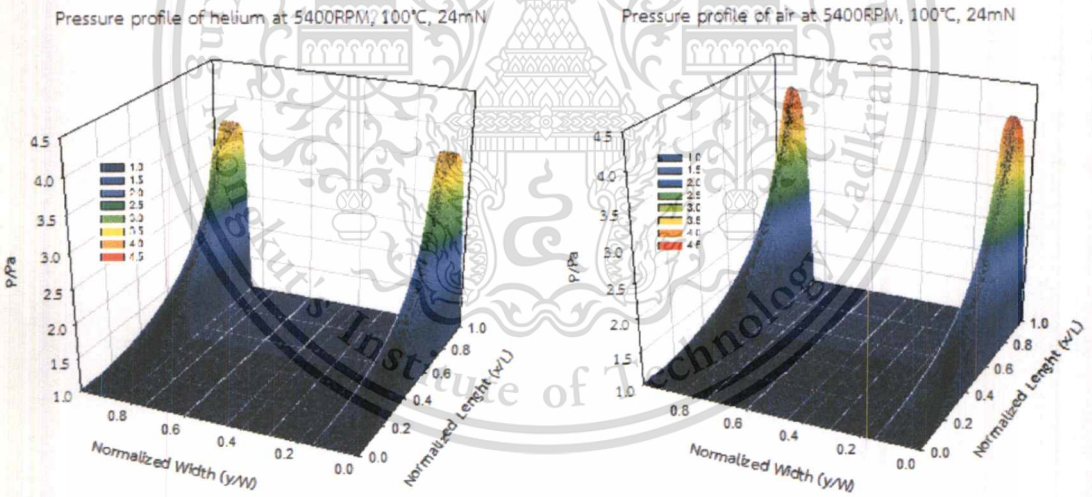

Fig 5.15 Comparison on the pressure profile along the slider head of helium and air at 5400RPM, 100°C, 24mN

This material is reserved for educational use only, not allowed for commercial use.
Forbidden to modify the content, and cite the document when use.

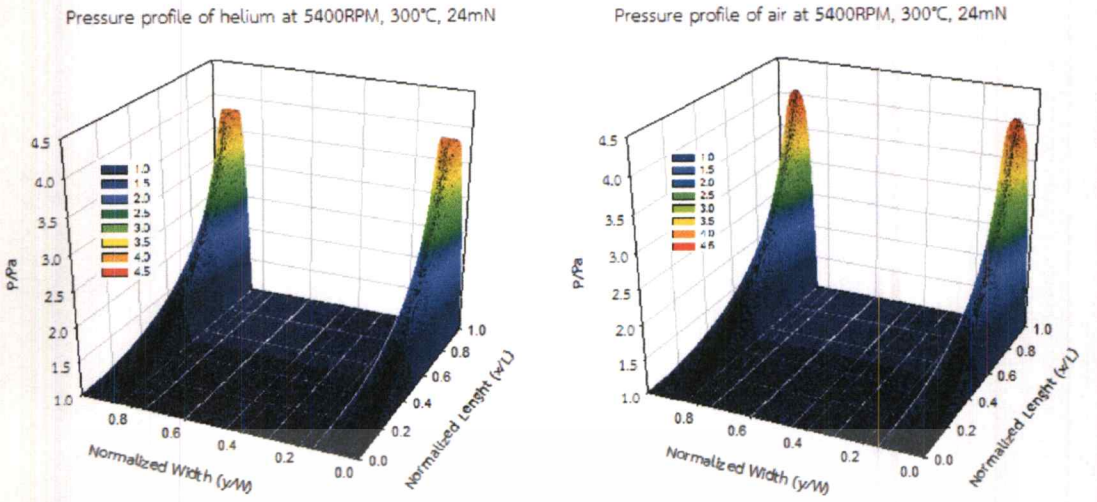

Fig 5.16 Comparison on the pressure profile along the slider head of helium and air at 5400RPM, 300°C, 24mN

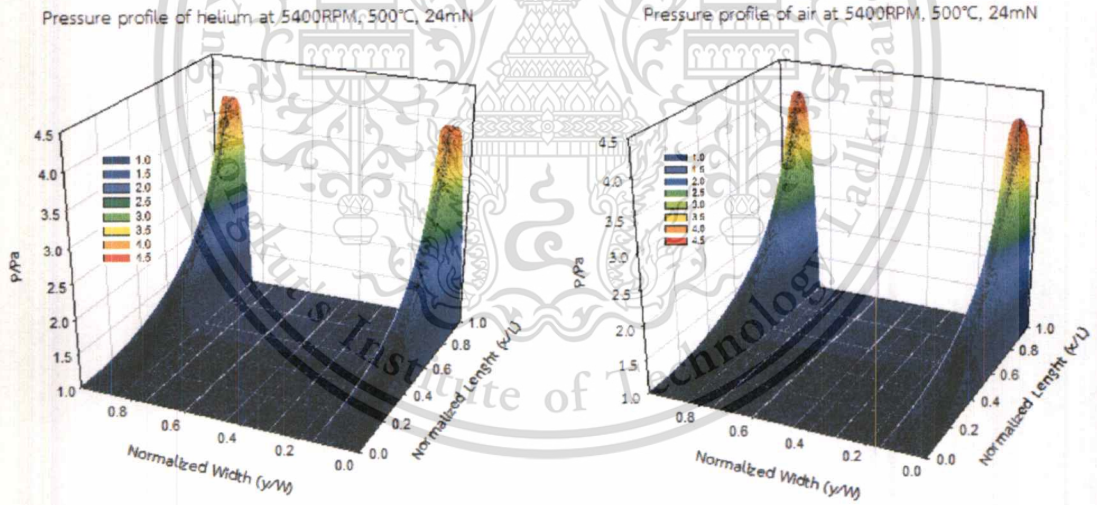

Fig 5.17 Comparison on the pressure profile along the slider head of helium and air at 5400RPM, 500°C, 24mN

This material is reserved for educational use only, not allowed for commercial use.
Forbidden to modify the content, and cite the document when use.

5.3 Defined the parameter for Tri-pad

In this study we focused on the characteristic of flying height when the parameters in the list are changed, in Table 5.2. The simulation is performed with the FEMTO form factor of slider dimension, 700μm in width and 850μm in lenght (Fig 5.18) on Tri-pad ABS.

TABLE 5.2

THE PARAMETERS OF THE SLIDER HEAD FOR SIMULATION FOR TRI-PAD

Symbol	Discretion	Dimension		Unit
		Helium	Air	
L	Slider lenght	850		μm
W	Slider width	700		μm
B_1	Slider rail width	200		μm
B_2	Slider rail width	200		μm
X_1	Slider rail lenght	650		μm
X_2	Slider rail lenght	100		μm
U	Disk velocity (2.5")	4000 - 10000		PRM
f_0	Loading force	20-25		Nm
P_a	Ambient Pressure	1.013x10-5		Pa
T	Temperature	20 - 160		$°C$
η	Viscosity	$1.956x10^{-5}$	1.821x10-5	$Pa.s$
ρ	Density	0.167	1.205	kg/m^3
k	Thermal Conductivity	0.148	0.026	W/mk
λ	Mean Free Path	165.5	63.5	nm

This material is reserved for educational use only, not allowed for commercial use.
Forbidden to modify the content, and cite the document when use.

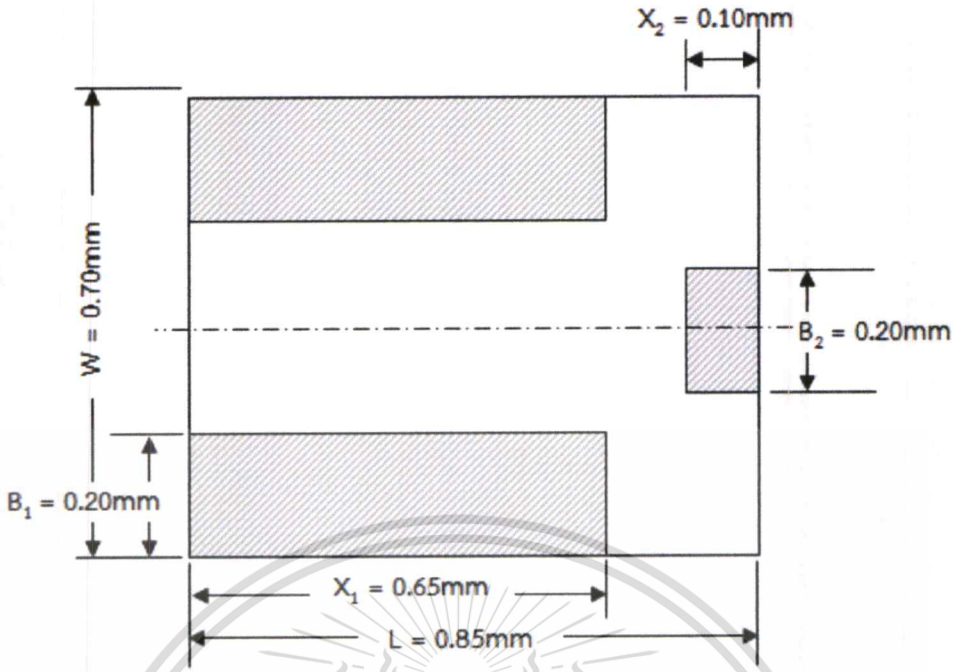

Fig 5.18 The FEMTO form factor of slider dimension for Tri-pad

5.3.1 Influence of disk velocity on static characteristics

Fig 5.19 compared flying height on Tri-pad of helium and air with various disk velocities at 20mN force and 20°C. The simulation results showed the flying height on helium is smaller than the air. Based on the air bearing property, in higher velocity will get the high air bearing number. Then loading force is significant effect on flying height for both helium and air. By the way, if the loading force is not suitable (larger) then the slider head can hit with the disk surface. So, the optimization for best loading force is required.

This material is reserved for educational use only, not allowed for commercial use.
Forbidden to modify the content, and cite the document when use.

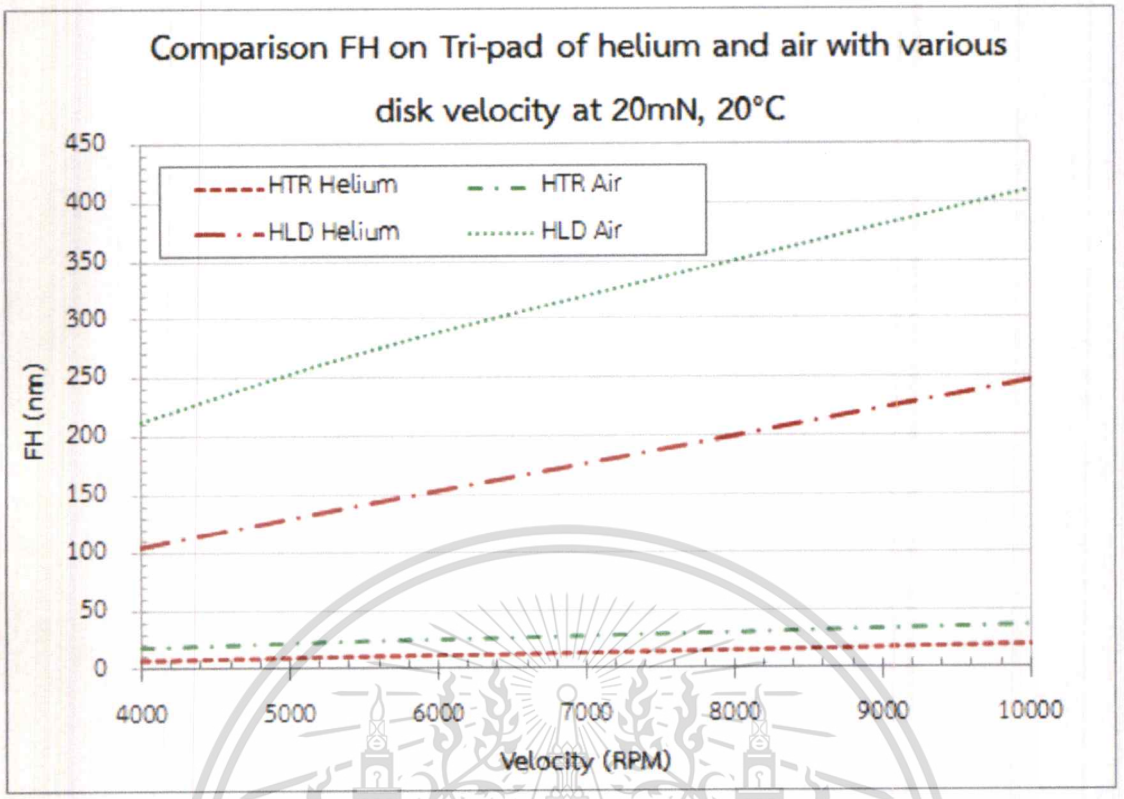

Fig 5.19 Comparison FH on Tri-pas of helium and air with various disk velocities at 20mN, 20°C

When consider on the pressure profile of helium along the slider head at 5400RPM, 7200RPM and 10,000RPM, as showed in Fig 5.20, no significant effect for pressure distribution on helium. As all of them is comparable for maximum pressure for each changed on disk velocity.

In Fig 5.21, 5.22 and 5.23 showed comparison pressure profile of helium and air in each RPM, 5400RPM, 7200RPM and 10,000RPM at 20°C, 20mN loading force, in the same trend of air that pressure is high when disk velocity is increased.

Fig 5.24 and 5.25 showed pressure profile on contour plot for helium and air with various disk velocities, respectively.

This material is reserved for educational use only, not allowed for commercial use.
Forbidden to modify the content, and cite the document when use.

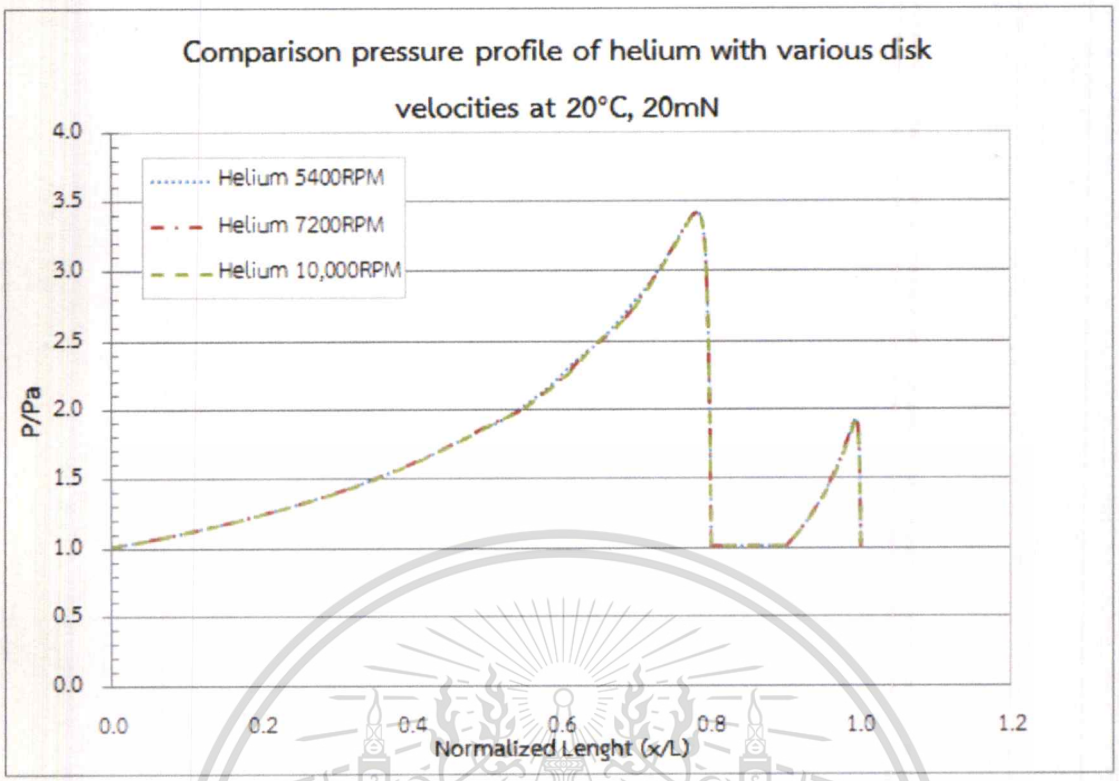

Fig 5.20 Comparison pressure profile of helium with various disk velocities at 20°C, 20mN

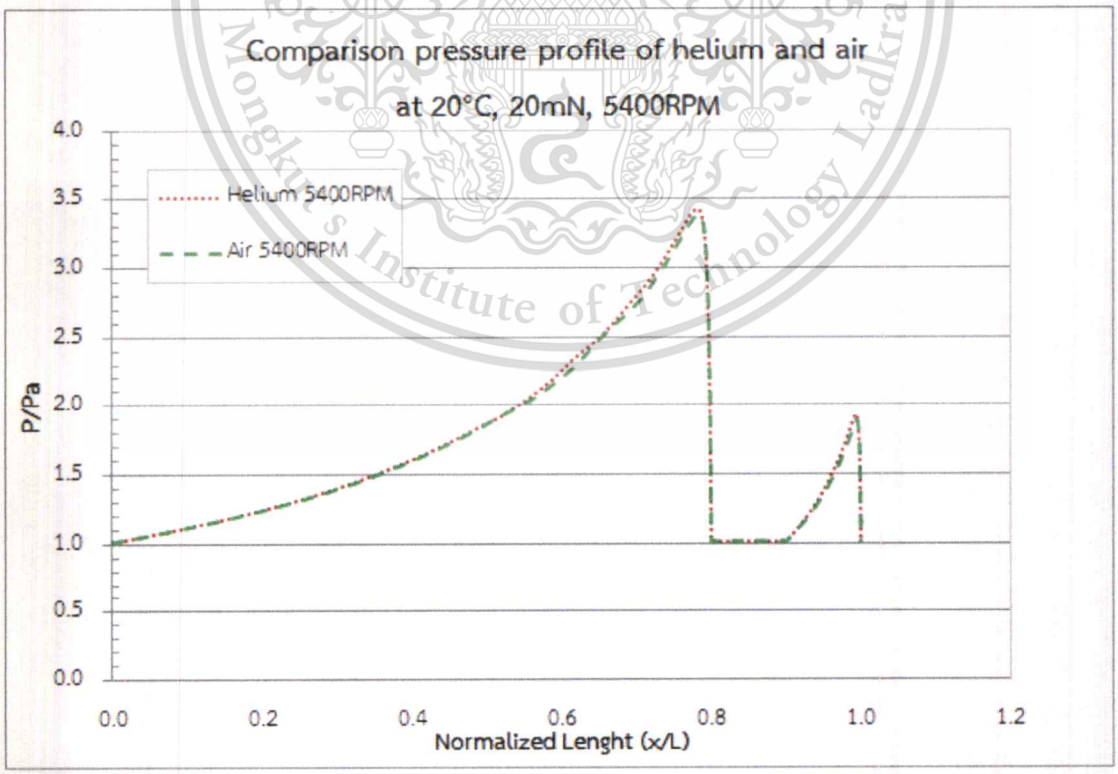

Fig 5.21 Comparison FH on Tri-pad of helium and air at 20°C, 5400RPM, 20mN

Pressure profile of helium at 5400RPM, 20mN, 20°C

This material is reserved for educational use only, not allowed for commercial use.
Forbidden to modify the content, and cite the document when use.

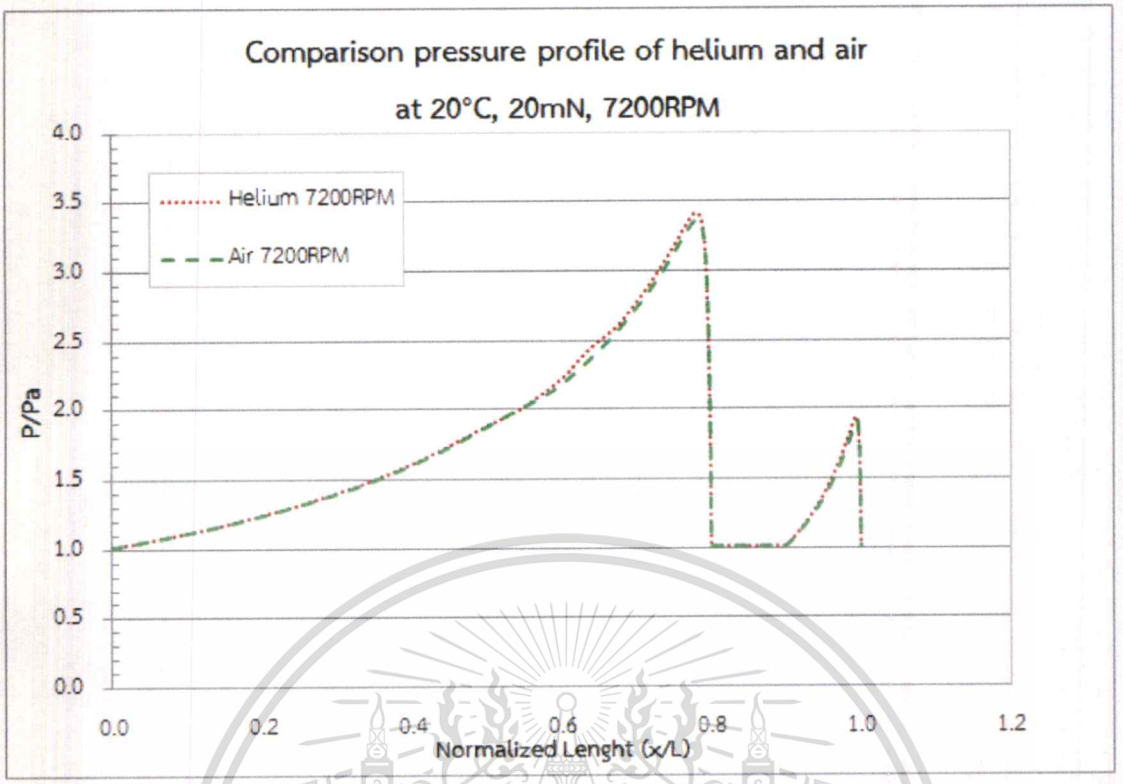

Fig 5.22 Comparison FH on Tri-pad of helium and air at 20°C, 7200RPM, 20mN

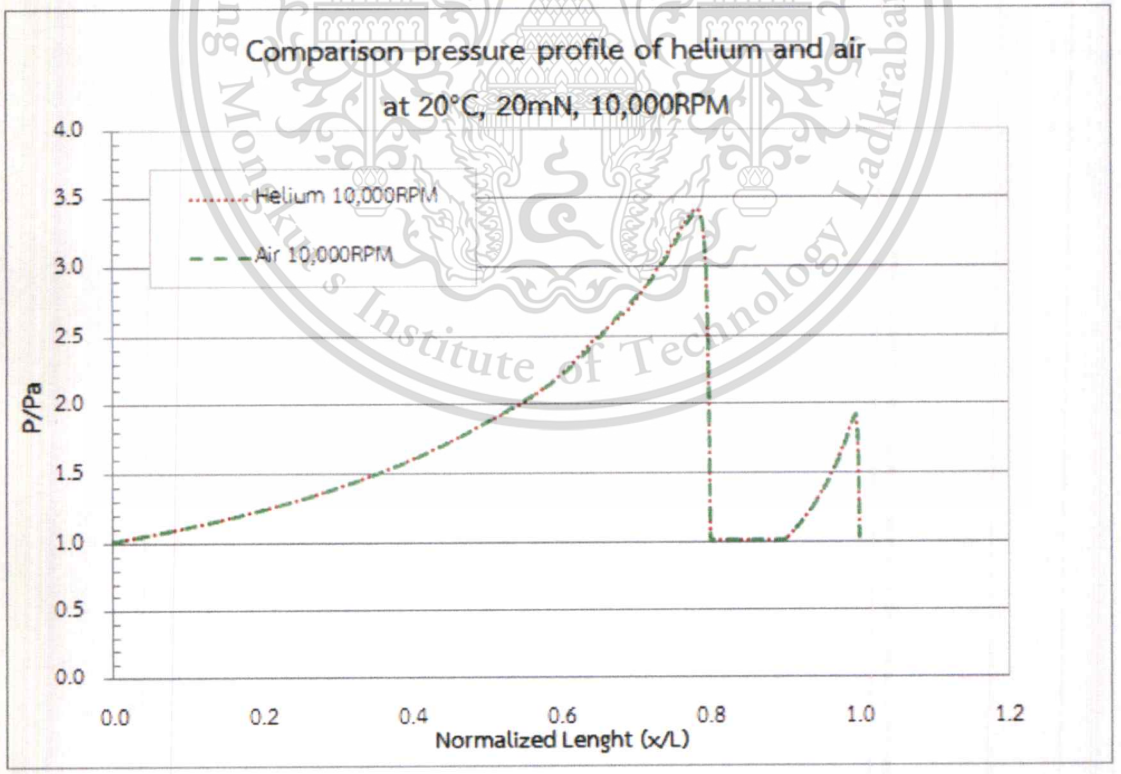

Fig 5.23 Comparison FH on Tri-pad of helium and air at 20°C, 10000RPM, 20mN

This material is reserved for educational use only, not allowed for commercial use.
Forbidden to modify the content, and cite the document when use.

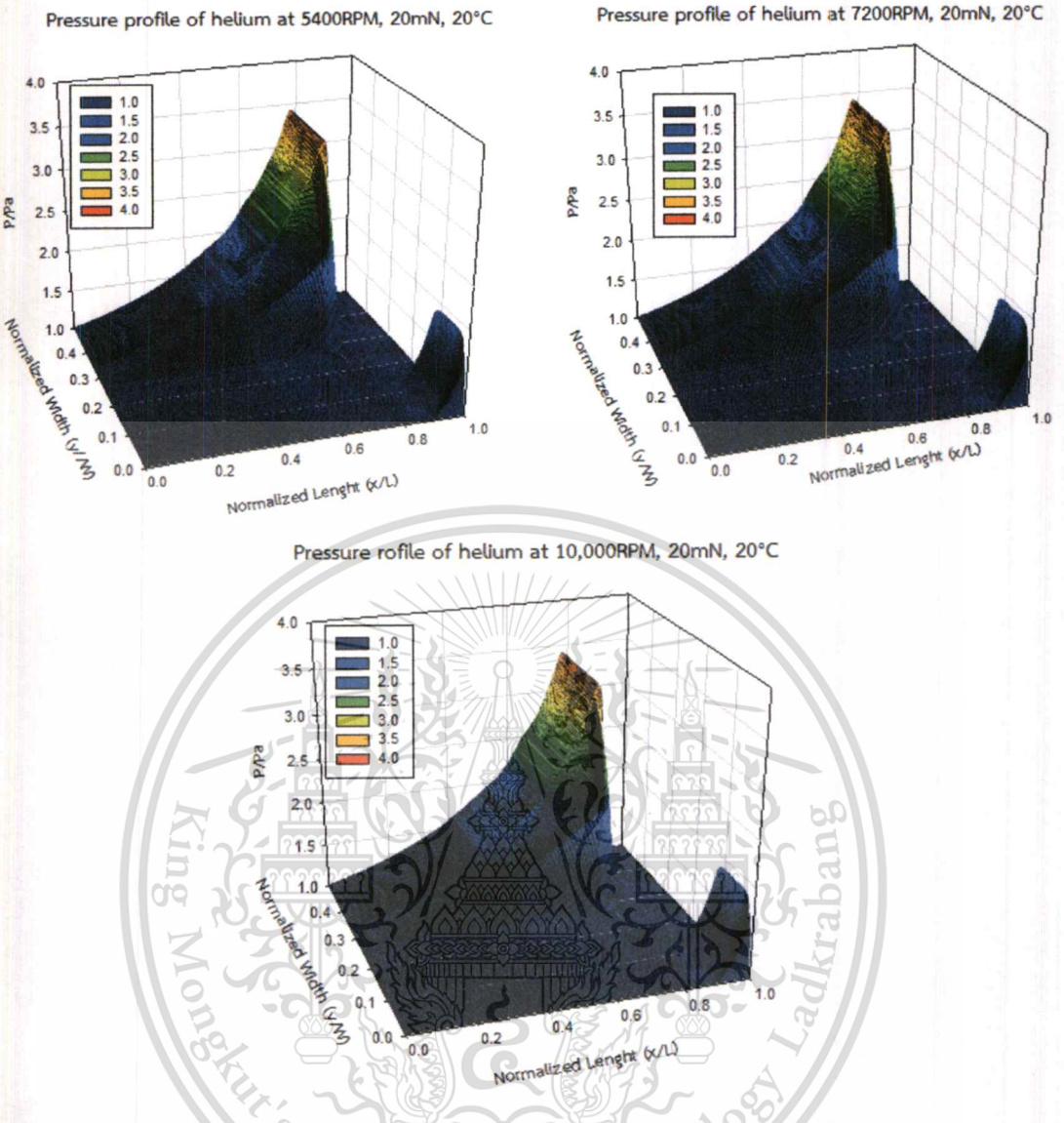

Fig 5.24 Comparison on the pressure profile along the slider head of helium with various disk velocities – 5400RPM, 7200RPM, 10,000RPM

This material is reserved for educational use only, not allowed for commercial use.
Forbidden to modify the content, and cite the document when use.

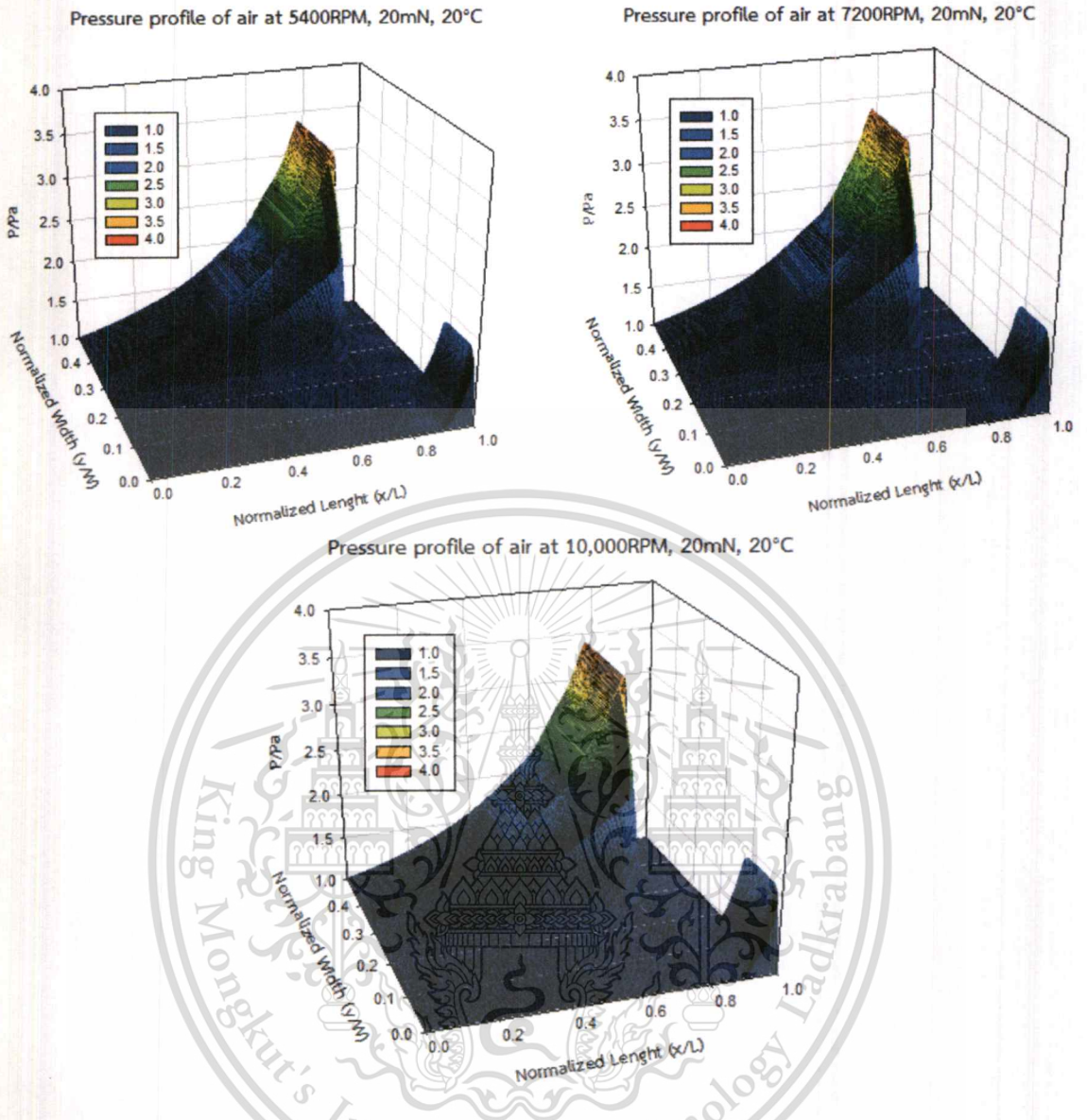

Fig 5.25 Comparison on the pressure profile along the slider head of air with various disk velocities – 5400RPM, 7200RPM, 10,000RPM

This material is reserved for educational use only, not allowed for commercial use.
Forbidden to modify the content, and cite the document when use.

5.3.2 Influence of loading force on static characteristics

The loading force is the one factor that effect to the flying height, from Fig 5.26 showed the loading force can help to reduce the flying height. We can see that at high loading force, the flying height is reduced for both helium and air condition. By the way, if the loading force is large the slider head can be hit to the disk surface. Then the optimization for best loading force is required. When compared between helium and air, we will get lower flying height in the helium. From the simulation result, we can conclude that the helium filled drives is good enough to develop the lower flying height in magnetic recording system.

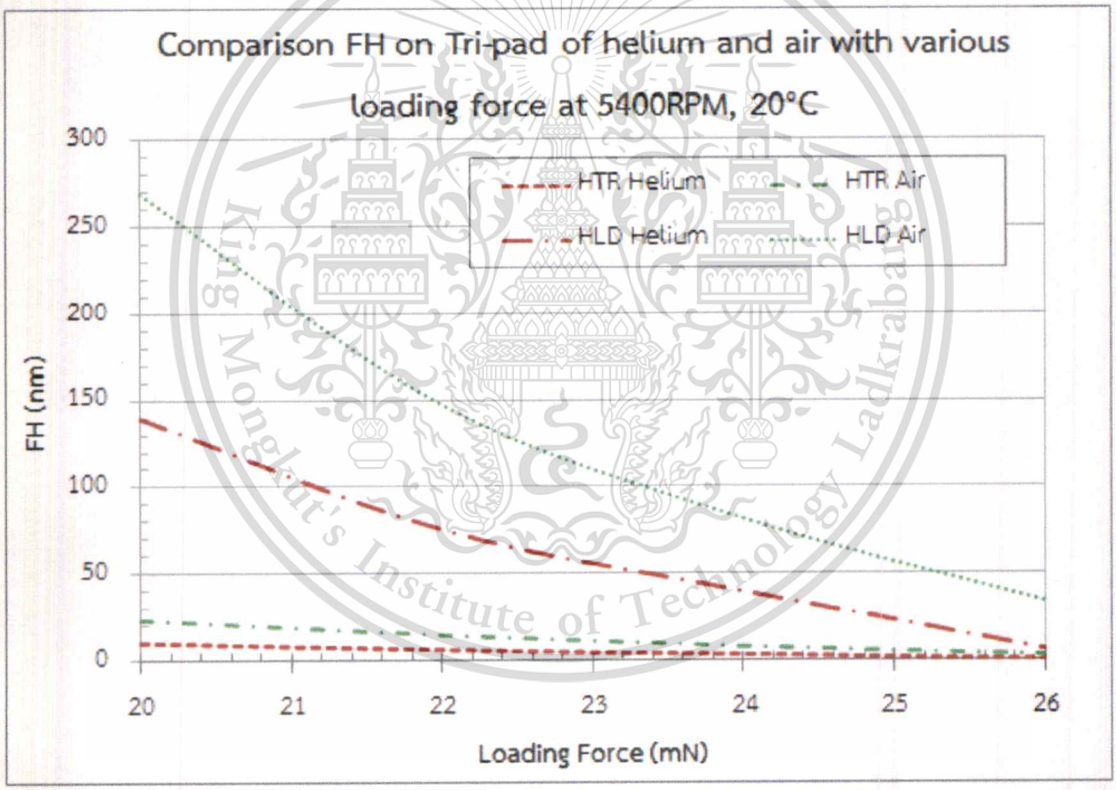

Fig 5.26 Comparison FH on Tri-pas of helium and air with various loading force at 5400RPM, 20°C

This material is reserved for educational use only, not allowed for commercial use.
Forbidden to modify the content, and cite the document when use.

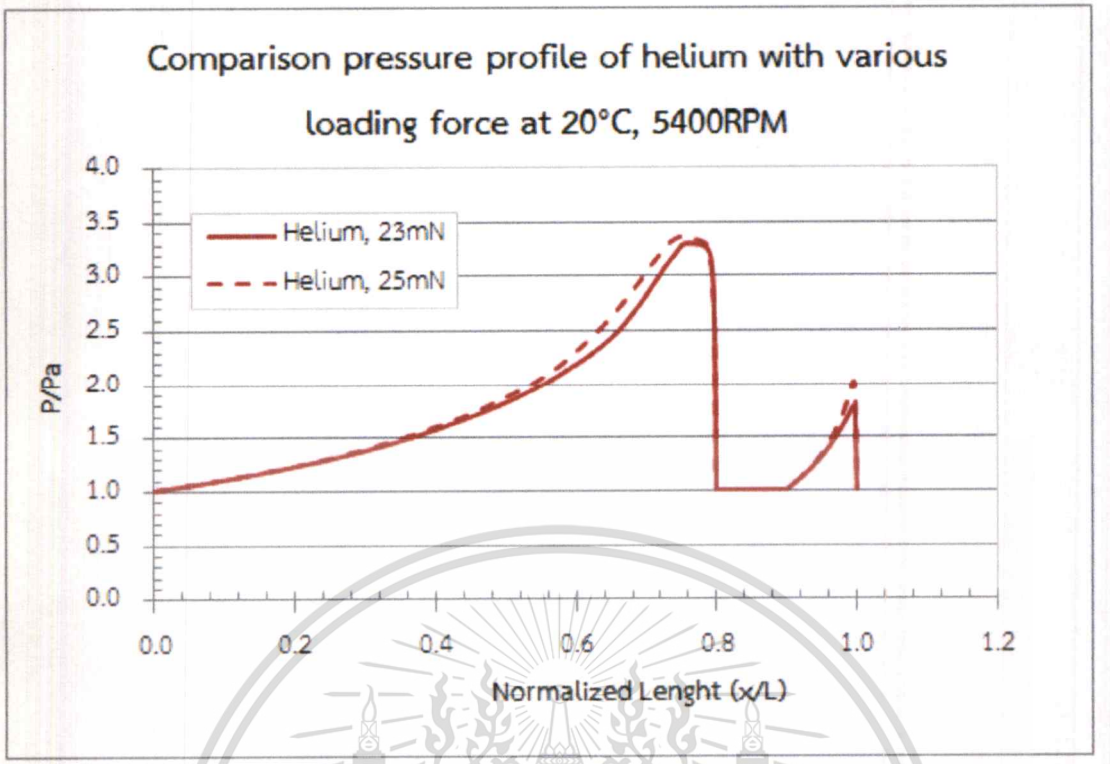

Fig 5.27 Comparison pressure profile on Tri-pad of helium with various loading force at 5400RPM, 20°C

The comparison pressure profile of helium with various loading force at 20°C, 5400RPM by focusing on 23mN and 25mN. We can see that in 25mN, maximum pressure is slightly higher than maximum pressure in 23mN for bigger pad but significant different on small pad at trailling edge (per Fig 5.27). The contour plot is on Fig 5.28, this just for half width of slider head dimension.

This material is reserved for educational use only, not allowed for commercial use.
Forbidden to modify the content, and cite the document when use.

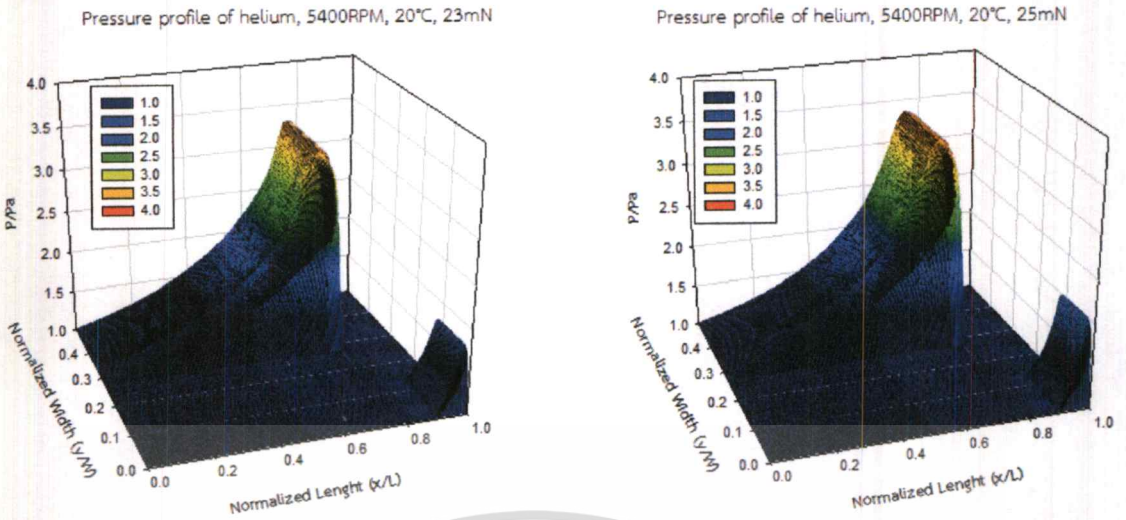

Fig 5.28 Comparison pressure profile on Tri-pad of helium with various loading force (23mN and 25mN) at 5400RPM, 20°C

5.3.3 Influence of temperature on static characteristics

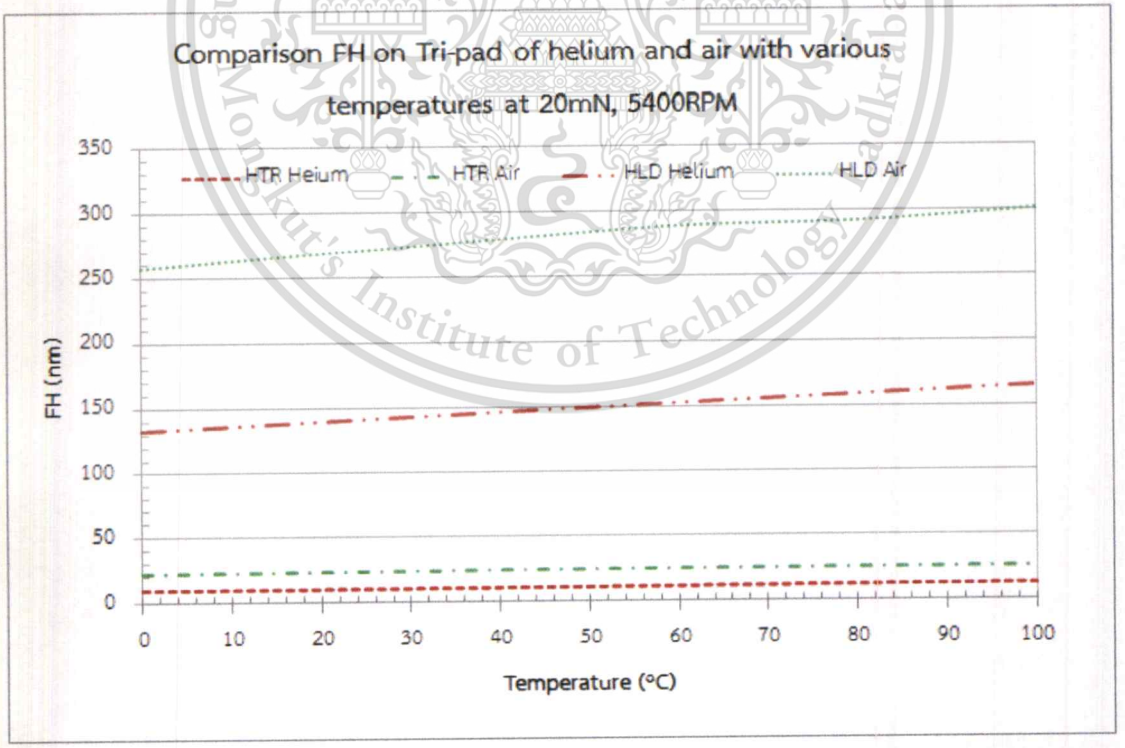

Fig 5.29 Comparison FH on Tri-pad of helium and air with various temperatures

This material is reserved for educational use only, not allowed for commercial use.
Forbidden to modify the content, and cite the document when use.

Flying height comparison between helium and air with various temperatures is showed in Fig 5.29, this one is focus at 20mN force and velocity 5400RPM. In higher temperature, the flying height is slightly increased for both helium and air by the way helium still provided lower flying height when compare with air. This simulation is based on a condition of fully seal drive without leakage problem. The mainly caused by the temperature is effected of the mean free path, which increase the Knudsen number and air bearing number.

Fig 5.30 showed the air bearing number for both helium and air when the temperature is changed. In high temperature provided high air bearing number. Fig 5.31 showed the viscosity on helium and air when the temperature is changed, the viscosity is higher in high temperature. This is same trend for both helium and air due to the viscosity property itself. Also, Fig 5.32 showed that comparison on density of helium and air when the temperature is increased, then density will be decreased.

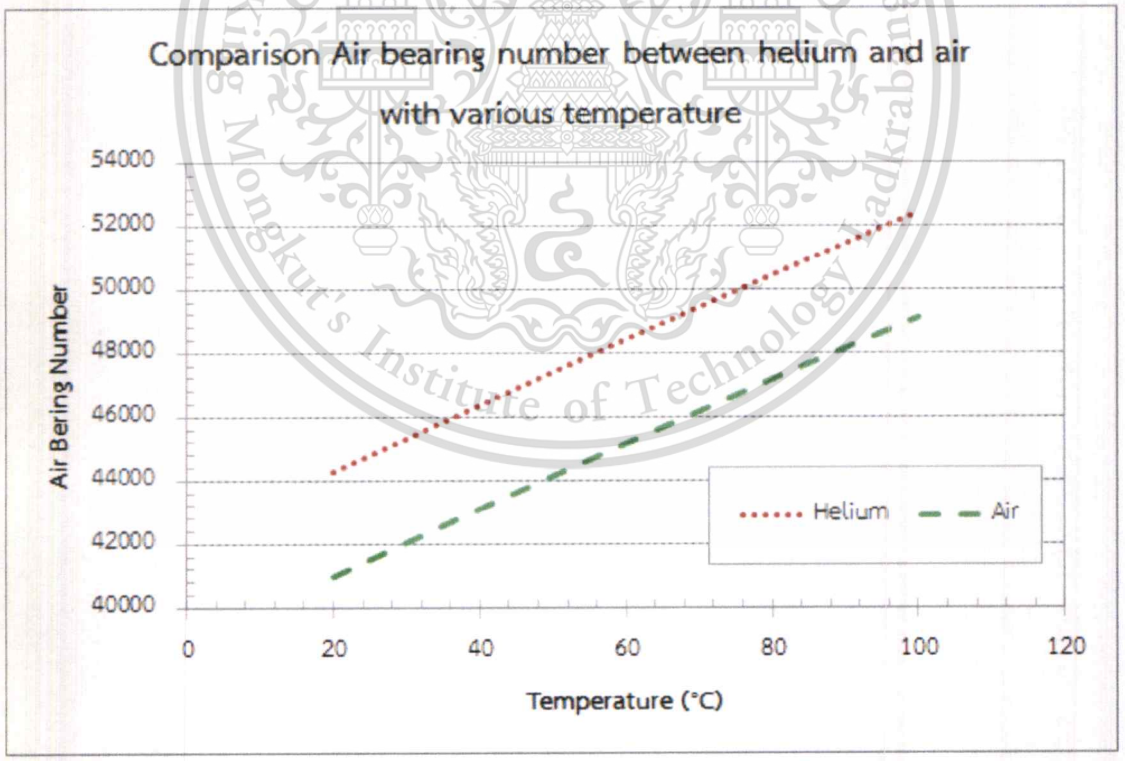

Fig 5.30 Comparison Air bearing number between helium and air with various temperatures

This material is reserved for educational use only, not allowed for commercial use.
Forbidden to modify the content, and cite the document when use.

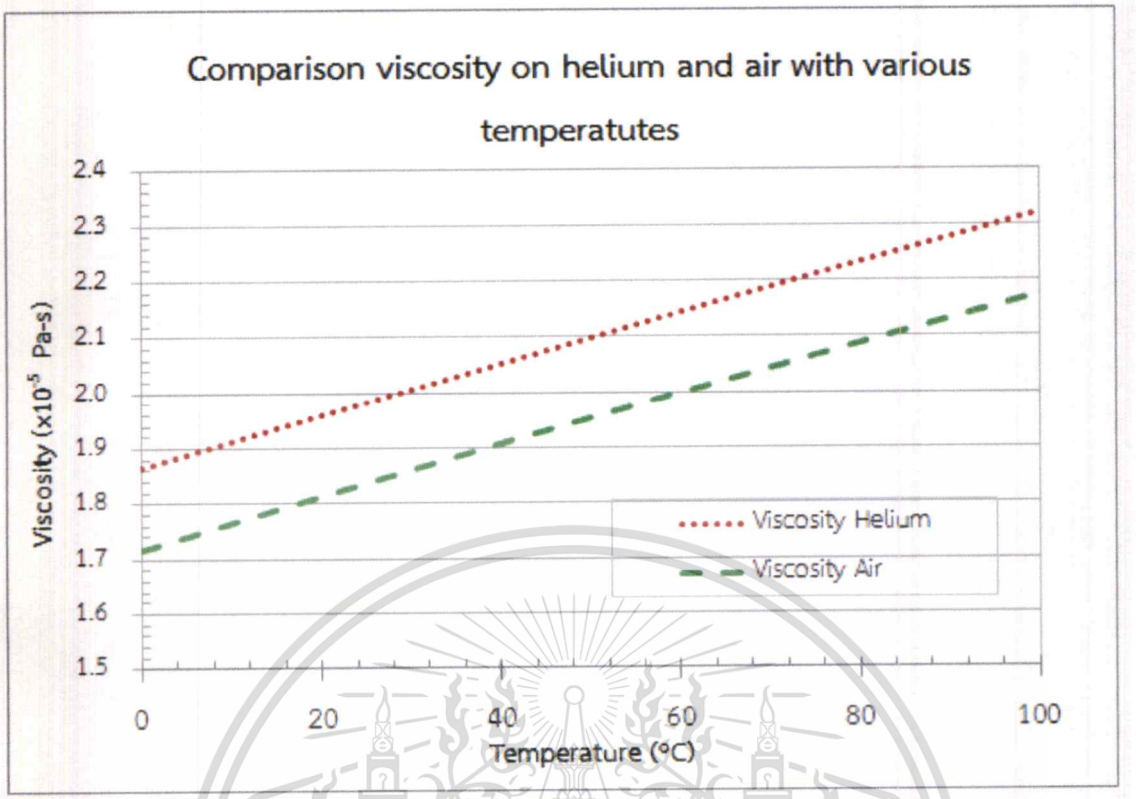

Fig 5.31 Comparison viscosity on helium and air with various temperatures

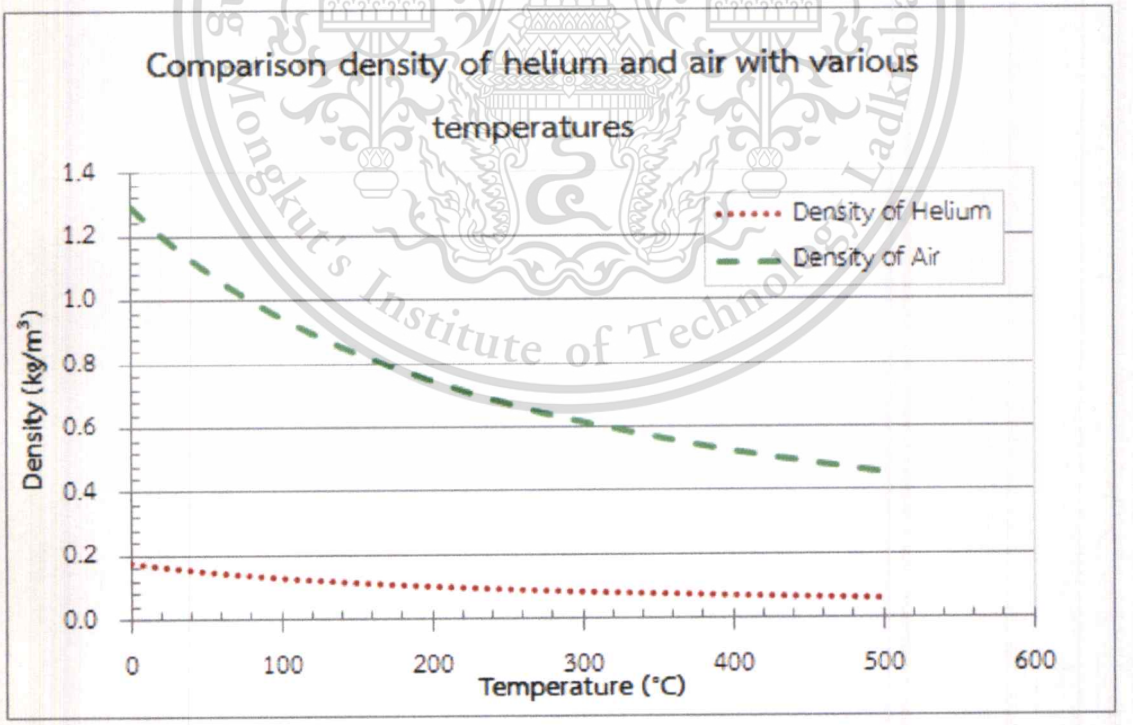

Fig 5.32 Comparison density on helium and air with various temperatures

This material is reserved for educational use only, not allowed for commercial use.
Forbidden to modify the content, and cite the document when use.

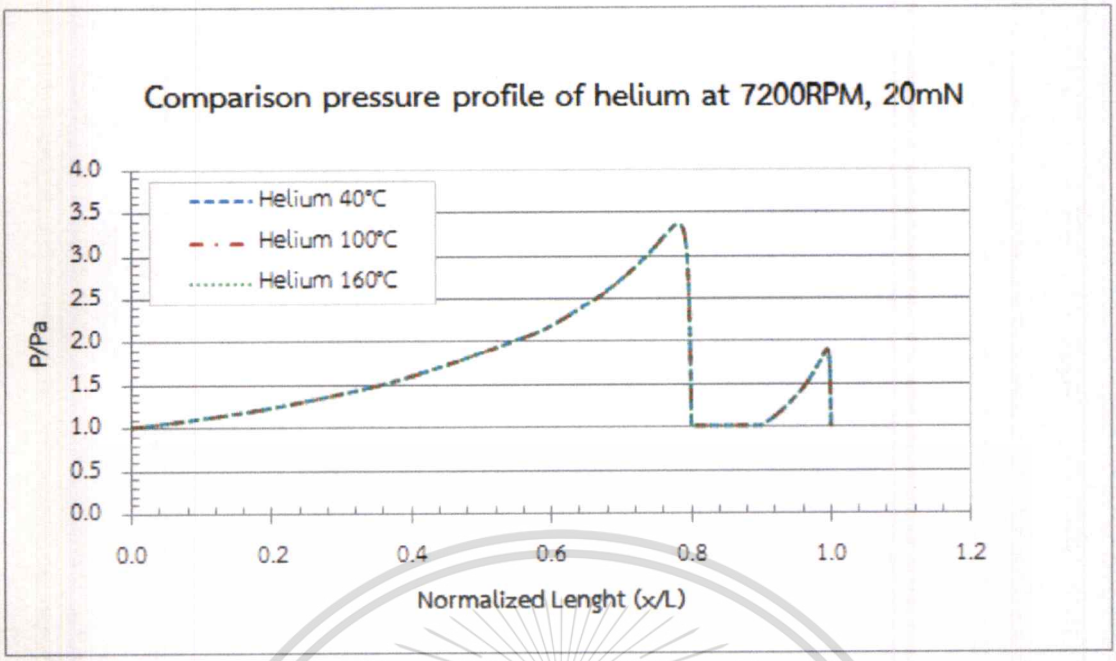

Fig 5.33 Comparison Pressure profile of helium with various temperatures at 7200RPM, 20mN

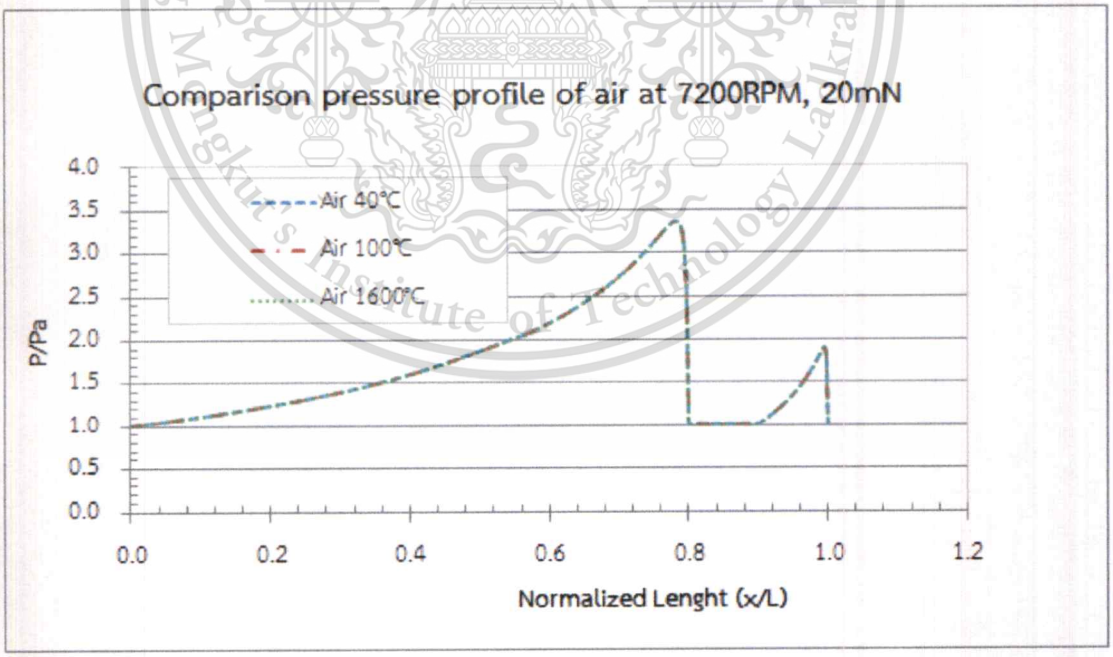

Fig 5.34 Comparison Pressure profile of air with various temperatures at 7200RPM, 20mN

This material is reserved for educational use only, not allowed for commercial use.
Forbidden to modify the content, and cite the document when use.

Fig 5.33 and Fig 5.34 showed pressure profile on helium and air at 7200RPM, 20mN with various temperatures, respectively. By the way, the maximum pressure for both helium and air is not difference when the temperature increased because the temperature range is not much changed. Fig 5.35 showed contour plot for helium with various temperatures.

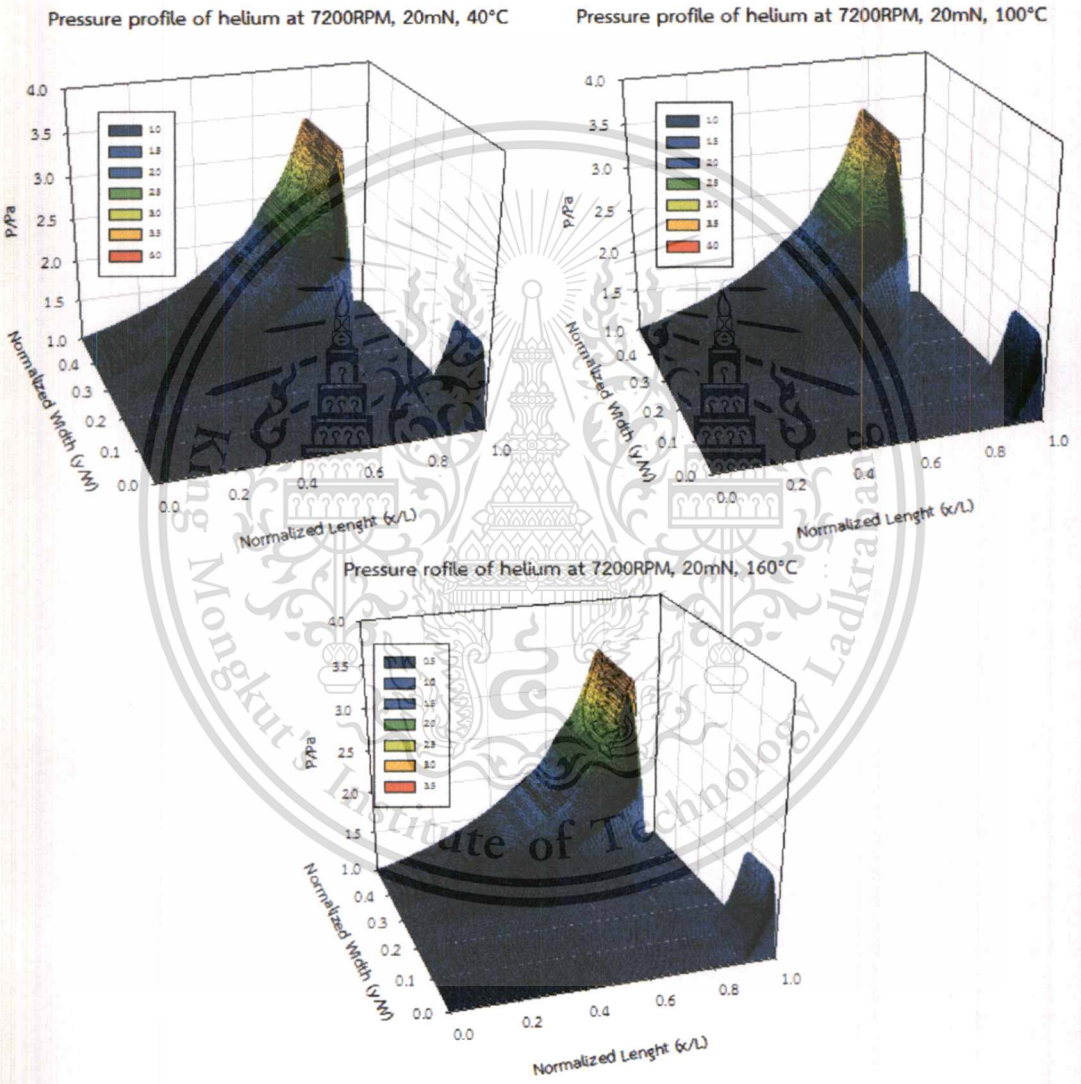

Fig 5.35 Comparison Pressure profile of helium with various temperatures at 7200RPM, 20mN

This material is reserved for educational use only, not allowed for commercial use.
Forbidden to modify the content, and cite the document when use.

CHAPTER 6

CONCLUSIONS

6.1 Conclusions

Currently, the inert gas has been implemented in magnetic recording system to reduce the flying height slider head in order to increase the areal density and interface performance of magnetic recording in hard disk drive technology.

This research was focused on the characteristic of flying height on slider head with various on disk velocity, loading force and temperatures. The static characteristic of slider head was numerically predicted.

We can summarize the characteristics of a slider head with each condition as follows:

1) High disk velocity directly affects the flying height due to higher disk velocity making the induced air flow inside the hard disk drive then it pushes the slider head out from the disk surface. Thus the flying height is higher with high disk velocity. When comparing the helium-filled and the air-filled drive, the flying height in helium still can be smaller than in air.

2) At higher loading force there can be a smaller flying height. The flying height with the helium-filled drive is smaller than the air one.

3) The flying height at leading edge increase significantly when the temperature is increased. This effect is due to the decreasing of gas's density and the increasing of gas's viscosity. Therefore, the pressure is increase at high temperature. This means the gas slider bearing operate under severe condition.

This study shows that the flying height of the helium-filled drive is lower than the flying height of the air-filled drive. However, the air bearing surface design and the dimension of slider are also important to the flying height characteristics.

This material is reserved for educational use only, not allowed for commercial use.
Forbidden to modify the content, and cite the document when use.

6.2 Suggestion for future work

This thesis was used finite difference method by using the grid was divided into square grids which it is not suitable with more complicate slider head and many grids is required much more computation time and high performance of computer.

Future study is on mixing between air and helium to investigate the characteristic of slider flying height which is required more study on model and properties of each condition and also pole tip protrusion is interested. As it can be more help on reducing the flying height and cost reduction in mass production.

This material is reserved for educational use only, not allowed for commercial use.
Forbidden to modify the content, and cite the document when use.

REFERENCES

[1] Gary Francis, (2012). "Storage: The Insatiable Demand, when does it end?" Oracle, Share Technology. Session 10939: 15.

[2] Zhou, W. D., B. Liu, et al. (2009). "Inert Gas Filled Head-Disk Interface for Future Extremely High Density Magnetic Recording." Tribology Letters 33(3): 179-186.

[3] Juang, J.Y., Bogy, D.B. "Air-Bearing effects on actuated thermal pole-tip protrusion for hard disk drives. ASME J. Tribol. 129, 570–578 (2007). doi:10.1115/1.2736456.

[4] Aruga, K., M. Suwa, et al. (2007). "A study on positioning error caused by flow induced vibration using helium-filled hard disk drives." Ieee Transactions on Magnetics 43(9): 3750-3755.

[5] Strom, B. D., S. Zhang, et al. (2007). "Effects of humid air on air-bearing flying height." IEEE Transactions on Magnetics 43(7): 3301-3304.

[6] Liu, N., J. L. Zheng, et al. (2009). "Thermal flying-height control sliders in hard disk drives filled with air-helium gas mixtures." Applied Physics Letters 95(21).

[7] Weidong Zhou, Bo Liu, Shengkai Yu, Wei Hua, and Chee How Wong. (2010). "Effects of environmental temperature and humidity on thermal flying height adjustment" Microsyst Technol (2010) 16:49–55. DOI 10.1007/s00542-008-0748-3.

[8] Computer history, history of the hard drive. Kioskea.net website [Online].
Available: http://en.kioskea.net/contents/237-history-of-the-hard-drive

[9] BrunoMarchon, Thomas Pitchford, Yiao-Tee Hsia,3 and Sunita Gangopadhyay. (2013) "The Head-Disk Interface Roadmap to an areal density of 4Tbit/in2". Advances in Tribology Volume 2013, Article ID 521086, 8 pages.

[10] Tutorial, hardware Tutorial. [Online]
Available: http://ajayannext.blogspot.com/search/label/HARDWARE%20TUTORIAL

[11] Scott Mueller. (2006) "Upgrading and Repairing PCs", 17th Edition. Que Publishing

[12] Lui gough. (2013). "Tech Flashback" [Online]
Available: http://goughlui.com

[13] Charles M. Kozierok, (2001). "The PC Guide" [Online]
Available: http://www.PCGuide.com

[14] Peter J. Vis. "Hard Disk Recovery Head Stack" [Online]

This material is reserved for educational use only, not allowed for commercial use.
Forbidden to modify the content, and cite the document when use.

Available: http://www.petervis.com

[15] Data Recovery Tools, Head Actuator of Hard Disk Drives [Online]

Available: http://www.datarecoverytools.co.uk/

[16] Goal, (2012). "Very silent Homemade Hamster Wheel using an old Hard Disk Drive". Cocodrilabs. [Online]

Available: http://cocodrilabs.wordpress.com

[17] Hard Disk Drives, Wikipedia [Online]

Available: http://th.wikipedia.org/

[18] S.C. Chapra and R.P. Canale, "Numerical Methods for Engineers", 4th Ed. New York: McGraw-Hill Inc., 2002.

[19] W.L. Briggs, V.E. Henson and S.F. McCormick, "A Multigrid Tutorial", 2nd Ed. Philadelphia. SIAM, 2000.

[20] William L. Briggs. "A Multrigrid Tutorial". Center of Applied Scientific Computing Lawrence Livermore National Laboratory. W-7405-Eng-48.

[21] BrunoMarchon,Thomas Pitchford, Yiao-Tee Hsia, and Sunita Gangopadhyay, "The Head-Disk Interface Roadmap to an Areal Density of 4 Tbit/in2," Hindawi Publishing Corporation, Advances in Tribology, Volume 2013, Article ID 521086, 8 pages

[22] B.Marchon and T. Olson, "Magnetic spacing trends: fromLMR to PMR and beyond," IEEE Transactions on Magnetics, vol. 45, no. 10, pp. 3608–3611, 2009.

This material is reserved for educational use only, not allowed for commercial use.
Forbidden to modify the content, and cite the document when use.

APPENDIX

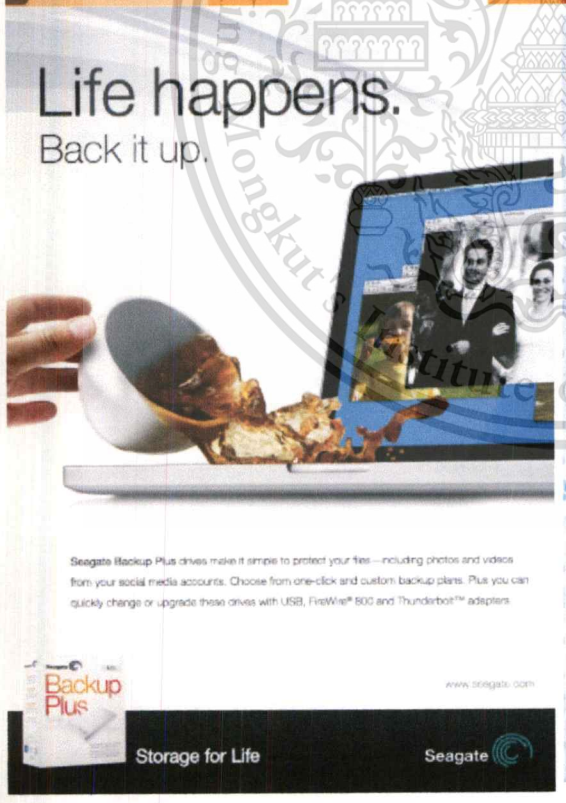

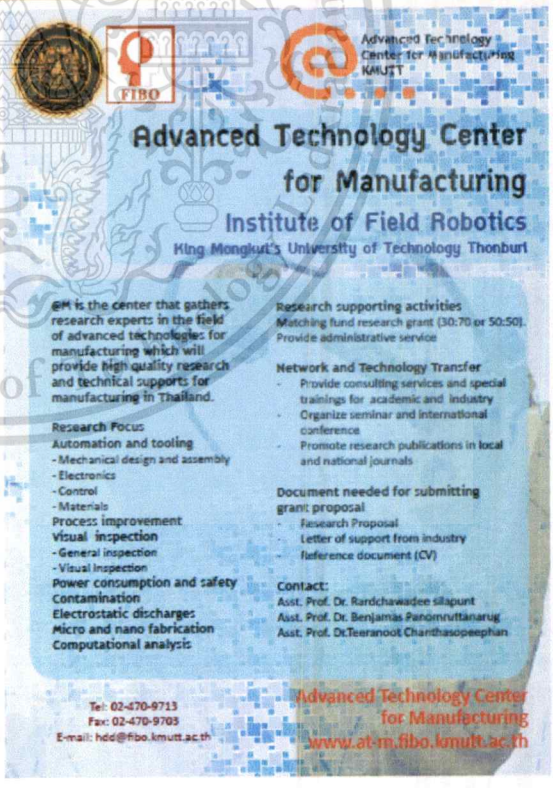

This material is reserved for educational use only, not allowed for commercial use.
Forbidden to modify the content, and cite the document when use.

P-15

Flying Height Characteristics in Helium-Filled Drive

S. Palita[1], and M. Mongkol[2]
[1]Department of Data Storage technology and Application,
King Mongkut's Institute of Technology Ladkrabang
Ladkrabang, Bangkok 10520, Thailand
[1]spalita.w@gmail.com
[2]Department of Mechanical Engineering
King Mongkut's Institute of Technology Ladkrabang
Ladkrabang, Bangkok 10520, Thailand
[2]kmmongko@gmail.com

Abstract— The digital explosion brought on by the proliferation of the internet fuelled significant growth in digital content creation and consumption. Coupled with a phenomenal growth in digital tools and equipment, researchers and analysts have put the growth of storage at a 40% compound annual growth rate. The traditional method of increasing tracks per inch (TPI) and bits per inch (BPI) to increase areal density still prevails. However, increasing TPI past a certain point requires other technologies to stabilize performance. Using an inert gas such helium is one technology to use. This has a positive effect on the thermal actuation of the slider head and reduces the vibration of hard disk drives due to large air bearing stiffness. The slider bearing is self acting with straight rails for the magnetic storage in a hard disk drive. The modified Reynolds equations were formulated. A numerical scheme based on the finite difference method with the Newton-Raphson method was implemented

This material is reserved for educational use only, not allowed for commercial use.
Forbidden to modify the content, and cite the document when use.

to obtain the static characteristics of slider head in steady state. The main objective of this topic is to investigate the flying height of a slider head in a helium filled-drive when the disk velocity, loading force and temperature are changed. The simulation results shows that the flying height of the slider head in the helium-filled drive is smaller than the flying height in air-filled drives for various disk velocities, loading forces, and the temperatures.

Keywords— Helium filled-drive, modified Reynolds equation, flying height, static characteristics of self acting air bearing.

King Mongkut's Institute of Technology Ladkrabang

This material is reserved for educational use only, not allowed for commercial use.
Forbidden to modify the content, and cite the document when use.

Kmutt Copyright Form (Bound to DST-CON 2013)

Proceeding of the 5th International Conference on Data Storage Technology (DST-CON) held during February 14-15, 2013 at The Sukosol, Bangkok

Title of work ____ Flying Height Characteristics in Helium-Filled Drive_____

_____

_____

Author(s)

1. ____ Palita Suthamma_____ 2. __Mongkol Mongkolwongrojn_____

3. _____ 4. _____

5. _____ 6. _____

Transfer of Copyright Agreement

Copyright to the above work (including without limitation, the right to publish the work in whole or in part in any and all forms of media, now or hereafter known) is hereby transfer to **King Mongkut's University of Technology Thonburi (KMUTT)** effective as of the date of this agreement on the understanding that the work has been accepted for publication by DST-CON 2013 Conference.

However, each of the Authors retains the following rights:

- All other proprietary rights except copyright (and the publication rights transferred to KMUTT), such as patent rights.
- The right to reuse any portion of the work, without fee, in future works of authors' own.

This form must be signed by the Author (one of the authors who is authorized to transfer copyright on behalf of other co authors), before processing of the manuscript for publication can be completed. Authors should understand that consistent with the policy of KMUTT in encouraging dissemination of information of each published paper will appear with the following notice:

"Permission to make digital or hard copies of part or all of this work for personal or classroom used is granted without fee provided that copies are not made or distributed for profit or commercial advantage and that copies bear this notice and the full citation on the first page. Copyrights for components of this work owned by others than KMUTT must be honored. Abstracting with credit is permitted. To copy otherwise, to republish, to post on servers or to redistribute to lists, require prior specific permission from KMUTT which may entail a fee."

Signature: ___Palita Suthamma_____

Print name: ___Miss Palita Suthamma _____

Date: _____18 December 2012_____

This material is reserved for educational use only, not allowed for commercial use.
Forbidden to modify the content, and cite the document when use.

Flying Height Characteristics in Helium-Filled Drive

S. Palita[1], and M. Mongkol[2]

[1]*Department of Data Storage technology and Application,*
King Mongkut's Institute of Technology Ladkrabang
Ladkrabang, Bangkok 10520, Thailand
[1]spalita.w@gmail.com

[2]*Department of Mechanical Engineering*
King Mongkut's Institute of Technology Ladkrabang
Ladkrabang, Bangkok 10520, Thailand
[2]kmmongko@gmail.com

Abstract— **The digital explosion brought on by the proliferation of the internet fuelled significant growth in digital content creation and consumption. Coupled with a phenomenal growth in digital tools and equipment, researchers and analysts have put the growth of storage at a 40% compound annual growth rate. The traditional method of increasing tracks per inch (TPI) and bits per inch (BPI) to increase areal density still prevails. However, increasing TPI past a certain point requires other technologies to stabilize performance. Using an inert gas such helium is one technology to use. This has a positive effect on the thermal actuation of the slider head and reduces the vibration of hard disk drives due to large air bearing stiffness. The slider bearing is self acting with straight rails for the magnetic storage in a hard disk drive. The modified Reynolds equations were formulated. A numerical scheme based on the finite difference method with the Newton-Raphson method was implemented to obtain the static characteristics of slider head in steady state. The main objective of this topic is to investigate the flying height of a slider head in a helium filled-drive when the disk velocity, loading force and temperature are changed. The simulation results shows that the flying height of the slider head in the helium-filled drive is smaller than the flying height in air-filled drives for various disk velocities, loading forces, and the temperatures.**

Keywords— **Helium filled-drive, modified Reynolds equation, flying height, static characteristics of self acting air bearing**

I. Introduction

The need to expedite new technological advances in areal density in order to fulfil continuing increase in hard disk drive (HDD) demand exists. Areal recording density increases about 30-40% every year as shown in Fig.1 [1]. Therefore, the study and development on areal density of hard disk drive is very important. There are many factors affecting the design of high capacity storage. One factor which is interesting to study is the reduced distance between the slider head and the disk surface (or what we call "Flying height"). The high precision of the read (playback) / write (recording) process will need to be increased when the flying height is small in order to maintain a suitable distance and avoid causing damage to the disk surface. A wide range of development and research

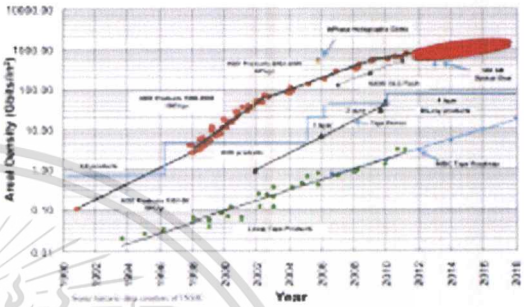

Fig.1 INSIC Storage Technologies Areal Density Trends of 2011 from Oracle Corporation. Courtesy of Gary Francis [1]

projects have focused on the flying height of the slider head, but these projects are restricted by the properties of the air. Thus the use of an inert gas such helium is studied in order to improve the flying height of slider head. Research on using inert gas started in the 1980s when 14 inch disks were normally used [2]. The results showed that the windage loss is reduced by 1/4 and the disk flutter is also reduced by 1/4.6 in helium-filled drives [2]. Also, the vibration from mechanical disturbance is reduced in the helium filled drive, and the positioning error in helium filled drive is less than half of the positioning error in an air-filled drive. These improvements are because of the low density property of helium [3]. In this topic we use the simulation method to study the flying height of the slider head in the helium-filled drives when the disk velocity, the loading force and the temperature are changed in the fully sealed drives and there is no discussion on the leakage problem.

II. Principles and Theories

The characteristics of flying height in steady state can be demonstrated by Modified Reynolds Equations.

A. Modified Reynolds Equations

This material is reserved for educational use only, not allowed for commercial use.
Forbidden to modify the content, and cite the document when use.

Consider the Molecular slip of air with dimensionless formula for Modified Reynolds equations in steady state [4].

$$\frac{\partial}{\partial X}\left(Q\frac{\partial P}{\partial X}\right)+R^2\frac{\partial}{\partial Y}\left(Q\frac{\partial P}{\partial Y}\right)=\Lambda\frac{\partial}{\partial T}(PH) \quad (1)$$

$$\text{with} \quad Q(PH)=\phi(P,H)PH^3 \quad (2)$$

Here P is the pressure, H is the distance between the air bearing surface and the disk surface, Q is the flow factor, λ is the ratio between length and width of the slider head, the expression Λ is the bearing number in the X position, and $\emptyset(P,H)$ is the Poiseulille flow factor [5, 6]

Defined as the following

$$Q(PH)=a_0+a_1\left(\frac{K_n}{PH}\right)+a_2\left(\frac{K_n}{PH}\right)^2+a_3\left(\frac{K_n}{PH}\right)^3 \quad (3)$$

$$\Lambda=\frac{6\mu_0 UL}{p_a h_m^2} \quad (4)$$

$$\mathrm{R}=\frac{L}{W} \quad (5)$$

where U is the disk velocity in X position, W is the width of the slider head, K_n is Knudsen Number, p_a is the ambient pressure, h_m is the minimum thickness of the gas film and μ is the dynamic viscosity of the gas. To consider at the boundary condition as below

$$\mathrm{P}(0,Y)=P(1,Y)=P\left(X,\frac{1}{2}\right)=P\left(X,-\frac{1}{2}\right)=1$$

B. Film Thickness Equations

Fig. 2 shows the characteristics of a slider head above the disk including the force and moment which are acting on the head.

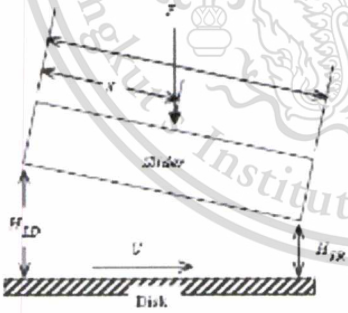

Fig. 2 The characteristic of slider head above the disk surface

The dimensionless formula for air bearing film thickness: where $0 \le X \le X_0$

$$H_{X,Y}=H_{TR}+(1-X)(H_{LD}-H_{TR})+\left(\frac{L}{h_m}\right)(X_0-X)tan\emptyset \quad (6)$$

where $X_0 \le X \le 1.0$

$$H=H_{TR}+(1-X)(H_{LD}-H_{TR}) \quad (7)$$

C. Balance Force and Moment Equations

From Fig.2, the dimensionless formula for the balance force acting on the slider head is

$$\int_{-\frac{1}{2}}^{\frac{1}{2}}\int_{0}^{1}(P-1)dXdY=\frac{f_0}{p_a LW} \quad (8)$$

The dimensionless formula for the balance moment is

$$\int_{-\frac{1}{2}}^{\frac{1}{2}}\int_{0}^{1}X(P-1)dXdY=X_G\left(\frac{f_0}{p_a LW}\right) \quad (9)$$

D. Newton – Raphson Method

Newton Raphson is the suitable method to determine the root of the Teylor series. This method is used for finding the function at position x from function value and derivative value which has any order at respective position x_0 that is given by

$$f(x)\cong f(x_0)+(x-x_0)f'(x_0)+\frac{(x-x_0)^2}{2!}f''(x_0)+\cdots \quad (10)$$

Consider at

$$f(x)\cong f(x_0)+(x-x_0)f'(x_0)=0 \quad (11)$$

$$x-x_0=\frac{f(x_0)}{f'(x_0)} \quad (12)$$

Then re-calculate between old and new value, to get

$$x_{k+1}=x_k+\Delta x_{k+1} \quad (13)$$

$$\Delta x_{k+1}=-\frac{f(x_k)}{f'(x_k)} \quad (14)$$

This material is reserved for educational use only, not allowed for commercial use.
Forbidden to modify the content, and cite the document when use.

The error is defined by

$$\left|\frac{X_{k+1}-X_k}{X_{k+1}}\right| < \varepsilon, \varepsilon = 10^{-5} \quad (15)$$

Then Reynolds equation will be performed as

$$\left[\frac{\partial F_{i,j}}{\partial P_{i,j}}\right]\{\Delta \bar{P}_{i,j}\} = -\{F_{i,j}\} \quad (16)$$

III. Simulation Result

In this paper we focus on the characteristic of flying height when the disk velocity and the loading force are changed. The simulation is performed with the tri-pad Air Bearing Surface (ABS) design 750μm x 850μm (W x L) and pad's width (B) 112.5μm. The properties for helium and air at 1 atm ambient pressure and temperature 20°C are shown in Table1 [1,7].

TABLE I
The properties of helium and air [2]

Properties	Helium	Air
Density, $\rho(kg/m^3)$	0.167	1.205
Dynamic viscosity, $\mu(Pa.s)$	1.956E-05	1.821E-05
Thermal Conductivity, $k(W/mk)$	0.148	0.026
Mean Free path, $\lambda(nm)$	165.5	63.5

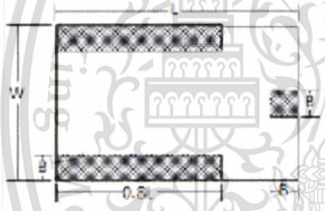

Fig.3 Characteristic of the slider head (simple tri-pad)

3.1 Flying height characteristic

Fig.4 shows the flying height characteristic of the trailing edge of the head slider at various disk velocities. The result shows that the flying height is raise up at the higher disk velocity. This is due to the air flow induced will push the slider head out from the disk surface. In the helium-filled drive, the flying height of the slider head is smaller than for the air-filled drive. The slope of the flying height on the helium-filled drive is less than the slope of the air-filled drive. This difference is because of the low density of helium and then the force generated from the air flow inside the HDD

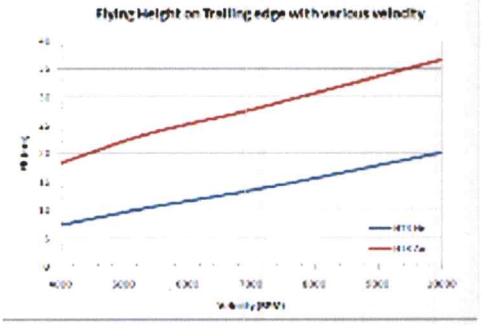

Fig.4 Flying Height on Trailing Edge change with various disk velocity

is not strongly enough to sustain the slider head at higher flying height in the helium filled drive.

Fig.5 shows the flying height characteristic of a slider head trailing edge at various loading forces. When the loading force is increased then the flying height is decreased. Normally, the loading force is in the range of 20-25 mN. If the loading force is outside of this range, the flying height is close to the disk surface and it will be result in impact of the slider head on the disk surface. However, this restriction is based on the air bearing surface design and the slider's dimension. From the results, the helium-filled drives provide a flying height that is twice as low as the flying height of the air-filled drives.

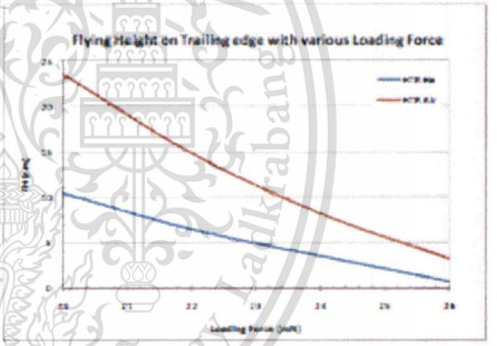

Fig.5 Flying Height on Trailing Edge change with various Loading Force

Fig.6 shows the flying height characteristics for various temperatures. The flying height is increased with higher temperature. This is same trend for both helium-filled and air-filled drives due to this study on fully sealed drives and there is no discussion on the leakage problem. This effect is due to the dynamic viscosity of gas and because pressure increases when the temperature is increased. Therefore, when the temperature is increased, the flying height is also increased.

This material is reserved for educational use only, not allowed for commercial use.
Forbidden to modify the content, and cite the document when use.

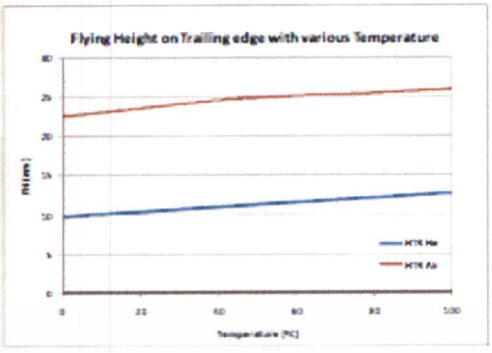

Fig.6 Flying Height on Trailing Edge change with various Temperature

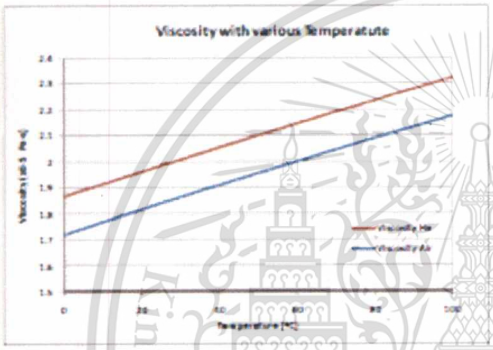

Fig.7 Viscosity with various Temperatures

Fig.7 shows the dynamic viscosity of helium and air with various temperatures.

IV. Conclusions

In this topic, we can summarize the characteristics of a slider head with each condition as follows:

1. High disk velocity directly affects the flying height due to higher disk velocity making the induced air flow inside the HDD then it pushes the slider head out from the disk surface. Thus the flying height is higher with high disk velocity. When comparing the helium-filled and the air-filled drive, the flying height in helium still can be smaller than in air.
2. At higher loading force there can be a smaller flying height. The flying height with the helium-filled drive is smaller than the air one.
3. The flying height is increased when the temperature is increased. This effect is due to the properties of the dynamic viscosity of gas and the increase of pressure inside the drive.

This study shows that the flying height of the helium-filled HDD is lower than the flying height of the air-filled HDD. However, the air bearing surface design and the dimension of slider are also important to the flying height characteristics.

Acknowledgment

The authors wish to acknowledge National Science and Technology Development Agency (NSTDA) and KMITL for financial support under Grant number DSTAR-R&D 02-02-53 and also would like to thank Western Digital (Thailand) Co., Ltd. for the scholarships in graduate study at KMITL.

References

[1] Gary Francis, "Data Storage - Trends and Directions", Oracle 2011 Technology Roadmap – PMR and Beyond", December 2006. Available: http://www.idema.org/wp-content/downloads/1615.pdf

[2] W. D. Zhou, B. Liu, S. K. Yu and W. Hua, *Inert Gas Filled Head-Disk Interface for Future Extremely High Density Magnetic*, Tribo Lett Springer, 2009, vol. 33, p.179-186. Doi:10.1007/s11249-008-9405-3

[3] K. Aruga, and M. Sawa, *A study on Positioning Error Caused by FIV using Helium Filled Hard Drives*, IEEE Trans. Magn., 2007, vol. 43(9), p.3750-3755. Doi:10.1109/TMAG.2007.

[4] B. J. Hamrock, *Fundamentals of fluid film lubrication*, Marcel Dekker Inc., New York, USA. ISBN: 0-8247-5371-2

[5] S. Fukui and Kaneko, *Analysis of Ultrathin Gas Film Lubrication Based on Linearized Boltzman Equation*, ASME Journal of Tribology, 1988, vol. 110, p. 335-341

[6] B. J. Shi and T. Y. Yang, *Simplified model of Reynolds equation with linearized flow rate for ultra-thin gas film lubrication in hard disk drives*, Springer-Verlag (2010 Doi: 10.1007/s00542-010-1107-8

[7] Helge Petersen, *The properties of Helium: Density, Specific Heats, Viscosity, and Thermal Conductivity at Pressure from 1 to 100 bar and from Temperature to above 1800K*, Danish Atomic Energy Commission Research Establishment Riso, 1970. Riso Report No. 224

This material is reserved for educational use only, not allowed for commercial use.
Forbidden to modify the content, and cite the document when use.

AUTHOR BIOGRAPHY

Name; Miss Palita Sudachun

Birthday; 14 January 1984

Address; 125/93 Moo4 YothayaVillage, Kunglan sub district, Bangpa-In district, Phanakornsriayudthaya, 13160

Education; 2005, Graduated in Bachelor of Engineering, Majoring in Mechanical Engineering, Suranaree University of Technology.

2013 (Present), Master degree of Engineering in Data Storage Technology and Application, International College of King Mongkut's Institute of Technology Ladkrabang.

Published research;

"Flying Height Characteristics in Helium-Filled Drive", the fifth International Data Storage Technology Conference 2013 (DST-CON2013) on February 14-15, 2013, Bangkok, Thailand.

This material is reserved for educational use only, not allowed for commercial use.
Forbidden to modify the content, and cite the document when use.